Progress and Prospects in Reverse Electrodialysis for Salinity Gradient Energy Conversion and Storage[1]

Ramato Ashu Tufa[a],*, Sylwin Pawlowski[b],*, Joost Veerman[c],*, Karel Bouzek[a], Enrica Fontananova[d], Gianluca di Profio[d], Svetlozar Velizarov[b], João Goulão Crespo[b], Kitty Nijmeijer[e],*, Efrem Curcio[d,f],*

[a]*Department of Inorganic Technology, University of Chemistry and Technology Prague, Technická 5, 166 28 Prague 6, Czech Republic*

[b]*LAQV-REQUIMTE, DQ, FCT, Universidade NOVA de Lisboa, 2829-516 Caparica, Portugal*

[c]*REDstack BV, Pieter Zeemanstraat 6, 8606 JR Sneek, The Netherlands*

[d]*Institute on Membrane Technology of the National Research Council (ITM-CNR), c/o University of Calabria, via P. Bucci, cubo 17/C, 87036 Rende, CS, Italy*

[e]*Membrane Materials and Processes, Eindhoven University of Technology, P.O. Box 513, 5600 MB Eindhoven, The Netherlands*

[f]*Department of Environmental and Chemical Engineering, University of Calabria (DIATIC-UNICAL) via P. Bucci CUBO 45A, 87036 Rende (CS) Italy*

*Corresponding authors: tufaa@vscht.cz; s.pawlowski@fct.unl.pt;

j.veerman@redstack.nl; d.c.nijmeijer@tue.nl; efrem.curcio@unical.it

Abstract

Salinity gradient energy is currently attracting growing attention among the scientific community as a renewable energy source. In particular, Reverse Electrodialysis (RED) is emerging as one of the most promising membrane-based technologies for renewable energy generation by mixing two solutions of different salinity. This work presents a critical review of the most significant achievements in RED, focusing on membrane development, stack design, fluid dynamics, process optimization, fouling and potential applications. Although RED technology is mainly investigated for energy generation from river water/seawater, the opportunities for the use of concentrated brine are considered as well, driven by benefits in terms of higher power density and mitigation of adverse environmental effects related to brine disposal. Interesting extensions of the applicability of RED for sustainable production of water and hydrogen when complemented by reverse osmosis, membrane distillation, bio-electrochemical systems and water electrolysis technologies are also discussed, along with the possibility to use it as an energy storage device. The main hurdles to market implementation, predominantly related to unavailability of high performance, stable and low-cost membrane materials, are outlined. A techno-economic analysis based on the available literature data is also performed and critical research directions to facilitate commercialization of RED are identified.

Keywords: Salinity Gradient Power, Reverse Electrodialysis, Ion Exchange Membranes, Fouling, Low-energy Desalination, Hydrogen Production, Techno-economic Analysis

1. Introduction

Energy is one of the key resources determining the overall socio-economic development: a robust energy supply must be secured for a sustainable growth and an improved living standard. Global energy consumption is increasing at an exponential rate: it is estimated that global energy consumption will rise by 48% between 2012 and 2040 [1]. Moreover, the anticipated population increase in the coming decades will generate two billion new energy consumers in emerging economies by 2050 [2, 3]. During the same time interval, global energy-related carbon dioxide emissions are expected to increase by 46%, corresponding to 45 billion metric tonnes [1, 3, 4]. In this context, the development of alternative energy resources able to alleviate the skyrocketing demand for clean energy and related environmental issues are urgently required [5].

Salinity gradient energy or Salinity Gradient Power (SGP), also referred to as 'Blue Energy', is generated by converting the chemical potential difference between two salt solutions with different concentrations into electrical or mechanical energy [6-12]. It is a completely clean and sustainable energy source with no toxic gas emissions. Commonly (but not exclusively) river and seawater are used as salt solutions. Other potential resources of SGP involve brine solutions from anthropogenic sources (industrial streams, solar ponds [13-15]) or natural sources (*e.g.* the Dead Sea), saline wastewater from industrial processes or domestic source, thermolytic solutions (*e.g.* ammonium bicarbonate) etc. The SGP concept was first proposed by Pattle in 1954 [16]. A number of patents were filled and pioneering research was performed at that time [9, 16-19]. However, technological progress was hampered mainly by the unavailability of suitable membranes. The fast-growing rate of today's membrane market, in conjunction with the increasing demand for renewable energy, currently represents the main driving force of interest in SGP.

The unexploited estuarial SGP released by mixing seawater and river water, which has an estimated maximum global potential of 2.6 TW, is the second largest marine-based energy source next to ocean waves (see Table 1) [7, 8, 20]. With reference to the most relevant water bodies, the gross global potential of salinity gradient energy

is estimated to be higher than 27,000 TWh/year, the extractable part of which being around 2000 TWh/year which is more than 10% of the total global potential of renewable energy resources [21]. This estimate may vary, depending on technical and operational factors, such as flow rate, temperature, recovery rate, efficiency, salinity levels, fouling behavior and other aspects, including ecological and legal constraints [22]. Of the total global potential of SGP, about 0.98 TW is estimated to be available for extraction. In addition, efficient utilization of the global SGP could potentially yield 38 Mt/yr of hydrogen, a clean and versatile energy carrier [23]. The SGP potential from wastewater discharged into an ocean is estimated to be 18 GW [7]. Novel SGP applications based on closed-loop systems using excess waste heat could also potentially enable the production of more than 120,000 GWh/year [24].

Table 1. Comparison of salinity gradient energy global potential with other marine renewable energy resources [20, 25-27].

Marine renewable energy resources	Driving force	Global potential (TW)
Salinity gradient energy	Salinity difference	2.6
Thermal energy conversion	Temperature difference	2.0
Ocean waves	Kinetic energy transfer	2.7
Tides	Water flow and Gravitational forces	0.03
Ocean currents	Temperature difference and water flow	0.005

Unlike intermittent wind and solar energy sources, SGP can be exploited continuously 24 hr per day and 365 days a year. The natural water cycle illustrated in Figure 1 exemplifies the concept of SGP as a renewable energy resource that potentially originates when river water, brackish water, seawater or brine are mixed with each other.

This review focuses on RED technology which is currently witnessing a significant development and, so far, the only pilot plant producing power from SGP using RED technology [28-30]. Furthermore, positive net power density values have been already achieved in RED stacks operated over extended periods of time with either natural river water and seawater [31-33] or brackish water/seawater and brine [29, 30, 34, 35]. The present work presents a detailed critical assessment of the potential of RED to harvest salinity gradient energy. Major research advances from the past decades up to now are presented and discussed, with a special focus on material development, system design, membrane stability against fouling, process optimization, and advanced

applications in the logic of process intensification. The most significant research outcomes in terms of ion exchange membrane preparation, characterization and testing in RED are reported. Suitable membrane materials still remain the key components determining the overall performance and economics of RED for commercial success. Applications based on hypersaline salt solutions are evaluated and compared with respect to conventional RED operations using river water and seawater. The applicability of RED for sustainable production of water and hydrogen in integrated process schemes with RO, MD, bio-electrochemical systems and water electrolysis technologies is presented, including potential use as an energy storage device (concentration gradient
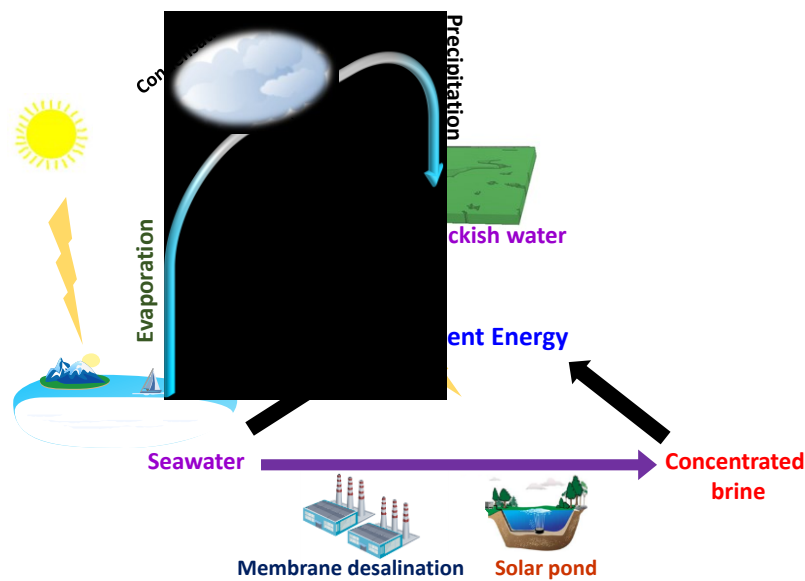
flow battery). Technological challenges and economic aspects, outlining the future research perspectives required for large-scale implementation are also discussed.

Fig. 1 The natural water cycle illustrating the possibility of continuous exploitation of SGP; concentrated brine can be obtained from anthropogenic sources like seawater desalination plants and/or solar evaporators (ponds).

2. Thermodynamic potential of salinity gradients

The Gibbs energy of mixing (ΔG_{mix}) is released when two solutions of different salinity are mixed. For the i-th component in a solution, the chemical potential μ_i (J/mol), i.e. its partial molar Gibbs energy, is defined as [36]:

$$\mu_i = \mu_i^\circ + v_i \Delta p + |z_i| F \Delta \psi + RT \ln \gamma_i x_i \tag{1}$$

where v is the partial molar volume (m³/mol), Δp the pressure difference (Pa), z the valence (equiv./mol), F the Faraday constant (96,485 C/equiv.), $\Delta \Psi$ the electrical potential difference (V), R the gas constant (8.314 J/(mol K), T the absolute temperature (K), γ the activity coefficient and x is the mole fraction. Under constant pressure and in the absence of an electrical field, Eq. 1 simplifies to:

$$\mu_i = \mu_i^{\circ} + RT \ln \gamma_i x_i \tag{2}$$

The Gibbs energy (G) is defined as follows:

$$G = \sum_i \mu_i n_i \tag{3}$$

where n is the number of moles of each component, expressed in terms of molar concentration c *(mol/m³)* and total volume V (m³) as:

$$n_i = c_i \cdot V \tag{4}$$

Therefore, ΔG_{mix} is calculated from the difference between the Gibbs free energy of the mixed solution (G_b) and the Gibbs free energy of the initial solutions (G_c *and* G_d) with subscripts "c", "d" and "b" referring to the concentrate solution, dilute solution, and to the brackish salt solution which remains after mixing, respectively [37]:

$$\Delta G_{mix} = G_b - (G_c + G_d) \tag{5}$$

Combining equations 1 to 5 then results in:

$$\Delta G_{mix} = \sum_i (c_{i,t} V_t RT \ln \gamma_{i,t} x_{i,t}) - (c_{i,c} RT \ln \gamma_{i,c} x_{i,c} + c_{i,d} V_d RT \ln \gamma_{i,d} x_{i,d}) \tag{6}$$

Figure 2 compares the theoretically available amount of Gibbs energy from mixing different salt solutions at room temperature. The theoretically available amount of free energy from mixing 1 m³ of seawater (0.5 M NaCl) and 1 m³ of reverse osmosis (RO) brine (1 M NaCl) is about 420 kJ. Mixing of 1 m³ of seawater (0.5 M NaCl) and 1 m³ of membrane distillation (MD) brine (5 M NaCl) yields about 10500 kJ, corresponding to an equivalent energy of 2.93 kWh, which is about 25 times higher than the amount harvested when mixing seawater (0.5 M NaCl) and RO brine (1 M NaCl). In fact, the lower amount of OCV from mixing seawater (0.5 M NaCl) and RO brine (1 M NaCl) is

due to the reduction of deriving force imposed by the low salinity ratio of 2. Moreover, ΔG_{mix} from 1 m^3 of brackish water (0.1 M) and 1 m^3 of MD brine (5 M NaCl) results in 15000 kJ. A higher amount of energy (16800 kJ) is obtained when mixing the same volume of MD brine and river water reversibly, although the high amount of Ohmic
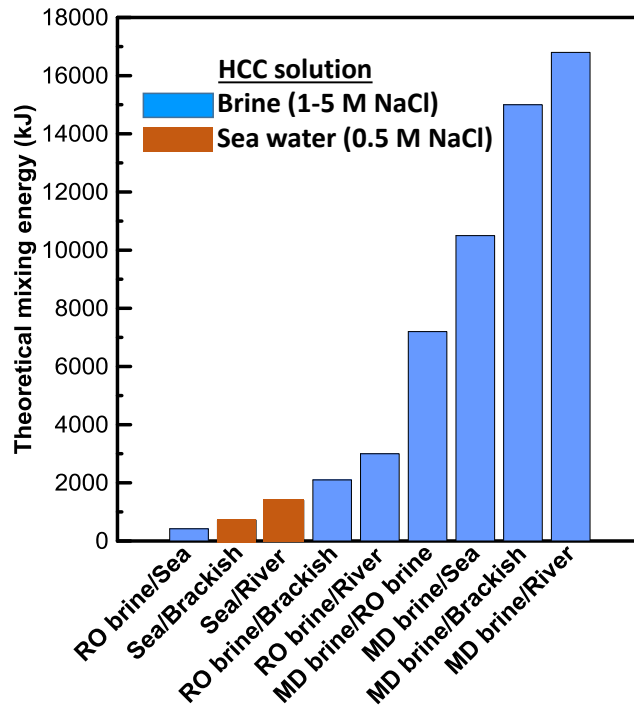
losses associated with the low salt concentration of the river water limits the maximum extractable power density [47].

Fig. 2 Comparison of the theoretical amount of ΔG_{mix} (kJ) obtained from mixing 1 m^3 of concentrated solution and 1 m^3 of diluted solution; river water (0.01 M NaCl), brackish water (0.1 M NaCl), reverse osmosis (RO) brine (1 M NaCl), membrane distillation (MD) brine (5 M NaCl); HCC: high concentration compartment.

3. Technologies for Salinity Gradient Power

SGP can be generated by different technologies: Reverse Electrodialysis (RED) [21, 34, 35, 38-49], microbial RED [50-53], capacitive mixing (CAPMIX)[54, 55], mixing entropy batteries (MEB) [56], pressure retarded osmosis (PRO)[57-68] and vapor pressure difference utilization (VPD) [69]. RED and PRO are the two promising membrane-based technologies which are at the most advanced stage of development.

4. Reverse Electrodialysis

Despite the fact that the concept of RED technology was reported long ago in 1954 [16], the most remarkable trend of research advances has been recorded from 2007 onwards [42, 49]. Figure 3 shows the number of papers on RED published yearly over the past decade, and the key research topics so far have covered process analysis, testing and optimization [39, 41, 70-76], stack design [77-81], membrane design and development [82-85], fouling [32, 86] modeling and simulations [87-98], hybrid applications [38, 47, 50, 51, 99-102] and extensions to energy storage as a flow battery [103, 104]. Moreover, RED operability has recently been extended from relatively low
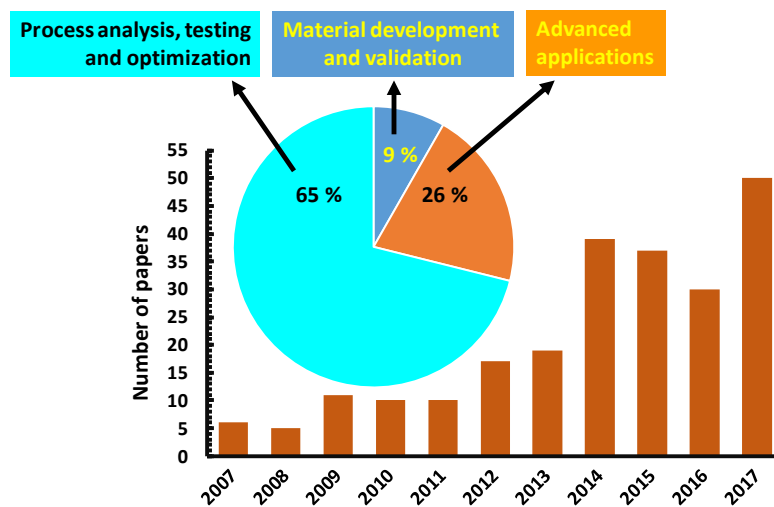
saline solutions to highly saline industrial effluents and thermolytic solutions regenerated in a closed loop [105-107].

Fig. 3 Progress in RED research: number of publications and topics (Source: Scopus 2017).

4.1. Theoretical background

RED is an emerging membrane-based technology for renewable energy generation via salinity gradients. Figure 4 illustrates a typical RED unit operated on two solutions of different salinity. In RED, cation exchange membranes (CEMs) and anion exchange membranes (AEMs) are alternately stacked to create a series of adjacent high concentration compartments (HCCs) and low concentration compartments (LCCs) fed with high concentration solutions and low concentration solutions, respectively. Salinity gradient and charge segregation induced by ion exchange membranes (IEMs) generate an electrochemical potential. The resulting ionic flux is converted into electricity by a redox reaction occurring at the electrodes connected to an external circuit. Low overpotential of the electrode is maintained by proper selection of electrode materials and use of appropriate electrode rinse solutions [42, 108-113]. In RED, two adjacent

IEMs constitute a single 'cell' (sometimes called a 'cell pair'), consisting of an AEM, an LCC, a CEM and an HCC. A RED stack usually includes a large number of cells.
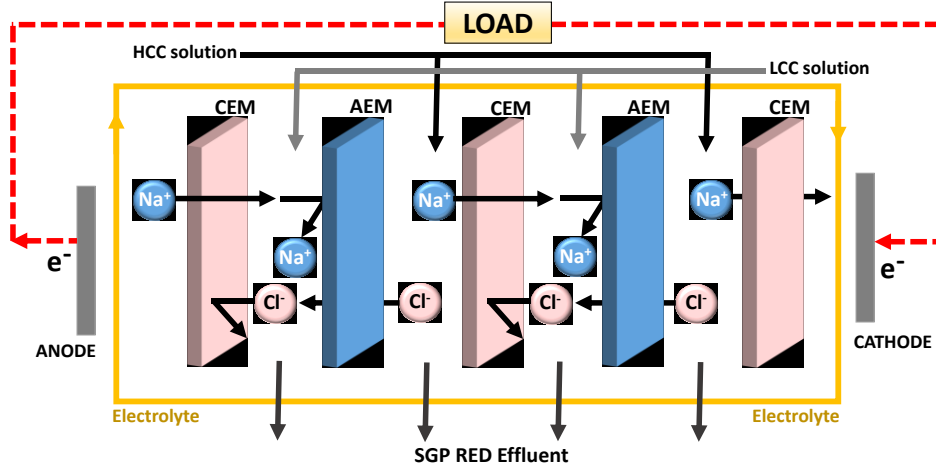
Fig. 4 Schematic illustration of a RED stack: the electrochemical potential is generated when feeding each high concentration compartment (HCC) and low concentration compartment (LCC) created by aligning alternatively a CEM and an AEM. The salinity gradient drives the selective transport of ions across the membranes towards electrodes where a redox reaction allows continuous generation of electricity.

The total electromotive force generated in RED, which is the sum of the Nernst potential over each cell, is the Open Circuit Voltage (OCV), theoretically calculated by the Nernst equation:

$$OCV = \frac{NRT}{F}\left[\frac{\alpha_{CEM}}{z_{ct}}\ln\frac{\gamma_{c,ct}c_c}{\gamma_{d,ct}c_d} + \frac{\alpha_{AEM}}{z_{an}}\ln\frac{\gamma_{c,an}c_c}{\gamma_{d,an}c_d}\right] \tag{7}$$

where N is the number of membrane pairs (cell pairs), α is the permselectivity of the ion exchange membrane, subscripts '*an*' and '*ct*' stand for 'anion' and 'cation', respectively. OCV is mainly dependent on the membrane permselectivity, the concentration gradient and the valence of the transported ions. The membrane permselectivity (α) represents the ability of the material to selectively transport only counter-ions (i.e. cations in CEMs or anions in AEMs) and to exclude co-ions (i.e. anions in CEMs or cations in AEMs) [114-117]. For membranes operating in a RED

stack, an "apparent permselectivity" (α_{app}) can be calculated as the ratio between the measured (E_m) and the theoretical membrane potential (E_t) [73]:

$$\alpha_{app} = \frac{E_m}{E_t} \cdot 100\% \tag{8}$$

Theoretically, a potential of about 0.12 V, 0.16 V and 0.2 V can be generated from a pair of IEMs (considering 100% permselective membranes) by mixing brine (5 M NaCl)/seawater (0.5 M NaCl), sea water (0.5 M NaCl)/river water (0.017 M NaCl) and brine (5 M NaCl)/brackish water (0.1 M NaCl), respectively.

In fact, the local electromotive force over the membranes varies spatially due to changes in concentration between the RED inlet and outlet as well as concentration polarization phenomena (defined next) [72].

In RED, ion exchange membrane attracts counter-ions, whose concentration is much larger than that of co-ions due to the Donnan exclusion. Concentration polarization phenomena occur due to the presence of a net charge on the membrane surface which affects the ions distribution at the interface of membrane and solution. This results in an increase of the concentration of counter-ions, the so-called electrical double layer (EDL), having a thickness in the order of nanometers [118]. Moreover, when ions are transported through the membrane from the HCC to LCC driven by an electrochemical potential gradient, the flux difference between the co-ion and the counter-ion along with the difference in transport number of the ions between the membrane and solution phase determines the formation of a diffusion boundary layer (DBL), having a thickness of several hundred of micrometers [119, 120]. The diffusion boundary layer non-ohmic resistance is due to change in salt concentration in the unstirred (stagnant) liquid films close to the membrane surfaces [72, 121-123]. Thus, the internal stack resistance of RED is accounted by several resistances as described next.

In RED, the internal stack resistance R_i, is composed of the Ohmic resistance R_{Ohm}, the non-Ohmic resistance and the resistance of the electrode system R_e. The Ohmic resistance inside the stack due to ionic transport limitations through the stack components is mainly accounted for by the resistance of the membranes and resistance of the feed compartments. The non-Ohmic resistance is ascribed to the diffusion boundary layer resistance R_{dbl} and electrical double layer resistance R_{edl} [72, 122-124].

Experimentally, R_{dbl} and R_{edl} can be traced by using powerful analytical tools like electrochemical impedance spectroscopy (EIS) [122, 123]. This technique enables investigation of the non-Ohmic contribution to the total stack resistance. However, there is also a non-Ohmic effect due to mixing in a RED stack which is best understood in co-current operation: the salinity gradient is decreased during the passage through the flow paths. The sum of all these non-Ohmic effects can be achieved with chronopotentiometric measurements [72, 125, 126]. In practice, the contribution of non-Ohmic resistance to R_i of RED is low, especially when working with highly concentrated brine solutions. The non-Ohmic losses are amplified in operations involving low concentration feed solutions [122] and can be ascribed to the mixing effect. The resistance of the electrode system is ascribed to the Nernst voltage of the redox reaction, to overpotential and to Ohmic part in the solution. Due to a stagnant diffusion boundary layer on the electrode, these parts are dependent on electrical current density, temperature, concentration and flow velocity. Considering the operability of RED on a large scale, the resistance of the electrodes can be neglected. Thus, R_i can be calculated as [72]:

$$R_i = R_{Ohm} + R_{dbl} + R_{edl} \tag{9}$$

R_i can be determined experimentally. R_{Ohmic} can be represented as the sum of the resistance of the membranes (R_{AEM} and R_{CEM}) and the solution compartments (R_{LCC} and R_{HCC}):

$$R_{Ohm} = N\left(R_{AEM} + R_{CEM} + R_{LCC} + R_{HCC}\right) \tag{10}$$

In a RED stack, the salt concentration near the membrane surface at the HCC side is lower than the bulk and at the other side, the concentration near the membrane is higher than the LCC bulk. Thus, the Ohmic resistance of the cell pair is mainly determined by the LCC and the thin enrichment layer at the LCC side and the thin depletion layer at the HCC side barely affect the total Ohmic resistance of the cell pair. This is opposite to an ED stack were the depletion layer is situated at the LCC side; the high resistance of this layer makes a considerable contribution to the total Ohmic resistance. The resulting difference in concentration across the depletion layer i.e concentration polarization is less pronounced at the HCC side because of the higher screening effect of the attractive electrical interactions between the counter-ions and fixed charged groups of the membrane, with respect to the LCC [42, 122, 123, 127].

The negligible effect of electrical double layer resistances at high NaCl concentration (up to 4 M) has been demonstrated by using electrochemical impedance spectroscopy [123].

If there is no spacer, the resistance of the solution compartments can be calculated from the specific conductivity σ (S/m) of the salt solution, the area A_{cell} (m^2) and the compartment thickness δ (m). Otherwise, a correction factor is used for the volume occupied by the spacer material. The void factor f_v expresses the relative volume available for the solution (void volume):

$$R_{LCC} = \frac{\delta}{f_v \sigma_{LCC} A_{cell}}$$
(11)

$$R_{HCC} = \frac{\delta}{f_v \sigma_{HCC} A_{cell}}$$
(12)

An ideal RED stack without significant shortcut currents behaves like a normal battery and its current I depends on the electromotive force (E), the internal stack resistance R_i and the load resistance R_L:

$$I = \frac{E}{R_i + R_L}$$
(13)

The power dissipated in the external resistance R_L, which is the power density P_d generated in a RED stack, can be calculated as:

$$P_d = I^2 R_L = \left(\frac{E}{R_i + R_L}\right)^2 R_L$$
(14)

For an ideal RED stack, the maximum power density $P_{d,max}$ (W/m^2: Watt per m^2 of total membrane area) is obtained when the load resistance equals the internal stack resistance ($R_L = R_i$). Considering that the sum of E across all cells equals OCV, and indicating with A (m^2) the active membrane area, Eq. (14) is adapted to calculate the maximum power density $P_{d,max}$ (W/m^2) as follows:

$$P_{d,max} = \frac{OCV^2}{4AR_i}$$
(15)

Generally, some electrical energy is consumed by pumping the feeds into the RED stack and circulating the electrode rinse solution. As a consequence, the net output

power $P_{d,net}$ is calculated by subtracting the power dissipated over the pumps (hydrodynamic loss) P_h from the gross power density P_d:

$$P_{d,net} = P_d - P_h \qquad (16)$$

The hydrodynamic loss P_h can be obtained from the theoretical pumping power required to recirculate the solutions through HCC and LCC, which depends on the pressure drop along the compartment Δp (Pa) and the volumetric feed flow rate Q (m³/s) normalized by the total cell pair area of the stack ($N{\cdot}A$). Thus, Eq. (16) is re-written as:

$$P_{d,net} = P_d - \frac{\Delta p_{HCC}Q_{HCC} + \Delta p_{LCC}Q_{LCC}}{N \cdot A} \qquad (17)$$

The ultimate objective of a RED operation is to achieve the highest possible value of net power density. It is important to note that net power density depends on several parameters related to the intrinsic electrochemical performance of IEMs, stack configuration (number of cell pairs, channel length), hydrodynamics, nature of available saline streams (ionic composition, the presence of foulants).

Transport phenomena in RED is mainly governed by the transport of ions in the membranes and the solutions within the SGP-channel. This consists the convective flux within the spacer-filled SGP channels and the electro-migrative flux of ions towards the proximity and within IEMs [91, 96, 128, 129].

For an IEM (*e.g.* CEM) in contact with a dilute electrolyte (NaCl solution) solution, the concentration of counter-ions (Na⁺) in the membrane will be much higher than the concentration in the solution, due to the presence of the fixed charges in the IEM. In contrary, the concentration of co- ions (Cl⁻) in the membrane will be much lower than in the solution. As a result, ions start to migrate from one side to another to maintain electro-neutrality in the membrane and the bulk solution. This creates an electric field in the direction opposite to the direction of the diffusional flow, and when the electric field balances the diffusional driving force, a Donnan equilibrium is reached. The potential difference between the membrane and the solution is given by Donnan potential. Thus, the mole fraction of ions in the membrane phase ($x_{i,\,m}$) and solutions phase ($x_{i,\,c}$ *and* $x_{i,\,d}$) can be obtained by the theory of the Donnan equilibrium (K) [115, 130]:

13

$$\frac{x_{i,m}}{x_{i,c}} = K \qquad (18)$$

To keep electro-neutrality, the total charge in the membrane phase need to be balanced:

$$\sum z_{i,m} x_{i,m} = 0 \qquad (19)$$

where $z_{i,m}$ is the valence of ions in the membrane phase.

In RED, unequal NaCl concentrations of the external solutions at both sides of an IEM results in a chemical potential gradient over the membrane which induces an ionic diffusion and osmotic water transport (Figure 5). The total mass transport T_m (mol/s) of NaCl from the HCC to the LCC in the stack can be determined from the difference between the output and input flow of feed solutions:

$$T_m = \phi_d^o c_d^o - \phi_d^i c_d^i \qquad (20)$$

where ϕ is the volumetric flow rate of feed solutions, superscripts 'o' and 'i' stands for 'out' and 'in', respectively. Salt transport is contributed by the counter-ion (columbic) transport and co-ion transport. Back transport is also be expected in the case of a mixture of solutions consisting of multivalent ions. On the other hand, water transport can take place by osmosis from the LCC to HCC or electro-osmosis from HCC to LCC [74]. In practice, there could also be the transport of co-ions in IEMs depending on the external salt concentration. The osmotic flow rate (ϕ_c^o) can be depicted from the salt concentrations and solution flow rates as [74]:

$$\phi_{os} = \frac{\phi_c^o \left(c_c^i - c_c^o \right) - \phi_d^o \left(c_d^i - c_d^o \right)}{\left(c_c^i - c_d^i \right)} \qquad (21)$$

Both the co-ion transport and osmosis have a negative impact on the power density of RED. A recent study focusing on development of RED models incorporating the influence of co-ion transport indicated upto 20% reduction of power density due to this phenomenon [91]. Osmotic effects in RED are less influential as it is counterbalanced by the electro-osmosis. However, its determinental effect to same level as co-ion transport have recently been demonstrated by model calculations [128].
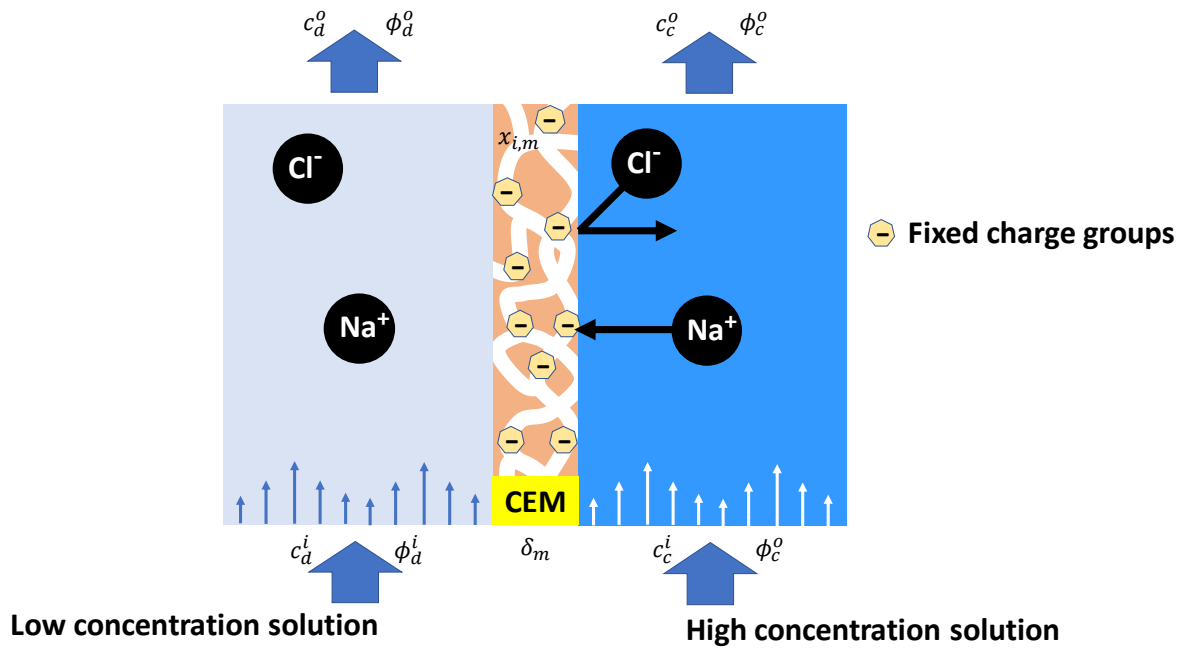
Fig. 5 Illustration of transport in CEM contacted with a NaCl feed solution.

In our opinion, there is a set of important questions/challenges which deserve special attention in order to turn RED into a competitive technology for power generation. Such fields of research are related to membrane properties (electric resistance and permselectivity) and cost, fluid dynamics (stack arrangement, profiled membranes) and stability against fouling associated with the use of natural saline streams. RED is currently an inherently sustainable and clean technology mainly limited by the cost and performance of membranes. The cost of low resistance membranes is still high (above 94 €/m^2) [75, 131]. Cheap membranes on the market, which mainly lack low resistance, do not meet the technical requirements for RED applications. Moreover, the permselectivity of current IEMs is reduced by a high salinity gradient, leading to a limited Donnan exclusion effect [34, 90]. To overcome the current limitations, advanced technological innovations are required targeting the design and development of new IEMs with low resistance and high permselectivity at an affordable cost.

4.2. *Membrane development*

4.2.1. *Tailor-made membranes*

At the heart of RED are ion exchange membranes (IEM) which significantly affect the overall process performance. The requirements of optimal IEMs for RED application include high permselectivity (above 95%), low electrical resistance (below

1 Ωcm^2), acceptable mechanical and chemical stability and long lifetime (minimum of 5 years) [132]. Besides, membranes should be of low cost: Membrane costs below 4.3 €/m² have been depicted to be a break-even prices for financial feasibility of seawater electricity generation by RED [81].

Low resistance and high ionic conductivity are the key requirements for membranes applied in electrochemical energy systems [122, 133-136]. Permselectivity also plays an important role in maintaining selective transport of counter-ions, which enhances the OCV. Additionally, both membrane resistance and permselectivity are a function of other electrochemical properties, such as the ion exchange capacity (IEC) and fixed charge density [91, 114, 123, 124, 126, 137, 138]. These properties are inherently sensitive to the chemical structure of the polymeric materials for IEMs, and there exists a trade-off between the two parameters depending on the structure-property relationships [114, 133, 139]. The water transfer coefficients of IEMs need to be minimized as well [140].

Most IEMs employed in electrochemical processes like fuel cells and electrolyzers are specifically tailored for high ionic conductivity, stability, and good mechanical properties [133, 134, 141-154]. For example, highly conductive and chemically perfluorinated membranes are compatible with a strongly acidic environment in polymer electrolyte water electrolyzers or fuel cells [133, 134, 149, 155-159].

Membrane requirements for RED slightly differ from previously mentioned systems, being IEMs mostly operated in a neutral environment (pH~7) with Na⁺ and Cl⁻ ions playing a major role in the ion transport process, taking place in the presence of divalent ions like Mg^{2+}, Ca^{2+} and SO_4^{2-}. Figure 6 correlates IEM properties and manufacturing parameters. Basically, membranes designed for RED should be thin, often without reinforcement, have high permselectivity and moderate mechanical properties [82, 131, 133, 160]. With the aim to alleviate the current cost limitation of commercially available IEMs, low-priced hydrocarbon polymers are good candidates as starting material for membrane fabrication.
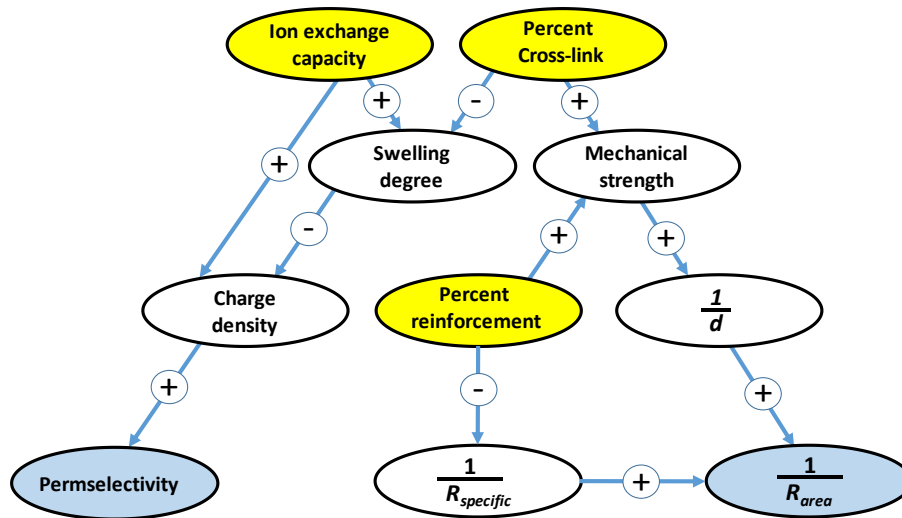
Fig. 6 Relationships between membrane manufacturing parameters (yellow) and most important operational RED parameters (blue); between them are the common membrane properties (white). Arrows indicate a positive (+) or negative (-) effect. For better clarity, specific resistance ($R_{specific}$), area resistance (R_{area}) and thickness (d) are displayed as reciprocal.

Although innovative IEMs tailored for RED have been manufactured in recent years, under an EU-funded research projects (i.e. REAPower, RED Heat to Power [161, 162]), the majority of experimental tests reported in the literature are performed using commercial IEMs.

Długołecki *et al*. [163] measured and compared the electrochemical properties (ionic resistance, permselectivity and charge density) of various commercial IEMs for use as input for model calculations to determine the maximum theoretical power density. Table 2 summarizes some of the electrochemical properties of commercial IEMs and tailor-made IEMs for potential application in RED. In general, a high IEC results in high permselectivity and low resistance. The propensity to swelling caused by high IEC is usually controlled by chemical cross-linking and mechanical reinforcement of the membrane structure. Table 2 shows that CEMs have higher permselectivity while AEMs exhibit lower resistance.

Table 2. Properties of commercial and tailor-made IEMs for potential applications in RED.

Membranes	Type	δ (μm)	α (%)	R_a (Ωcm²)	SR (Ωcm)	IEC (meq/g)	SD (%)	CD (meq/mL)	Ref.
Tokuyama Co., Japan									
Neosepta CM-1	CEM	120-170	97.2	1.67	115	2.30	20	11.5	[163, 164]
Neosepta CMS	CEM	150	-	2	133	2	38	5.3	[165]
Neosepta CMX	CEM	140-200	99.0	2.91	171	1.62	18	9	[132, 164]
Neosepta AM1	AEM	130-160	91.8	1.84	127	1.77	19	9.3	[163, 164]
Neosepta ACM	AEM	120	-	4.5	375	1.5	15	10	[165]
Neosepta AFN	AEM	150-200	88.9	0.70	40	3.02	43	7.0	[163, 164]
Neosepta AMX	AEM	160-180	90.7	2.35	138	1.25	16	7.8	[132, 164]
FuMA-Tech GmbH, Germany									
FKE	CEM	50-70	98.6	2.46	410	1.36	12	11.3	[163, 164]
FKD	CEM	90-100	89.5	2.14	225	1.14	29	3.9	[132, 164]
FAD	AEM	80-100	86.0	0.89	99	0.13	34	0.4	[163, 164]
FAS	AEM	100-120	89.4	1.03	94	1.12	8.0	14.0	[132, 164]
MEGA a.s., Czech Republic									
Ralex CMH-PES	CEM	764	94.7	11.33	148	2.34	31	7.5	[163]
Ralex CM-PP	CEM	<450	>90	<8	178	-	-	-	[166]
Ralex AMH-PES	AEM	714	89.3	7.66	107	1.97	56	3.1	[163]
Ralex AM-PP	AEM	<450	>90	<8	178	-	-	-	[166]
Asahi Glass Co. Ltd., Japan									
Selemion CMV	CEM	130-150	98.8	2.29	164	2.01	20	10.1	[132, 164]
Selemion AMV	AEM	110-150	87.3	3.15	242	1.78	17.0	10.5	[132, 164]
Selemion DSV	AEM	121	89.9	1.03	85	1.89	28	7.1	[163]
Selemion APS	AEM	138	88.4	0.68	49	0.29	147	0.2	[163]
Hangzhou QianQiu Industry Co., China									
Qianqiu CEM	CEM	205	98.8	1.97	96	1.21	33.0	3.7	[132]
Qianqiu AEM	AEM	294	86.3	2.85	97	1.33	35.0	3.8	[132]
Tailor-made									
Fe_2O_3-SO_4^{2-}-sPPO	CEM	10	87.7	0.97	970	1.40	26	5.4	[84, 160]
sPVA/PPO	CEM	50	87.17	1.54	308	~2	93.9	>1.68	[167]
SPEEK 40	CEM	53	95.3	2.05	387	1.23	23	5.3	[132]
SPEEK 65	CEM	72	89.1	1.22	169	1.76	35.6	4.9	[132]

Table 2. *(Continued)*

		δ	α	R_a	SR	IEC	SD	CD	
KIER-CEM1	CEM	26	97.8	0.34	131	2.64	26.9	9.8	[168]
KIER-CEM2	CEM	27	99.2	0.72	267	1.42	21.7	6.5	[168]
PECH A	AEM	77	90.3	2.05	266	1.31	32.2	4.1	[82, 132]
PECH B-1	AEM	33	86.5	0.82	248	1.68	49.0	3.4	[82, 132]
PECH B-2	AEM	77	87.2	0.94	122	1.68	49.0	3.4	[82, 132]
PECH B-3	AEM	130	87.0	1.32	102	1.68	49.1	3.4	[82, 132]
PECH C	AEM	77	79.2	1.14	148	1.88	53.5	3.5	[82, 132]
KIER-AEM1	AEM	27	91.8	0.28	104	1.55	21.9	7.1	[168]
IMD-40-PAES	AEM	64	94.35	1.65	258	1.48	13	13.31	[166]
TMA-40-PAES	AEM	70	91.56	1.45	207	1.45	30	6.68	[166]
ABCO-40-PAES	AEM	66	93.53	1.59	241	1.48	17	10.55	[166]
Fujifilm Manufacturing Europe B.V., the Netherlands*									
Fuji T1	CEM	115	87-91	1.7	-	-	-	-	[169]
FujiCEM	CEM	114	-	2.97	261	1.1	-	-	[35, 123]
FujiAEM	AEM	129	89	1.55	120	1.4	-	-	[71, 123]
Fuji A-mono**	AEM	124	91	1.1	89	-	-	-	[83]

*Prepared on request to the company; **Monovalent selective ion exchange membrane prepared by modification of Fuji membranes. Symbols: δ - thickness; α - permselectivity; R_a - area resistance; *SR* - specific resistance; *IEC* - ion exchange capacity; *SD* - swelling degree; *CD* - charge density.

Permselectivity and resistance are usually determined using NaCl solutions. However, the mobility, dry ion radius, hydrated ion radius, polarizability, hydration energy and diffusion constant of Na^+ and Cl^- are very different. This difference in ionic properties influences membrane properties. For example, CEMs mostly display higher resistance compared to AEMs [123, 170] in NaCl solution due to the lower mobility of the Na^+ ion (4.98×10^{-8} m^2 $V^{-1}s^{-1}$) than that of the Cl^- ion (6.88×10^{-8} m^2 $V^{-1}s^{-1}$) [171]. The resistance of IEM also varies depending on the nature of electrolyte. Fontananova *et al*. [117] characterized membrane resistance in pure NaCl solution and a mixture of solution containing multivalent ions. A typical test in solution containing Mg^{2+} ion resulted in about 4-fold increase of CEM (Fuji CEM800) membrane resistance from 2.41 ± 0.08 Ωcm^2 in 0.5 M NaCl to 8.3 ± 0.2 Ωcm^2 in a mixture of 0.340 M NaCl and 0.054 M $MgCl_2$. Moreover, significantly high resistance of up to 158 Ωcm^2 was also reported for a highly cross-linked Neosepta CMS membrane in pure $MgCl_2$ (0.5 M) solution [172]. The same holds for the fixed charges (except diffusion constant and mobility) $\sim N(CH_3)_3^+$ and $\sim SO_3^-$. Ion exchange groups which strongly interact with specific ions lead to a reduction of the migration speed of the given ion through the membrane [170]. Geise *et al*. characterized IEMs in a wide range of salts including $NaHCO_3$. A lower permselectivity of Selemion CMV membranes in $NaHCO_3$ (78.9 %) than in NaCl (97.5 %) test solutions (0.1 M/0.5M) was observed [138]. Ammonium ion binds more strongly to the fixed charge groups of the CEMs than sodium ions, resulting in the neutralization of fixed charge groups that in turn leads to the reduction in the concentration of the fixed charge groups within the membrane. A similar effect has also been reported for Mg^{2+} ion that led to a reduction in permselectivity of CEMs [124]. The influence of external solution concentration and compositions on membrane properties and hence the RED performance are discussed in later sections.

For the hypothetical case of RED operated with optimal IEMs, model calculations predict the possibility of attaining a gross power density above 6 W/m^2 when mixing seawater and river water [163]. Veerman *et al*. [74] tested various commercial membranes to investigate the power density and thermodynamic efficiency of RED. Thin membranes with thickness (80-100 μm) and good electrochemical properties (permselectivity above 86 %, electrical resistance in the range of 2.14-0.89 Ωcm^2) resulted in a $P_{d,max}$ up to 1.2 W/m^2 obtained when using a combination of Fumasep and Selemion membranes.

Güler *et al.* [82] fabricated IEMs from polyepichlorohydrin (PECH), an active polymer backbone, and a tertiary diamine (1,4-diazabicyclo[2.2.2]octane, DABCO) in dimethyl sulfoxide (DMSO) as an aminating and crosslinking solution. Figure 7 shows the chemical reaction mechanism involved in the fabrication of PECH membranes via the membrane casting method. PECH membranes were blended with polyacrylonitrile (PAN) at blend ratios in the range of 0.100 - 1.04. As the blend ratio increases (above 0.333), the amount of active polymer and, consequently, the amount of ion exchange groups increases as well, leading to a decrease in area resistance (below 0.94 Ωcm^2). In parallel, permselectivity decreased due to an increase in swelling.
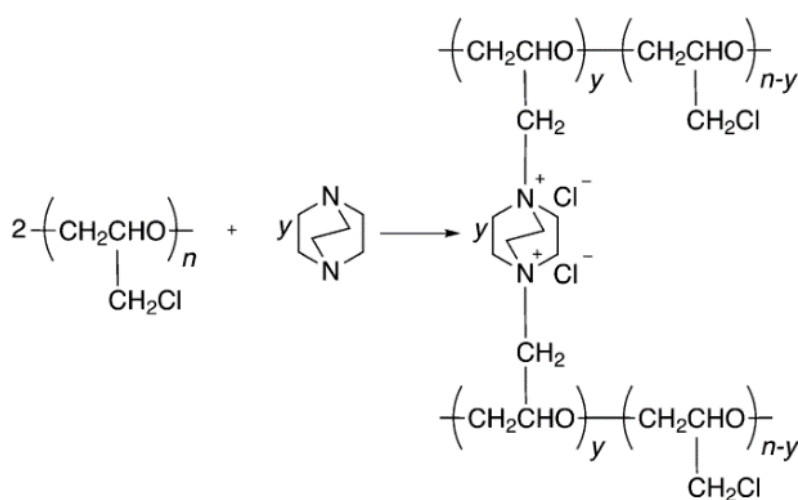
Fig. 7 Illustration of the reaction mechanism for the amination of PECH with DABCO. Reproduced with permission [82]. Copyright 2012 Wiley.

In another work, CEMs based on sulfonated polyetheretherketone (SPEEK) were prepared by a casting method [132]. Quite a high area resistance was recorded for the SPEEK membranes (above 1.22 Ωcm^2). The SPEEK membranes also indicated good permselectivity: a maximum of 95% permselectivity was measured at sulfonation degree of 40% (SPEEK40). Moreover, a RED test using SPEEK CEMs with a sulfonation degree of 60% (SPEEK65) and PECH B2 (blend ratio 0.333, the thickness of 77 μm) AEM membranes revealed a $P_{d,max}$ of 1.3 W/m^2 (Figure 8). IEMs based on poly(vinyl alcohol, PVA) and sulfonated polyetheretherketone (SPEEK) are generally considered to be economically viable and to have good electrochemical properties [133, 150, 173-180].
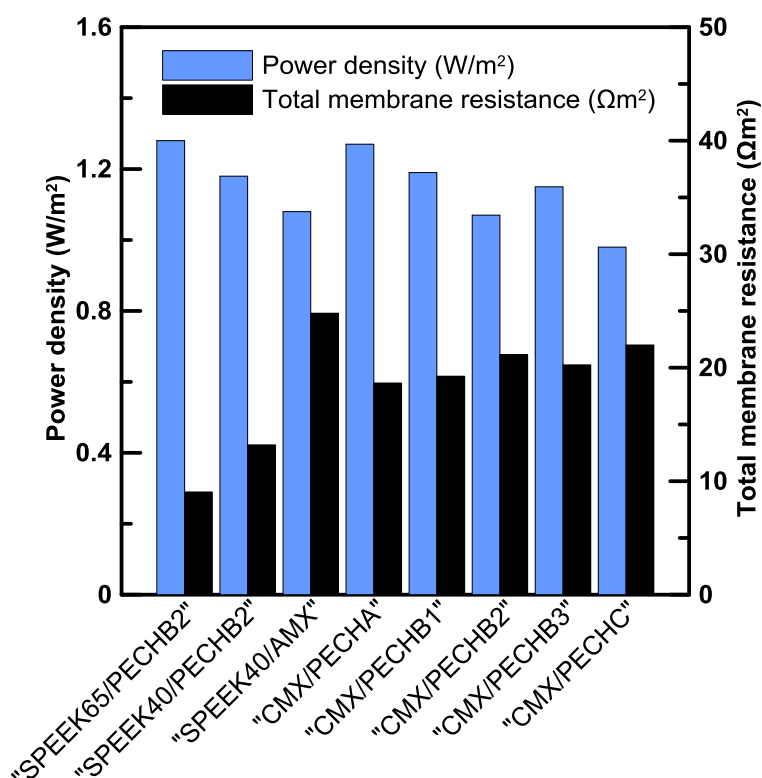
Fig. 8 Total membrane resistance and experimental power density determined for RED equipped with a combination of different tailor-made membranes combined with different membranes; SPEEK65 and SPEEK40: Sulfonated polyetheretherketone (SPEEK) with a sulfonation degree of 65% and 40% respectively; PECHA, PECHB1, PECHB2 and PECHB3, PECHC: Polyepichlorohydrin (PECH) membranes with a blend ratio of 0.208, 0.333 and 0.417 for A, B and C type membranes respectively; B1, B2, B3 type membranes have varying thickness of 33, 77 and 130 μm, respectively; The membranes CMX and AMX are commercial membranes (Tokuyama Co., Japan). RED tests were performed with artificial seawater (0.513 M NaCl) and artificial river water (0.017 M NaCl). Flow velocity: 1.75 cm/s. Adapted with permission [132]. Copyright 2013 Elsevier.

Fuji *et al.* [168] synthesized IEMs based on poly (vinyl alcohol) (PVA) and polyelectrolytes for applications in RED. Such membranes exhibited a power density of 0.4 W/m^2 at a salinity ratio of 20. Furthermore, model calculations indicated the superiority of PVA-based membranes in terms of performance and cost compared to commercial membranes (Neosepta AMX and CMX, Astom Co., Japan).

IEM based on inorganic-organic composite materials are gaining remarkable attention in the field of electrochemical technologies due to their synergistic advantages

compared to conventional membranes exclusively based on organic or inorganic materials. Inorganic-organic composite IEM materials have been applied in fuel cells [181-184], water electrolysis [185-188] and batteries [189-193]. Similarly, porous nanocomposite CEMs with inorganic functional groups have been prepared and tested for RED applications [84, 85, 194]. So far, composite membranes used for RED are based on sulfonated poly (2,6-dimethyl-1,4-phenylene oxide) (sPPO) polymer with sulfonated Fe_2O_3-SO_4^{2-} nanoparticles. Hong *et al*. [84] reported a power density of 1.4 W/m^2 for a RED stack equipped with composite membranes having an optimal loading of 0.7 wt% of nanoparticles in the polymer matrix. The use of organic-organic hybrid membranes can also be a promising approach for low-cost production of membranes for RED. In line with this, Zhang *et al*. [167] fabricated a series of hybrid CEMs by incorporation of sulphonated poly (vinyl alcohol) (sPVA) into poly (2,6-dimethyl-1,4-phenylene oxide) (PPO) polymer matrix using a solvent evaporation method. The area resistance of the membranes decreased with an increase in sPVA content reaching its minimum i.e. 1.43 Ωm^2 at 10 wt% of sPVA. In a RED test, the highest power density of 0.48 W/m^2 was recorded at 5 wt% of sPVA which was slightly (14 %) higher than the commercial Fumasep membranes tested under similar conditions.

Pore-filling type membranes enable control of electrochemical membrane properties by tuning preparation conditions. This membrane has been investigated for several applications including fuel cells [195-199]. The applications have also been investigated for RED by Kim *et al*. [168] who fabricated different pore-filling membranes. AEMs (KEIR-AEM1) were prepared by crosslinking microporous polyolefin polymer with *N,N*-bis(acryloyl)piperazine and (vinylbenzyl) trimethylammonium chloride at a molar ratio of 1 : 11, whereas CEMs (KEIR-CEM1) were prepared by crosslinking the same microporous polymer with *N,N*-ethylenebis(acrylamide) and vinyl sulphonic acid at a 1 : 8.8 molar ratio. The membrane exhibited extremely low thickness (26 μm for KEIR-CEM1 and 27 μm for KEIR-AEM1), very low area resistance (0.34 Ωcm^2 for KEIR-CEM1 and 0.28 Ωcm^2 for KEIR-AEM1) and permselectivity up to 97%. RED tests resulted in a gross power density of 2.4 W/m^2. Other polymeric materials recently used for fabrication of IEMs include trimethylammonium chloride at a molar ratio of 1 : 11, whereas CEMs (KEIR-CEM1) were prepared by crosslinking the same microporous polymer with *N,N*-ethylenebis(acrylamide) and vinyl sulphonic acid at a molar ratio of 1 : 8.8. The

membrane exhibited extremely low thickness (26 μm for KEIR-CEM1 and 27 μm for KEIR-AEM1), very low area resistance (0.34 Ωcm^2 for KEIR-CEM1 and 0.28 Ωcm^2 for KEIR-AEM1) and permselectivity up to 97%. RED tests resulted in a gross power density of 2.4 W/m^2.

Other polymeric materials recently used for fabrication of IEMs for RED application involve poly(2,6-dimethyl-1,4-phenylene oxide) (SPPO) [200], polyethylene [201] and poly(arylene ether sulfone) (PAES)[166, 202]. With the aim to investigate the effect of the pulsed electric field on the alignment of ion channels, Lee *et al.* prepared sulfonated CEMs based on poly(2,6-dimethyl-1,4-phenylene oxide) (SPPO) [200]. These membranes achieved electrical resistance below 0.86 Ωcm^2 with power density reaching 1.34 W/m^2 in RED tests [200]. In another work, Safronova *et al.* [201] prepared sulfonated CEMs by radiation grafting of styrene/divinylbenzene onto a polyethylene film. Different membranes with varying degrees of crosslinking and grafting were fabricated and characterized, indicating the possibility of achieving membranes with low area resistance (below 0.61 Ωcm^2). Theoretical calculations indicated the possibility of obtaining higher power densities (above 10%) with such optimally tailored membranes compared to the use of commercially available Neosepta CMX membrane in RED [201]. Cho *et al.* [166] fabricated CEMs based on poly(arylene ether sulfone) (PAES) with three different functional groups: 1-methyl-imidazolium (IMD), basic tetramethylammonium (TMA), and the salt form of 1-azabicyclo[2,2,2]octane (ABCO). The strategy was chosen with a perspective to prepare AEMs with high ion conductivity and permselectivity at low cost. The aminated AEMs exhibited good conductivity of up to 10.3 $mScm^{-1}$ and excellent permsectivity of up to 91-99 % which were both higher compared with a commercial AMX membrane with ionic conductivity of 4.68 $mScm^{-1}$ and permselectivity of 90.7 % [166].

The aforementioned methods for tailoring membranes allow a better choice of suitable strategies and potential membrane materials for efficient power generation by RED. For example, a route for the fabrication of homogeneous membranes without any reinforcement and reduced thickness can be followed to design IEMs with low resistance. However, in such scenario, membranes might show poor permselectivity. This is coherent with general trend observed in Figure 9 which shows the variation of area resistance with permselectivity of some commercial membranes, and selected tailor-made RED membranes: Less selective membranes generally display low

membrane resistance and highly selective membranes display high resistance. A similar scenario has also been reported by Długołecki *et al.* who characterized and compared the electrochemical properties of a series of commercial IEMs [163]. In fact, methods other than the one used to design thin membranes might also have an advantage depending on the required electrochemical property. When it comes to low-cost membrane design, not only the cost of raw material but also the cost of production plays a role. For example, in such scenario, a simple and fast UV induced polymerization technology might be of great interest [83].
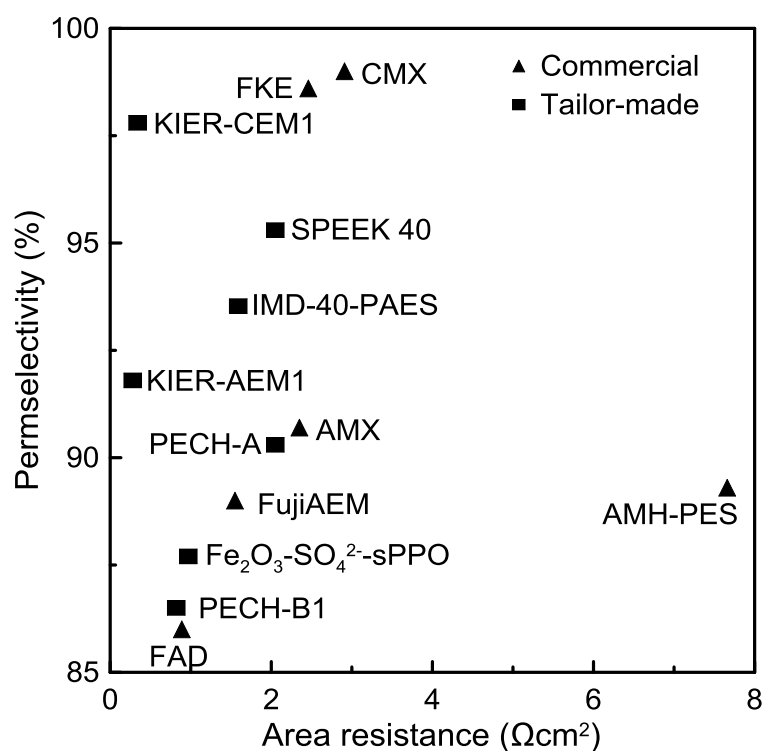
Fig. 9 The variation of area resistance with permselectivity for some commercial IEMs, and tailor-made IEMs for RED.

Overall, the tailor-made membranes developed so for RED seems to be promising as permeances are compared to the commercially available ones. Most of the tailor-made RED membranes display a comparable electrical resistance, and even lower than commercial membranes in some cases (Figure 9). In particular, the pore-filling membranes (KIER-CEM1) exhibit significantly low electrical resistance compared to other membranes, due to the intrinsic polymer properties as well as thinness. Other membrane based on polymers like SPEEK also show good permselectivity but comparatively higher membrane resistance. Despite the low membrane resistance, the

PECH and organic-inorganic hybrid membranes (Fe_2O_3-SO_4^{2-}-sPPO) require an improvement in permselectivity.

4.2.2. Monovalent selective membranes

Many ions other than sodium and chloride are naturally present in water, and multivalent ions like Mg^{2+} and SO_4^{2-} have been already reported to have a negative impact on RED performance [41, 46, 71, 203]. Thus, IEMs with improved monovalent ion selectivity are crucial for RED operating with real feed solutions.

A monovalent selective membrane allows rapid permeation of monovalent ions while blocking the passage of multivalent ions. The permselectivity between ions of the same charge in a mixture depends on several factors, including the differences in hydrated radii, the affinity of the ions with the membrane and the differences in migration rate in the membrane phase [137, 170, 204].

Preparation methods for IEMs with enhanced monovalent ion selectivity include the coating of a weakly basic anion exchange group layer on the membrane surface, the condensation of polymer aromatic amines and formaldehyde on either the surface or matrix of the membrane, the partial decomposition of strongly basic anion exchange groups on the membrane surface, the coating of a highly cross-linked or anionic polyelectrolyte layer on the membrane surface, modification by covalent grafting etc [205-219].

Separation of anions according to their hydration radius and size was achieved by physical adsorption of polyethylenimine (PEI) onto AEM [220, 221]: a positively charged thin-film composite nanofiltration membrane, prepared by in-situ interfacial polymerization of functionalized polyethyleneimine and terephthaloyl chloride, exhibited a distinct increase in selectivity towards Cl^- and SO_4^{2-}. Layer-by-layer deposition of alternating polyanions and polycations layers has also been considered [222, 223]. Mulyati *et al*. [224] reported that monovalent-anion selectivity is achieved by electrostatic repulsion between multivalent anions and the negative surface charge of the membrane. Li *et al*. [225] introduced polyquaternium-7 into a commercial CEM for application in electrodialysis (ED).

Güler *et al*. [83] adopted a simple and fast method based on UV curing to design a monovalent selective IEM for RED application. A standard commercial AEM (Fuji A) was coated with a layer formed by copolymerization of 2-acryloylamido-2-methylpropanesulfonic acid (AMPS) as the active polymer and N, N-

methylenebis(acrylamide) (MBA) as the cross-linker. Pristine Fuji-A and modified Fuji A-mono membranes were characterized in terms of morphology and permselectivity (Figure 10). The dense structure of the thin coating on both membranes exhibited structural similarity (Figure 10A); the high concentration of sulfonic acid functional groups present in the coating layer is confirmed by EDX sulfur mapping images reported in Figure 10B. 3D optical interferometric images indicate that the surface roughness of the coated Fuji A-mono membrane was lower than the original membrane due to the smoothening effect of the homogeneous coating layer (Figure 10C).
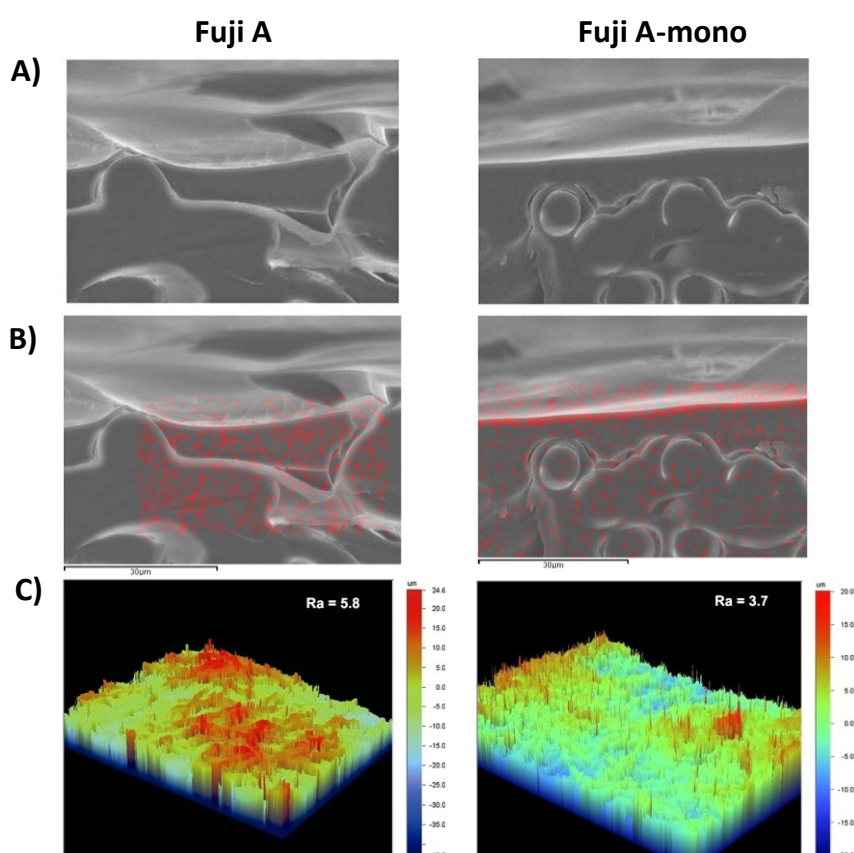
Fig. 10 A) Cross-sectional SEM images of pristine Fuji A and coated Fuji A-mono membranes; B) EDX sulfur mapping overlaid (red dots); C) Surface roughness by 3D optical interferometry; D) Electrochemical characterization in terms of limiting current density (LCD) and relative permselectivity measurements. Reproduced (adapted) with permission [83]. Copyright 2014 Elsevier.

Li *et al*. coated a commercial CEM with a Chitosan/Polyaniline (PANI) film by electrodeposition. The monovalent selectivity of the composite membrane was enhanced with PANI content up to a certain level [210]. This approach was extended to other composite membranes (organic-inorganic [226], sulfonated-PVDF/PVDF) to improve monovalent selectivity. Blend membranes of sulfonated poly(ether ether ketone) and poly(arylene ether ketone) derivatives containing crown ether units [227, 228], polyelectrolyte coated Nafion membranes [229], and surfactant-modified membranes [230] have also been proposed.

4.3. Process parameters

The key performance parameter in RED is power density; additional parameters of interest include OCV and internal stack resistance. Table 3 summarizes the RED conditions and power density values from the relevant literature.

The performance of RED is predominantly affected by feed characteristics (composition and concentration) and operating conditions (flow velocity and temperature) [231-238].

4.3.1. Effect of flow velocity

Flow velocity, defined as the mean fluid velocity (v) inside a single spacer-filled channel, affects the hydrodynamics of the RED system and the mass transfer of charges. Flow velocity can be estimated as:

$$v = \frac{Q}{\delta w \varepsilon} \tag{18}$$

where Q is the volumetric flow rate (m^3/s) in a single channel, δ the spacer thickness (m), w the compartment width (m) and ε the spacer porosity.

Table 3. RED conditions and power densities reported in the literature on testing and optimization.

Membrane				Spacers (δ, μm)	Electrolyte	Electrode	v (cm/s)	$P_{d, max}$ (W/m^2)	Ref.
Type	A (cm^2)	δ (μm)	N						
Neosepta ACS/CMS (Tokuyama Inc., Japan)	10x10	120-200	5	Woven (100)	0.1 M $K_3Fe(CN)_6$, 0.1M $K_4Fe(CN)_6$ and 0.5 M NaCl	Ti-RuO_2/IrO_2	4.2	3.8	[239]
FumasTech FAD/FKD (GmbH, Germany)	10x10	82	50	Woven spacers (200)	0.05 M $K_4Fe(CN)_6$, 0.05 M $K_3Fe(CN)_6$ and 0.25 M NaCl	Ti-RuO_2/IrO_2	4.2**	6.7 (60 °C)	[239]
Qianqiu AEM/ CEM, (Hangzhou Qianqiu Industry Co, China)	25x75	205-294	25	Woven spacers (200)	0.05 M $K_4Fe(CN)_6$, 0.05 M $K_3Fe(CN)_6$ and 0.25 M NaCl	Ti-RuO_2/IrO_2	2.5	~0.83	[240]
Selemion AMV/CMV (Asahi Glass, Japan)	10x10	110-150	5	Woven spacers (200)	~0.25 M NaCl	Ti-RuO_2/IrO_2	58.3	1.18	[74]
FumaTep FKD and FAD (GmbH, Germany)	10x10	40-80	25	Woven spacers (200)	~0.25 M NaCl	Ti-RuO_2/IrO_2	58.3	1.17	[74]
	10x10	82	50	Woven spacers (200)	0.05 M $K_4Fe(CN)_6$, 0.05 M $K_3Fe(CN)_6$ and 1 M NaCl	Ti-RuO_2/IrO_2	58.3	0.93	[39]
Qianqiu Heterogeneous AEM/CEM (Hangzhou QianQiu Industry Co., China)	10x10	40-80	5	Woven spacers (200)	~0.25 M NaCl	Ti-RuO_2/IrO_2	58.3	1.05	[74]
Fuji AEM/CEM (Fujifilm Europe B.V., The Netherlands)	10x10	114-129	25	Woven (270)	0.3 M $K_3Fe(CN)_6$, 0.3 0.3 M $K_4Fe(CN)_6$ and 2.5 M NaCl	Ti-Ru/Ir mesh	1	1.06	[241]

Table 3. (*Continued*)

|									
PC-SK and PC-SA (PCCell, Germany)	8x8	90-130	10	Non-conductive (500)	~0.6 M NaCl	Ti coated with Pt	3.5	~0.33	[76]
Neosepta AMX/CMX (Tokuyama Co., Japan)	10x10	134-164	5	Woven spacers (200)	~0.25 M NaCl	Ti-RuO$_2$/IrO$_2$	58.3	0.65	[74]
Neosepta AMX/CMX (Tokuyama Co., Japan)	10x10	134-164	4	Ion conductive AMX/CMX (320)	0.5 M NaCl	Ti-RuO$_2$/IrO$_2$	~0.8	0.8	[79]
Neosepta AMX/CMX (Tokuyama Co., Japan)	100	138 -181	3	Woven (200)	0.5 M NaCl	Ti-RuO$_2$/IrO$_2$	0.56	0.87	[73]
Neosepta CMX/AMX (Tokuyama Co., Japan)	100	138 - 181	3	Woven (485)	0.5 M NaCl	Ti-RuO$_2$/IrO$_2$	0.56	0.56	[73]
Neosepta CMX/AMX (Tokuyama Co., Japan)	6x13	30-37	5	Woven-modified (500)	0.05 M K$_3$Fe(CN)$_6$, 0.05 M K$_4$Fe(CN)$_6$ and 0.25 M NaCl	Ti-Ir plasma	1.25	0.59	[242]
FKS/FAS (FumaTech GmbH, Germany)	10x10	30-40	5	Woven (60)	0.025 M K$_3$Fe(CN)$_6$, 0.025 M K$_4$Fe(CN)$_6$ and 0.25 M NaCl	Ti-RuO$_2$/IrO$_2$	0.12	1.8	[72]
FKS/FAS (FumaTech GmbH, Germany)	10x10	30-40	5	Woven (100)	0.025 M K$_3$Fe(CN)$_6$, 0.025 M K$_4$Fe(CN)$_6$ and 0.25 M NaCl	Ti-RuO$_2$/IrO$_2$	~0.56	2.2	[72]
FKS/FAS (FumaTech GmbH, Germany)	10x10	30-40	5	Woven (200)	0.025 M K$_3$Fe(CN)$_6$, 0.025 M K$_4$Fe(CN)$_6$ and 0.25 M NaCl	Ti-RuO$_2$/IrO$_2$	~0.56	1.2	[72]
FKS/FAS (FumaTech GmbH, Germany)	10x10	30-40	5	Woven (485)	0.025 M K$_3$Fe(CN)$_6$, 0.025 M K$_4$Fe(CN)$_6$ and 0.25 M NaCl	Ti-RuO$_2$/IrO$_2$	~0.56	0.5	[72]

Table 3. (*Continued*)

Membrane	A	δ	N	Spacer	Feed	Electrodes	v	$P_{d,max}$	Ref
Neosepta CMX/AMX (Tokuyama Co., Japan)	10x10	134-164	2-30	Woven (200)	0.25 M NaCl	Capacitive electrodes (Ti-Pt with activated carbon)	~1.7	~0.95	[78]
Ralex CMH- PES/AMH-PES (MEGA, Czech Republic)	5x5	580±25	5	Normal spacer (143)	0.05 M $K_3Fe(CN)_6$, 0.05 M $K_4Fe(CN)_6$ and 0.25 M NaCl	Ti-Pt mesh	~18	~0.62	[243]
	5x5	580±25	5	2 layer, twisted spacers (64)	0.05 M $K_3Fe(CN)_6$, 0.05 M $K_4Fe(CN)_6$ and 0.25 M NaCl	Ti-Pt mesh	~16	~0.65	[243]
Ralex CMH/AMH, (MEGA AS, Czech Republic)	10x10	<725	5	Woven (200)	0.05 M $K_3Fe(CN)_6$, 0.05 M $K_4Fe(CN)_6$ and 0.25 M NaCl	Ti-Ru/Ir mesh	1.3	~0.26* (10 % $MgSO_4$ in NaCl)	[41]
Neosepta AMX/CMX (Tokuyama Inc., Japan)	10x10	155	5	Woven (200)	0.05 M $K_3Fe(CN)_6$, 0.05 M $K_4Fe(CN)_6$ and 0.25 M NaCl	Ti-Ru/Ir mesh	1.3	~0.42*	[41]
Fuji T1 CEM/ Fuji T1 AEM (Fujifilm Europe B.V., The Netherlands)	6.5x6.5	115	10	Woven (200)	0.1 M $K_4Fe(CN)_6$ / 0.1 M $K_3Fe(CN)_6$ with 0.25 M NaCl	Ti/Ru-Ir mesh	0.92	~0.7*	[172]
Neosepta CMX (Tokuyama Co., Japan)/ Fuji T1 AEM (Fujifilm Europe B.V., The Netherlands)	10x10	115	5	Woven (485)	0.05 M $K_4Fe(CN)_6$ / 0.05 M $K_3Fe(CN)_6$ with 0.25 M NaCl	Ti/Ru-Ir mesh	1	~0.2*	[169]

A: Active membrane area; N: Number of cell pairs; δ: thickness; $P_{d,max}$: Maximum power density; v: flow velocity; Feed conditions: Feed solutions of seawater (~0.5 M NaCl)/river water (~0.017 M NaCl);*Power densities reported for mixtures of solutions (10 % $MgCl_2$ in M NaCl: total salt concentration of 0.5 M/0.017 M

Overall, in a power generating RED stack, the concentration polarization causes a decreased salinity gradient over the membrane resulting in a lower membrane voltage. However, this voltage drop can be interpreted as an electrical resistance and depends on the geometry of the membrane surface and the flow velocity [72, 121-123]. High feed flow improves the hydrodynamic mixing and reduces both the concentration polarization phenomenon and the diffusion boundary layer resistance at the membrane interface due to the effect of the tangential stress on the boundary layer thickness [94, 122]. This consequently results in a higher potential difference across the IEMs inside the stack and, hence, in a high P_d [35, 76]. For RED operated with seawater and Membrane Distillation (MD) brine, Tufa *et al*. [35] reported an up to 35% increase in OCV (from 1.7 to 2.3 V) and up to 47% increase in P_d (0.75 to 1.1 W/m^2) when increasing the feed flow velocity from 0.7 to 1.1 cm/s. In fact, the net power density initially increases with flow velocity and drops down after a certain point due to large hydrodynamic losses (Figure 11), which also depends on the compartment thickness [72].
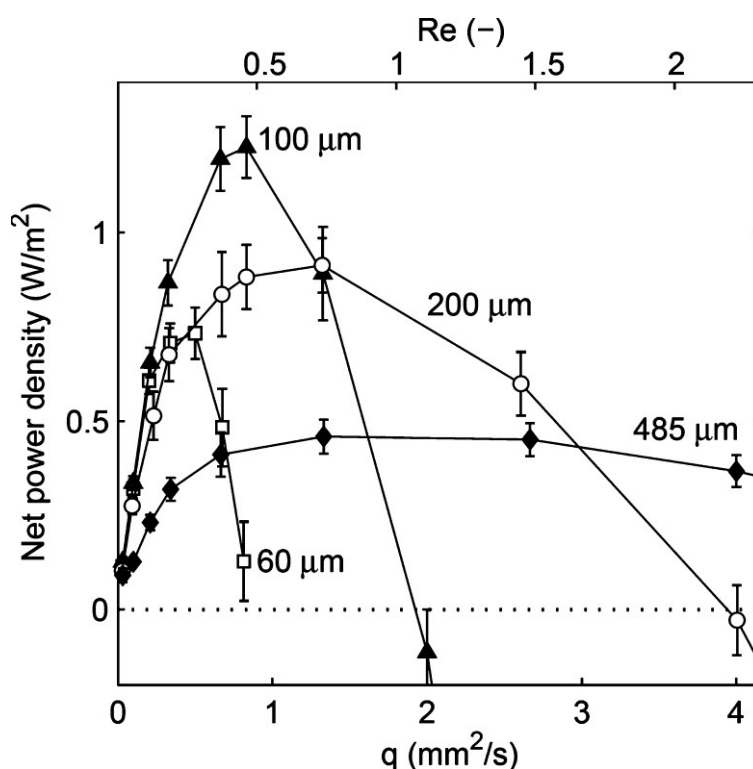

Fig. 11 Experimentally obtained net power density as a function of the flow rate per cell per unit width and intermembrane distance (60-485 µm). Reproduced with permission [72]. Copyright 2016 American Chemical Society.

Długołęcki *et al.* [122] observed that the total resistance, measured at low NaCl concentration (0.017M) under direct current conditions, strongly decreased by increasing the flow rate (investigated interval: 0.1-0.8 L/min). Additional investigations made by EIS revealed that the decrease in the overall resistance was due to the reduction of the diffusion boundary layer resistance (typically having a thickness of a few hundred micrometers) at a higher solution flow rate.

Fontananova *et al.* [123] observed a 60% reduction in electrical double layer resistance predominantly for CEMs when increasing the linear flow velocity from 1.5 to 4 cm/s in 0.5 M NaCl test solution (Figure 12A). Although diffusion boundary layer resistance usually dominates over the electrical double layer resistance, this particular observation in the case of CEMs was probably due to a higher thickness of the EDL, partly due to the large hydrodynamic radius of the counter-ion, and thus influence by flow velocity. The influence of the solution velocity is expected to be spread on the diffuse layer (DL) of the EDL, constituted by more loosely bond ions than the inner layer of the EDL, called Stern layer (SL) [123].
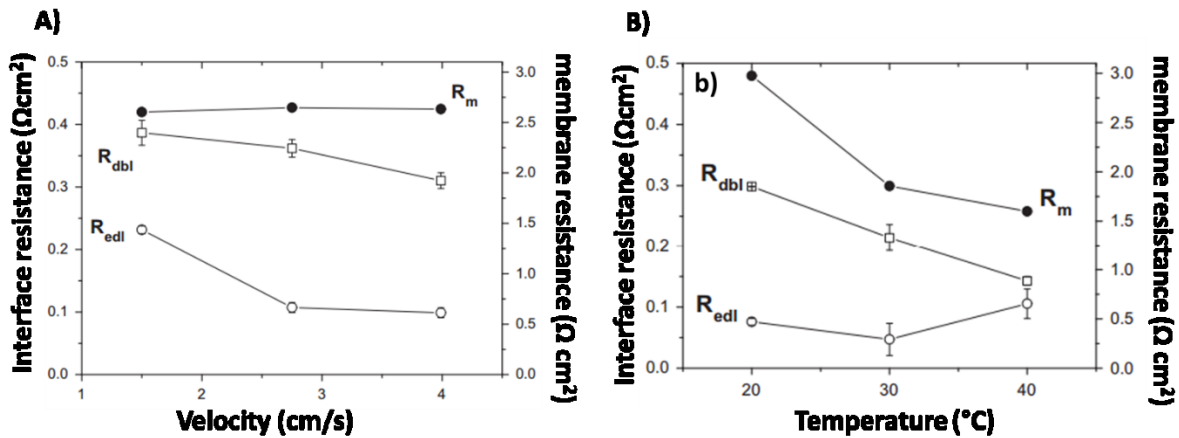
Fig. 12 The trend of membrane area resistance (R_m), diffusion boundary layer resistance (R_{dbl}) and electrical double layer resistance (R_{edl}) with flow velocity (A) and temperature (B) for a Fuji CEM in 0.5 M NaCl solution. Reproduced with permission [123]. Copyright 2014 Elsevier.

Overall, the changes in membrane and interface resistances i.e. the electrical double layer resistance and diffusion boundary layer resistances (non-Ohmic), along with compartment resistances i.e. the resistances of the HCC solutions and LCC solutions (Ohmic), directly influence the internal stack resistance (see Eq. 10). A

decrease of 0.14 Ω cm^2 in internal area resistance per 0.1 cm/s increase in fluid velocity has been observed for a RED unit operated with MD brine (0.5 M NaCl) and seawater (0.5 NaCl) [35].

Although P_d benefits from increasing feed flow velocity, higher flow rates require extra energy to feed the pumps, thus leading to a decrease in the net power density.

A loss of gross power density in the range of 23 - 39% was reported for RED operated with high-salinity brine solutions at decreasing flow velocity in the range of 0.7-1.1 cm/s [35]. Simultaneously, a significant decrease in the net power density was recorded by Tedesco *et al*. [34, 87] for RED operated at increasing flow velocity, attaining negative values above 1 cm/s. Moreover, high flow rates also lead to a shorter residence time of feed in the stack, which reduces the energy efficiency. A study by Weiner *et al*. [244] shows that an optimal stack design incorporating low feed flow velocity reduces the levelized cost of electricity produced by RED.

4.3.2. Effect of temperature

An increase in feed temperature has a positive impact on the performance of the RED system [34, 35, 239, 245]. A high temperature generally increases the feed conductivity, facilitates ionic mobilities, reduces Ohmic losses and, ultimately, increases the output power. Furthermore, a high temperature reduces the viscosity of the feed waters, resulting in lower hydrodynamic losses; OCV is only moderately affected by temperature [35, 246-249]. RED tests with brine and seawater resulted in a 44% increase in P_d (Figure 13A) and 47% decrease in internal area resistance (from 8.7 Ωcm^2 to 4.6 Ωcm^2) (Figure 13B) when the feed solutions were warmed up from 10 to 50 °C [35].
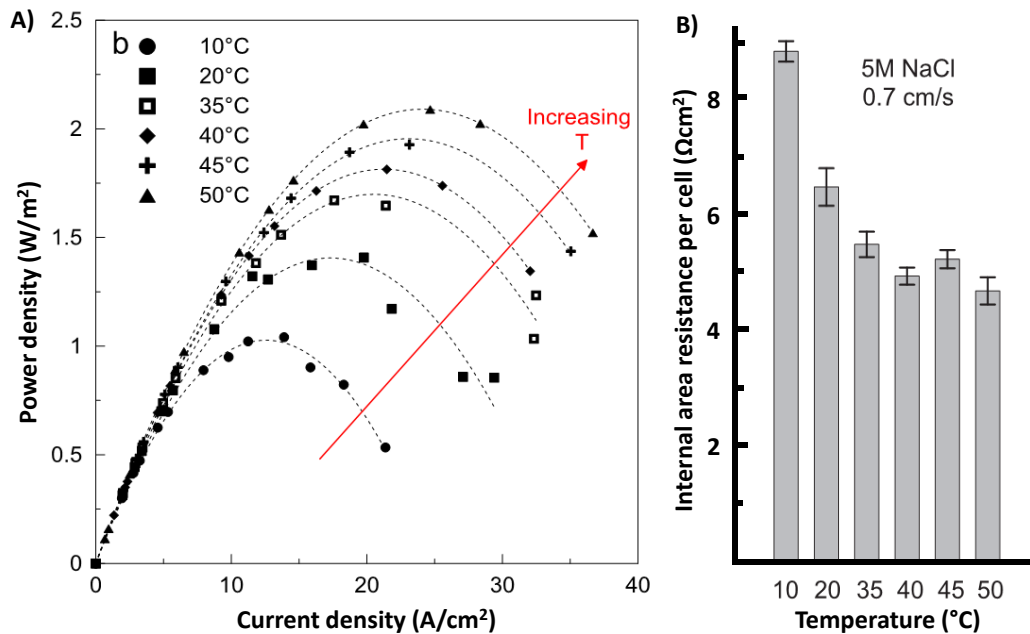
Fig. 13 A) Effect of temperature on RED performance; B) Internal stack resistance under varying operating conditions. LCC solution: 0.5 M NaCl (seawater), HCC solution: 5 M NaCl (MD brine). Reproduced with permission [35]. Copyright 2015 Elsevier.

Tedesco *et al*. [34] observed a power density increase in the range of 40 - 50% (up to 6 W/m^2) along with a 30 - 50% reduction in internal stack resistance when raising the temperature of feed solutions (brackish water and brine) from 20 to 40°C. Daniilidis *et al*. [239] reported that the power density almost doubled (from 3.8 to 6.7 W/m^2) when the feed solutions (river water and brine) were warmed up from 25 °C to 60 °C.

Electrochemical Impedance Spectroscopy studies prove that temperature also influences system resistances: Reduction of both membrane and interface resistances with increasing temperature has been observed by Fontanova *et al*. [123] in 0.5 M NaCl solutions: temperature increases ionic mobility both through the membrane and the interface (Figure 12B).

Although temperature has a positive impact on RED performance, high temperature might also be associated with some drawbacks: high temperature might increase ionic shortcut currents that reduce the permselectivity and energy efficiency of RED [169]. Besides, the extra energy required to warm up the feed solutions is not economically favorable; advantage can be taken from the availability of waste heat sources from industrial sources.
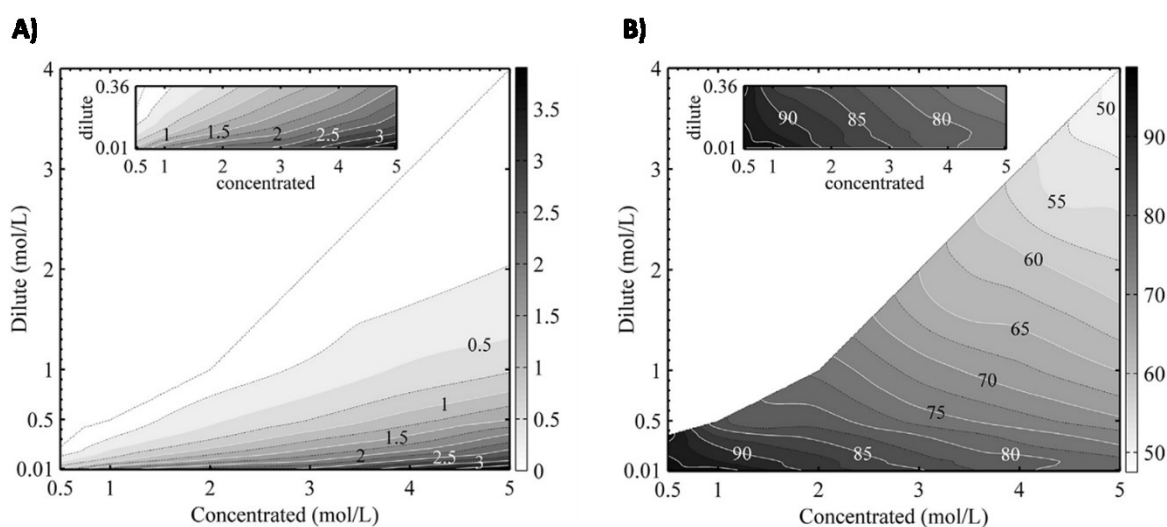
4.3.3. *Effect of feed concentration*

Operations at low feed concentration (*e.g.* river water) is associated with high Ohmic losses that limit the output power. In particular, low concentration of external solutions below 0.3 M NaCl significantly affects membrane conductivity [129, 250]. The conductivity of river water (1 g/L M NaCl, ~2 mS/cm) is about 25 times lower than that of seawater (30 g/L NaCl, ~49 mS/cm) and about 100 times lower than that of highly concentrated brine (200 g/L NaCl, ~226 mS/cm). In principle, low LCC solution concentration leads to high stack resistance and, consequently, low power density. On the other hand, a low LCC solution concentration leads to high Nernst voltage and, consequently, high power density. Therefore, there is an optimal value for the LCC solution concentration, which also depends on other operating and stack conditions such as linear flow velocity, temperature, channels length and thickness. Blending of river water with seawater was found beneficial in terms of power density [89, 251]. Veerman *et al*. [89] reported an optimal LCC solution concentration of 0.005 M in NaCl for a power density of ~ 0.83 W/m^2. For a RED stack operated with a feed velocity of 0.5 cm/s, Weiner *et al*. [251] reported an optimal LCC solution concentration of 0.01 M in NaCl for a power density of 1.72 W/m^2. Alternatively, the use of concentrated saline feed solutions (*e.g.* seawater) is beneficial in terms of reduction of Ohmic losses (Eq. 10), especially at the LCC solution [35, 70-72]. However, this increases the risk of fouling, specifically, scaling due to sparingly soluble salts precipitating on the surface of the membrane.

Investigations by Tufa *et al*. [35] with seawater (0.5 M NaCl) and brine (4-5.4 M NaCl) confirmed the benefits in terms of lower Ohmic losses and higher output power. An increase by 71 % in OCV (from 1.23 to 2.1 V) and by 67 % in power density (from 0.45 to 0.75 W/m^2) was recorded by increasing the brine concentration from 4 M to 5.4 M NaCl. For a RED stack equipped with 50 cells, Tedesco *et al*. [34] observed an increase in OCV from 1 to 3 V by increasing HCC solution concentration from 1 M NaCl to 5 M NaCl, at a fixed LCC concentration of 0.5 M NaCl. This was accompanied by a 4-fold increase in P$_d$ (from 0.4 W/m^2 to 2 W/m^2) whereas R_{stack} reduced by about 26%. Experimental studies of Daniildis *et al*. [239] indicate a remarkable increase in power density, from 1.5 W/m^2 to 3.8 W/m^2 on increasing the HCC solution concentration from 2 M NaCl to 5 M NaCl at LCC solution concentration of 0.01 M NaCl (Figure 14A). Zhu *et al*. [252] studied the performance of a RED unit by varying

HCC concentration from 0.6 M (NaCl) to saturation, and LCC solution concentration from 0 M (deionized water) to 3 M NaCl, and thereby obtaining a maximum power density in the range of 0.2-0.8 W/m^2 proportional to the concentration gradient.

Feed concentration also has a remarkable impact on the performance of IEMs [122-124, 253]. The use of highly concentrated solutions reduces the permselectivity of IEMs due to the fact that the co-ion exclusion (Donnan exclusion) is less effective. Daniliidis *et al.* [239] showed that permselectivity values fall below 90% for a HCC concentration greater than 2 M NaCl; low permselectivity down to 65% was recorded for LCC:0.5 M NaCl//HCC: 5 M NaCl [87] (Figure 14B).


Fig. 14 Contour plot for A) power density; B) permselectivity for the range of feed concentrations tested experimentally. Reproduced with permission [239]. Copyright 2014 Elsevier.

Fontananova *et al.* [123] investigated the behavior of membrane and interface resistances at a high salt concentration (up to 4 M NaCl) for different IEMs supplied by Fujifilm Europe B.V. (The Netherlands). EIS measurements showed a decrease in membrane resistance for an AEM-80045 anion exchange membrane, from 1.55 Ωcm^2 to 1.44 Ωcm^2, at increasing concentration; the opposite trend (from 2.97 Ωcm^2 to 3.50 Ωcm^2) was recorded for a CEM-80050 cation exchange membrane. The different behavior was mainly attributed to the difference in electrochemical membrane properties, such as the density of fixed charge groups and ion exchange capacity, as well as in morphological properties like membrane thickness [122, 123, 163, 254].

4.3.4. Effect of Feed Composition

Solution composition has a huge impact on RED performance and needs to be considered critically for practical implementation under natural conditions [71, 124, 241, 252]. A relatively low number of literature studies address the effect of multivalent ions (prevalently Mg^{2+} and SO_4^{2-}, the most abundant ions in natural waters after Na^+ and Cl^-) [41, 46, 71, 203, 241].

The transport of ions across an IEM is governed by several factors, including electric potential gradient (migration), chemical/concentration potential gradient (diffusion) and pressure gradient (convection). The direction and velocity of ions are not an obvious matter: the concentration gradient is just one of the possible variables, and ions could be transported even against their own concentration gradient (uphill transport) from the dilute to the concentrated compartments until valence-interdependent redistribution of counter-ions and Donnan equilibrium are achieved. Such uphill transport has been detected in RED for the case of divalent ions initially present in the dilute stream [41, 203, 255]. Vermaas et al. [41] investigated the influence of Mg^{2+} and SO_4^{2-} in RED stacks equipped with different membrane types. It was observed that an increase in $MgSO_4$ led to an increase in Ohmic resistance. For a combination of seawater and river water (both containing 10% of Mg^{2+} and SO_4^{2-} ions), a 29-50% reduction in power density was recorded with respect to pure NaCl solutions (Figure 15A). A similar trend (in the range of 15 - 43%) was reported by Hong et al. [46] for RED operated with artificial multi-ion solutions mimicking natural seawater and river water. Transport of divalent ions from the LCC solution to HCC solution reduce the net internal charge transport, thus leading to a lower number of electrons transported from anode to cathode and, ultimately, to lower current and generated power.
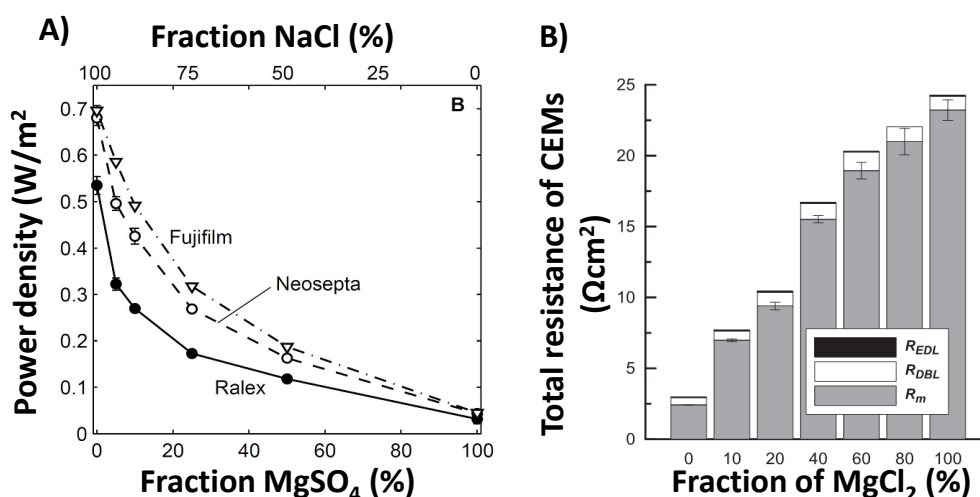
Fig. 15 A) Variation of power density with molar fraction of MgSO$_4$ in NaCl feed solution for a RED unit equipped with different membranes (Ralex, Neosepta or Fujifilm). Reproduced with permission [41]. Copyright 2014 Royal Society of Chemistry; B) Trend of membrane resistance (R_m), diffusion boundary layer resistance (R_{DBL}), and electric double layer resistance (R_{EDL}) with MgCl$_2$ content (4 m NaCl/0.5 m NaCl) for Fuji-CEM-80050 CEM. Reproduced with permission [241]. Copyright 2016 Elsevier.

Post *et al*. investigated the impact of solution composition on the power generation by RED [203]. LCC solution with a concentration of 3 mmol/L and HCC solution with a concentration of 0.45 mol/L NaCl was considered for the study. Initially, 0.05 mol/L of MgSO$_4$ was added to the HCC stream, and during the experiment, 0.2-0.4 mmol/L of MgSO$_4$ was added to the LCC stream. A decrease of OCV from 0.78 V to 0.74 V was observed when increasing the concentration of MgSO$_4$ from 2 mmoL/L to 4 mmol/L in the LCC solution.

The negative impact of multivalent ions is exacerbated when using a real brine. Tufa *et al*. [71] measured OCV and P_d of 2.77 V and 0.57 W/m^2, respectively, when operating RED with seawater (0.014 M in Mg^{2+}) and brine from solar pond (1.6 M in Mg^{2+}). In contrast, reported values of OCV and P_d were 3.4 V and 1.52 W/m^2, respectively, when using pure equimolar NaCl solutions under the same operative conditions.

Tedesco *et al*. [34] observed a 40 % reduction in P_d (from 1.35 W/m^2 to 0.8 W/m^2) on switching the feed solutions from artificial brackish water/brine (pure NaCl)

to real natural solutions. In a systematic study on the effect of Mg^{2+}, Avci $et\ al.$ [241] observed a ~94% decrease in power density (from 0.53 to 0.03 W/m^2) for HCC:4 M $MgCl_2$//LCC: 0.5 M $MgCl_2$ solution (m: molality) with respect to equimolal NaCl solutions.

A reduction of OCV in the presence of multivalent ions is predicted by the Nernst equation (Eq. 7). Additionally, uphill transport has aslo been mentioned as a cause of the negative impact of a multivalent ion on RED performance [41, 203].

When Mg^{2+} is transported from the dilute solution to the concentrated solution, for each amount of transported Mg^{2+} ions, double the amount of Na^+ is transported to the opposite direction in order to obey electro-neutrality on both sides of the membrane. The uphill transport of Mg^{2+} sacrifices the salinity difference of Na^+ without any net charge transport. Therefore, the presence of multivalent ions causes an irreversible loss of the available energy from monovalent ions, and hence a performance loss of RED operation [41, 203, 241].

The performance of IEMs is also negatively affected by multivalent ions [138, 241]: a reduction of CEM resistance was observed with increasing concentration of Mg^{2+} (Figure 15B). For Mg^{2+} ions, stronger electrostatic interactions with fixed charge groups were proven to restrict transport across membranes [138, 241], leading to ineffective Donnan exclusion of co-ions. SO_4^{2-} ions, having a large hydration radius, exhibit restricted transport across IEMs [41, 208].

In general, the development of IEMs with enhanced permselectivity to monovalent ions is required to limit the negative impact of multivalent ions due to uphill transport. For example, the use of monovalent selective CMS (Neosepta) indicated a nearly constant OCV and hence a reduced effect of uphill transport upon RED tests with natural seawater and river water [256]. Monovalent selective membranes can also be tailored, for example, by a layer-by-layer technique by increasing the number of deposited layers [224], but this leads to an increase in electric resistance of the membranes. As to an increase in membrane resistance due to the presence of multivalent ions, the use of membranes specifically designed for fast transport of these ions could be a strategic solution [256, 257]. In this regard, some works have recently been conducted focusing on membrane design and transport of divalent ions along with the performance tests in RED. CEMs designed to block the transport of multivalent ions (like Neosepta CMS) and Fuji T1 membranes which are specifically designed for fast

transport of multivalent ions (Fuji manufacturing Europe BV) were considered for this purpose [169, 172]. It was found out that the monovalent-selective CMS maintain an almost constant potential in pure NaCl (0.5/0.017 M) solutions and a mixture of MgCl₂ (10 %) and NaCl (90%) solution (total concentration: 0.017 M or 0.5 M), whereas the standard grade and multivalent ion-permeable Fuji CEMs (Fuji T1) indicated a reduction of OCV when exposed to divalent-ion containing feed solutions [172]. Owing to its fast transport of Mg^{2+}, the Fuji T1 membranes exhibits low resistance in a mixture of solutions (Figure 16a). A slightly higher power density was reported for Fuji T1 membranes compared to other membranes, mainly due to its low resistance (Figure 16b) [169]. In principle, both strategies (improved monovalent selectivity or increased multivalent ion permeability) would improve membrane performance, so it's tough to conclude one strategy is superior to the other. Further in-depth study is required to clarify the possibility to fabricating new membranes exhibiting both high selectivity and low resistance, together with transport analysis and performance tests in the presence of multivalent ions, which is a real challenge at this stage.
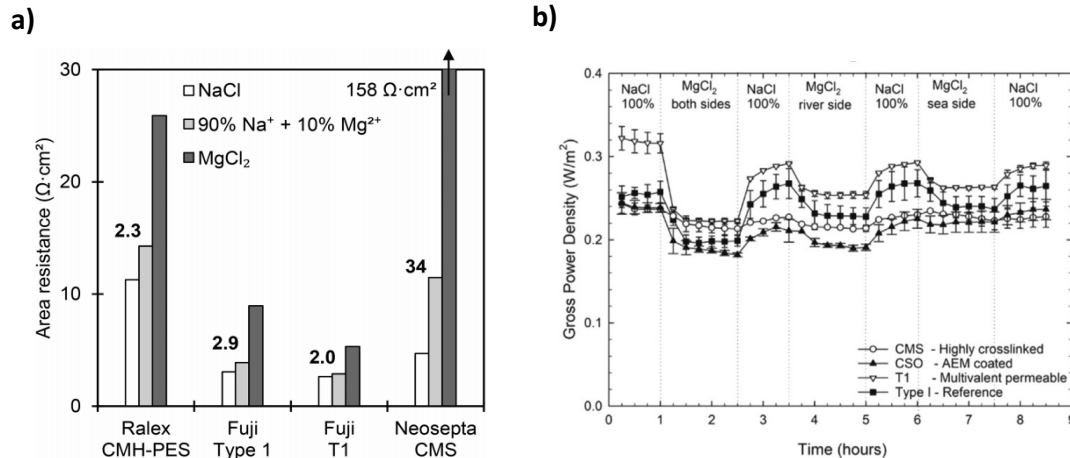
a)   b)

Fig. 16 a) Area resistance of different CEMs in 0.5 M NaCl, pure NaCl solutions and mixture of MgCl₂ (10 %) in NaCl solution (total concentration: 0.017 M or 0.5 M); Reproduced with permission [172]. Copyright 2016 Elsevier. b) Gross power density of different CEMs in MgCl₂ in the feed at both sides (1 - 2.5 h), MgCl₂ in the feed at the river water side (3.5 - 5 h) and (3) MgCl₂ in the feed at the seawater side only (6 - 7.5 h). Reproduced with permission [169]. Copyright 2016 Elsevier.

Pre-treatment of feed solutions by membrane filtration and/or chemical softening could be also envisaged. Separation of monovalent and divalent ions can be partially

achieved, for example, by nanofiltration [258, 259] and ion-exchange [260]. Nevertheless, the introduction of unitary operation for pre-treatment of saline streams introduces additional costs. In general, the design of suitable pre-treatment schemes for RED applications is a topic so far not sufficiently explored and still requiring intensive investigation.

4.4. Stack Design

4.4.1. Fluid Dynamics, Mass Transfer and Pressure Drop

One of the most frequently explored options to enhance power generation in RED has focused on improving hydrodynamic conditions within the RED stack. Fluid dynamics directly affect mass (ions) transfer and energy costs related to pumping. In order to increase mass transfer, concentration polarization (and diffusion boundary layer thickness) in the vicinity of membrane interfaces (Figure 17) must be reduced [126]; this is usually achieved by increasing fluid mixing and promoting convective phenomena. By this means, OCV (Eq. 7) increases because of the higher concentration difference across the membranes. However, increasing flow rate simultaneously leads to a higher pressure drop and higher pumping costs; thus, an optimal trade-off of between the operating parameters is needed to maximize the net power density (Eq. 17).
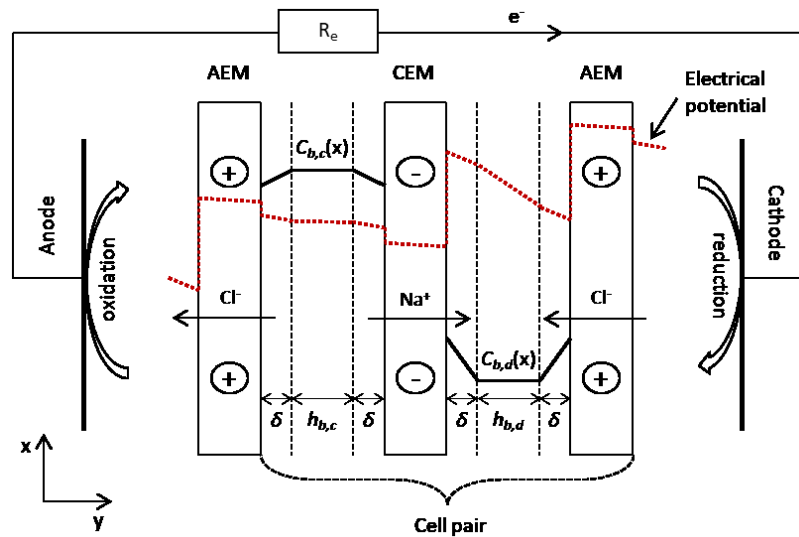
Fig. 17 Schematic representation of concentration and electric potential profiles in the compartments of a RED cell (CEM: cation-exchange membrane; AEM: anion-exchange membrane; R_e: external load resistance). Reproduced with permission [261]. Copyright 2015 Elsevier.

Some parameters, *e.g.* linear flow velocity, can be directly adjusted to obtain the highest net power density in a given stack [76]. Others, *e.g.* channel geometry/thickness and/or type of spacers (acting as mixing promoters), still need to be improved although they have already been extensively studied for other membrane processes (*e.g.* electrodialysis and pressure-driven filtrations) [243, 262, 263].

An intermembrane distance of 100 μm was found to allow an achievement of the highest values of the net power density when NaCl aqueous streams of 1 and 30 g/L were used [72]. Decreasing intermembrane distance leads to a decrease in solution resistance in the stack compartments (Eqs. 9-11), especially in the LCC, while the pressure drop simultaneously increases. At 60 μm, the increase in pressure drop (which depends on power -3 regarding the inter-membrane distance [264]) was observed to be stronger than the benefit of reducing the electric resistance. However, at different concentrations of dilute solution, different optimal intermembrane distances are expected. Furthermore, in the case of mixing natural river and seawaters, thin channels can be clogged by foulants present in real feeds, leading to a drastic increase in pressure drop [32].

The concentration gradient along a channel decreases since the ions are transported from concentrated to dilute saline solutions. Thus, for the same linear flow velocity, power generation is less effective in longer channels due to the lower concentration gradient [75]. Besides, the contribution of flow entrance effects, which enhance mass transfer by decreasing the thickness of the diffusion boundary layer, is more prominent as the channels are shorter [126]. Thus, as the length of the channels increases, the optimal linear flow velocity should also increase, even if the pressure drop increases, in order to grant a reasonably high salt concentration gradient across the membranes and minimize concentration gradients along the channel pathways [261].

The pressure drop in the fluid distribution system also contributes to the total pressure drop [264, 265]. With increasing number of cell pairs, the pressure drop in the manifolds/branches eventually becomes dominant; therefore, the inlet flow rate (or, indirectly, the linear flow velocity in the channel) is a parameter to be optimized [264]. Depending on the stack design, the fluid flow distribution through diverse channels may become highly non-uniform in the case of a large number of cell-pairs [264]. Pawlowski *et al.* [264] suggested that a more uniform fluid distribution can be achieved with a proper/variable sizing of the cross-flow section, increasing the number of beam

inlets/outlets to/from the flow compartment channels or by complete elimination of branch format as in stacks manufactured by REDstack BV (The Netherlands) [266]. Regarding hydrodynamics, breakthrough ideas are mostly appearing in the field of stack and channels design. Since the main resistance is usually located in LCC compartment due to the low conductivity of the dilute solution, the focus has been on modifications to that compartment. Zhang *et al*. [242] proposed inserting ion-exchange resin beds into dilute compartments to increase their conductivity. By this means, the electric resistance decreased, the OCV remained almost unchanged and, although the pressure drop increased, the net power density almost doubled at a relatively low flow rate [242]. The viability of this strategy in large stacks, in which pressure drop and pumping costs are higher, is not yet known. An alternative strategy to decrease electric resistance in the dilute compartment is offered by the breathing cell concept [267]. As shown in Figure 18, this system involves two operational steps. In the first step (Figure 18a), both seawater and river water flow through compartments of equal thickness. During the second step (Figure 18b), the seawater outlet is closed, and the subsequent build-up of pressure in the HCC reduces the thickness of the LCC and, therefore, the electric resistance in the latter compartment. An increase in cost of pumping energy was observed, in comparison to a fixed channel thickness, when breathing cell concept was implemented, nevertheless, since the pumping losses were relatively low (due to a high channel thickness - 480 µm), high values of net power density could have been obtained in a wide range of flow rates. As the pumping losses are relatively low, high values of net power density can be obtained in a wide range of flow rates. As stated by Moreno *et al*. [267], the advantages of applying this concept may be limited by internal leakages caused by membrane movements, and by mechanical stress on the membranes during oscillations.
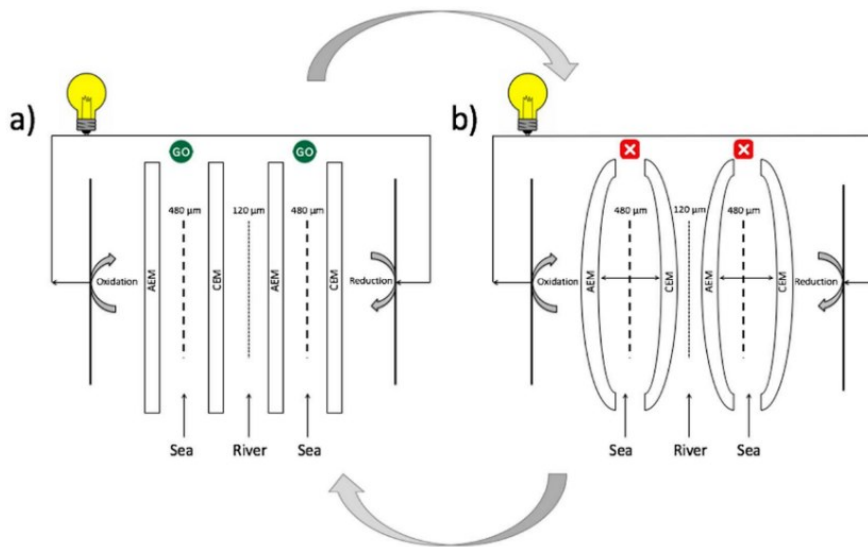
Fig. 18 Schematic presentation of the breathing cell: a) normal mode RED operation and (b) pressure build-up by preventing seawater outflow. Reproduced with permission [267]. Copyright 2016 American Chemical Society.

4.4.2. Spacers

Spacer geometry significantly influences the concentration and flow distribution along the channels and, consequently, RED performance. In a comparative study using different spacer geometries, Tamburini *et al*. [96] found out that a woven spacer provides a better compromise between pressure drop and concentration polarization compared to spacers with overlapping filaments (non-woven). The woven spacer design is believed to promote better mixing in RED [95, 96].

The net spacer material may also influence the channel fluid dynamics by affecting the slip/no-slip conditions [93]. Hydrophobic material reduces friction between the flowing solution and the spacer wires, thus resulting in up to a 40% reduction of the pressure drops compared to the hydrophilic material.

Non-conductive spacers partially cover the membrane surface and create longer paths for ions transport in solutions [79, 126, 243, 266]. This so-called "spacer shadow effect" can be responsible for almost doubling the Ohmic resistance [79, 126]. Although the spacer shadow effect can be reduced by increasing the open area of the spacer [168, 243] or by using a spacer mesh thinner than the surrounding gasket, its complete removal is preferable.

Spacers manufactured with ion- conductive materials can significantly reduce the spacer shadow effect. Długołecki *et al.* [79] prepared ion- conductive spacers (Figure 19) by cutting commercial membrane materials of CMX and AMX (Tokuyama, Japan) using a molding press with the desired geometry. A significant reduction in the internal resistance of RED (about 2-fold compared to the use of non-conductive spacers) was observed by placing the cation/anion conductive part of the spacer over the CEM/AEM; this led to an increase in power density by a factor of 3-4 [79].
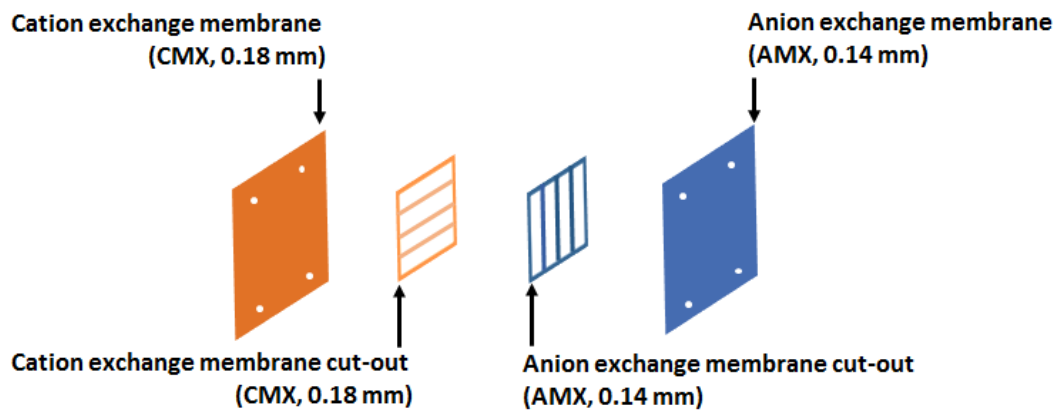
Fig. 19 Ion conductive spacers from an IEM and placement in the stack for performance tests. Reproduced with permission [79]. Copyright 2010 Elsevier.

### *4.4.3. Profiled membranes in RED stacks*

Profiled membranes, also called corrugated, microstructured or patterned-membranes, have the potential to drastically change the architecture of a flow channel. They are a viable alternative to spacers in RED [32, 52, 77, 83, 243, 266, 268]. A profiled membrane has reliefs formed on its surface, which keep two adjacent membranes separated while, at the same time, a channel is formed for fluid flow. Thus, spacers are no longer needed.

The power generated in RED using profiled membranes is higher than the equivalent RED units equipped with non-conductive spacers. A reduction of the Ohmic resistance due to the elimination of the spacer shadow effect is the main cause of the better performance observed. Examples of profiled membranes tested in RED are shown in Figure 20.

First attempts regarding the preparation of profiled membranes focused on reducing pressure drop and pumping energy costs [77, 83, 243]. Vermaas *et al.* [77] used profiled membranes with straight ridges oriented parallel to the fluid flow direction

(Figure 20A and G) and achieved a 10% higher net power density than in a stack with spacers, which was mainly caused by a 4 times lower pressure drop and elimination of the spacer shadow effect (thus 30% lower Ohmic resistance). Additionally, the channels formed by such profiled membranes proved to be less susceptible to fouling in comparison to channels with spacers [32]. Güler *et al*. [83] proposed utilization of profiled membranes with pillar structures (Figure 20C), which allowed for an even lower pressure drop and a 20% higher net power density in comparison to the stack with spacers (Figure 20E). However, the non-Ohmic resistance was significantly higher when using profiled membranes compared to using spacers [77, 83] which could be attributed to less efficient solution mixing and formation of a thicker diffusion boundary layer. The inclusion of sub-corrugations perpendicular to the flow between ridges or modification of the pillar shape (circular [83], diamond-like, teardrop-like or tipped star structures [269]) were found unsuccessful due to the formation of dead zones upstream to the corrugations and preferential channelling [243, 269].

Based on computational fluid dynamics (CFD) simulations, Pawlowski *et al*. [261] suggested the design of a "V"-shaped (so-called chevron) profiles (Figure 20F). To form a channel, two membranes with chevron profiles should align in opposite directions. By this means, a very specific fluid pathway is expected to be created, in which the linear flow velocity upstream to the corrugation is high, the dead zones are very small and multiple streams (vertical, diagonal and horizontal) cross the channel, thus promoting good fluid mixing. Despite a slightly higher pressure drop, utilization of such chevron-profiled membranes in a RED stack increased the net power density by 8-14% in comparison to that obtained in a RED stack with pillar-profiled membranes (Figure 21) [266].
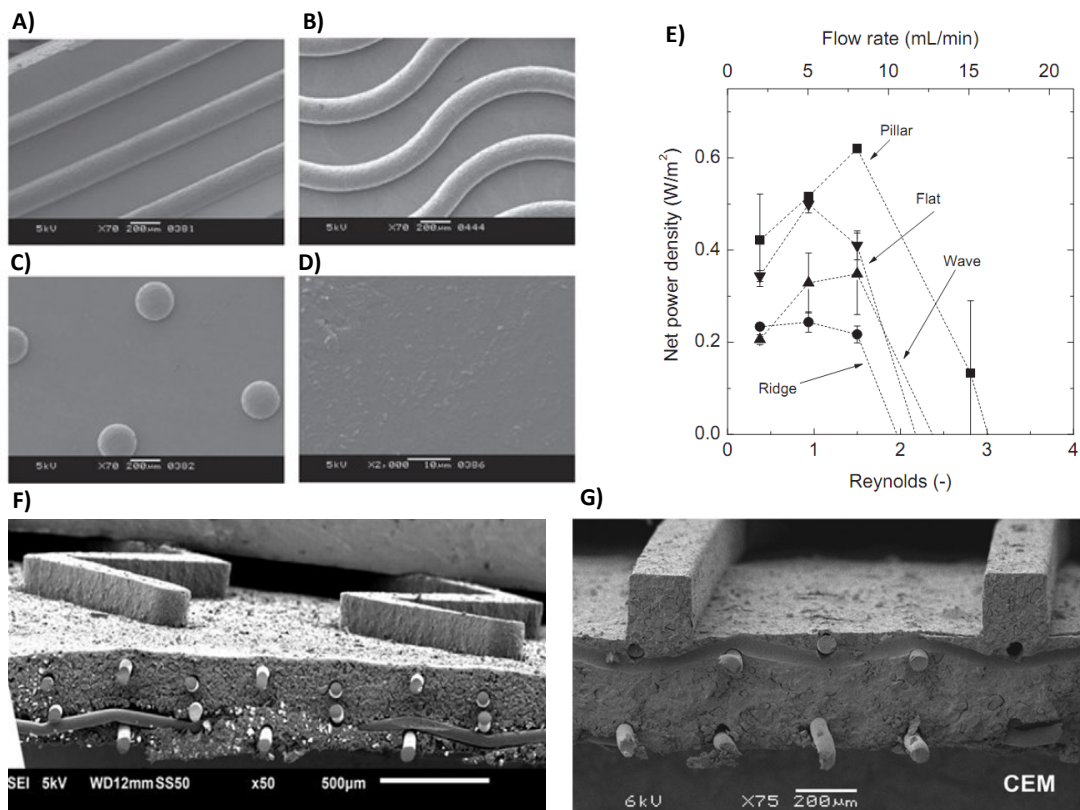
Fig. 20 SEM images of the surface morphology of patterned membranes designed in A) ridges, B) waves, C) pillars, and D) flat membranes. The membranes were prepared from Polyepichlorohydrin (PECH) and Polyacrylonitrile (PAN); E) Net power density measured in RED stacks using tailor-made AEMs with different profiles geometries (ridges, waves, and pillars): reproduced with permission [83]. Copyright 2014 Elsevier. SEM micrographs of a cross-section of: F) profiled AEM with chevron configuration (Reproduced with permission [266]. Copyright 2011 Elsevier), and G) CEM with ridge configuration (reproduced with permission [77]. Copyright 2011 Elsevier). Pristine AEM and CEM are commercial Ralex CMH and AMH (Mega a.s., Czech Republic), respectively.
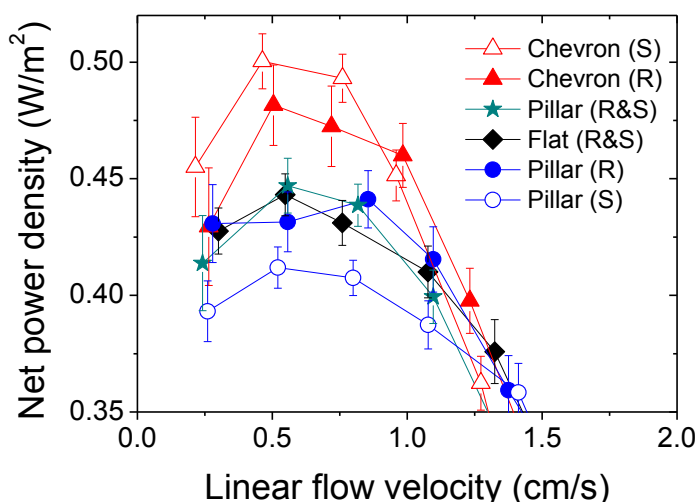
Fig. 21 Net power density as a function of linear flow velocity with flat, chevron- and pillar-profiled membranes in both river and sea (R&S), or only in river (R), or only in sea (S) compartments. Reproduced with permission [266]. Copyright 2017 Elsevier.

Due to absolute values of pressure drop, the stacks with chevron profiled membranes are expected to generate the highest net power below a certain linear flow velocity and channel length in comparison to pillar profiled membranes. For example, at an intermembrane distance of 0.5 mm, such linear flow velocity and channel lengths are approximately 1.5 cm/s and 80 cm, respectively [261]. For longer channels, a higher linear flow velocity is required in order to sustain the salinity gradient along the whole stack, thus pillar membranes become preferable as they cause a lower pressure drop. In general, profiles which promote an enhancement of fluid mixing are more suitable for shorter channels; on the other hand, profiles which minimize pressure drop are more suitable for longer channels. Based on CFD simulations, Pawlowski and Rijnaarts *et al*. [266] suggested a simplification of the chevron corrugation design in order to facilitate the assembly of larger stacks**.**

Profiled membranes can be manufactured by thermal pressing [77, 243, 266], membrane casting [52, 83, 269] or photo-polymerization [270]. Only thermoplastic materials can be thermally pressed; this limits utilization of this technique to heterogeneous IEMs with relatively high intrinsic electric resistance. Thermal pressing can also introduce some structural changes in membrane chemistry [77], and the consequent risk of membrane swelling must be well anticipated and controlled [266]. Utilization of the membrane casting technique, suitable for preparation of homogeneously dense ion-exchange polymeric membranes [83], avoids the previously

mentioned problems. This technique consists of casting the ion-exchange polymeric solution into a mold with the desired structure, followed by phase separation induced by solvent evaporation [52, 83]. The release of the profiled membrane from the mold is a problem in both methods. Stainless steel molds can be covered with an anti-adhesive coating to facilitate membrane release [77, 83, 266]. Photo-polymerization is relatively new process applied to the preparation of profiled membranes, similar to 3D printing technique [270]. Selected studies on tailor-made/modified and profiled membranes tested in RED are summarized in Table 4.

4.4.4. Flow modes

Adoption of different flow directions can potentially increase RED performance [87, 93, 271, 272]. As shown in Figure 22, the RED system has three basic configurations: counter-flow, co-flow and cross-flow. In most processes, the counter-flow operation is substantially more efficient since it promotes more uniform driving force along the device. Depending on flow rates, co-flow operations might be advantageous in some cases: Veerman *et al*. reported slightly higher power density of about 0.05 W/m^2 by co-flow operation compared to counter-flow operation in RED [240]. This effect is probably caused by less leakage between LCC and HCC due to the low local pressure differences between both compartments during co-flow operation.

Table 4. Power density values for different tailor-made and profiled membranes.

Membranes				Spacers	Electrode compartment		v	$P_{d, max}$	
Type	A(cm^2)	δ (μm)	N	(δ, μm)	Electrolytes	Electrodes	(cm/s)	(W/m^2)	Ref
Tailored SPEEK65 CEMs, Tailored PECH B2 AEMs	10x10	53-77	5	Woven (100)	0.05 M K$_3$Fe(CN)$_6$, 0.05 M K$_4$Fe(CN)$_6$ and 0.25 M NaCl	Ti/Ir-Ru	1.75	1.28	[132]
AEM (Selemeim® ASV),Tailored nanocomposite CEM (0.7 wt% blend ratio of Fe$_2$O$_3$, SO$_4^{2-}$)	4x9	30-120	3	Woven (250)	0.05 M K$_3$Fe(CN)$_6$, 0.05 M K$_4$Fe(CN)$_6$ and 0.25 M NaCl	Ti-Ir plasma	0.45	1.4	[85]
Tailored SPPO AEMs, Neosepta CMX (Astom Corp., Tokyo, Japan)	2x10	55-160	1	Non-conductive (80)	0.050 M FeSO$_3$ and 0.05 mM Fe$_2$(SO$_3$)$_3$, 1.2 M NaCl	Carbon cloth	10.4	~1.34	[200]
Neosepta AMX (Tokuyama Co., Japan), Tailored PAES CEMs	7x7	58-153	5	-	0.05 M K$_3$Fe(CN)$_6$, 0.05 M K$_4$Fe(CN)$_6$ and 0.25 M NaCl	Ti/Pt	17.1	1.05-1.2	[166]
Profiled (ridges) - Ralex AMH-PES /CMH- PES (MEGA, Czech Republic)	5x5	475-510	6	No spacer	0.05 M K$_3$Fe(CN)$_6$, 0.05 M K$_4$Fe(CN)$_6$ and 0.25 M NaCl	Ti/Pt	19	~0.82	[77]
Profiled (pillar) PECH AEM (Tokuyama Co., Japan), Neosepta CMX (Tokuyama Co., Japan)	10x10	200	3	Woven (100)	0.05 M K$_3$Fe(CN)$_6$, 0.05 M K$_4$Fe(CN)$_6$ and 0.25 M NaCl	Ti/Ir-Ru	6.7	1.3	[83]
Profiled (ridge) PECH AEM (Tokuyama Co., Japan), Neosepta CMX (Tokuyama Co., Japan)	10x10	200	3	Woven (100)	0.05 M K$_3$Fe(CN)$_6$, 0.05 M K$_4$Fe(CN)$_6$ and 0.25 M NaCl	Ti/Ir-Ru	6.7	~1.13	[83]
Profiled (Chevron) - Ralex AMH-PES/CMH- PES (MEGA, Czech Republic)	9.5x9.5	440-520	5	Woven (260)	0.1 M K$_3$Fe(CN)$_6$, 0.1 M K$_4$Fe(CN)$_6$ and 0.25 M NaCl	Ti/Pt	1.75	~0.68	[266]

A: Active area; N: Number of cell pairs; δ: thickness; $P_{d,max}$: Maximum power density; v: flow velocity; Feed solutions: seawater (~0.5 M NaCl, ~0.017 M NaCl).
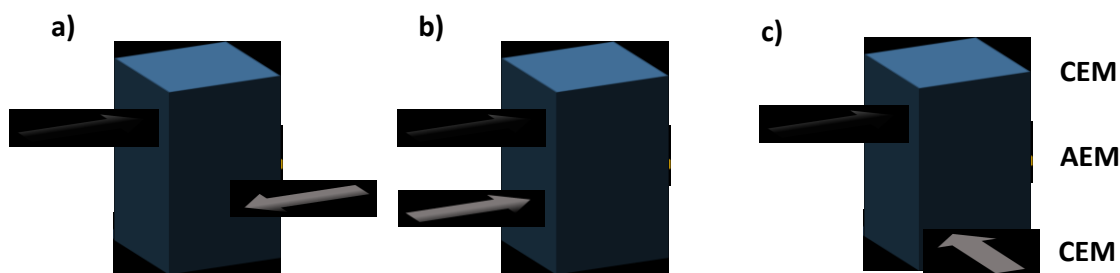
Fig. 22 RED flow configurations: a) counter- flow b) co-flow and c) cross-flow.

In the co-flow mode, the Nernst potential is at its maximum near the inlet and at a minimum near the outlet; however, the conductivity of the low concentration solution follows an opposing trend. This results in variable power density along the flow channel. Veerman *et al*. [89] investigated the behavior of a RED stack operated with co-flow and counter-flow mode using a modeling approach. As shown in Figure 23, a comparison of the two flow modes indicates that the local variation in power density along the flow channel is higher for the co-flow mode (from ~0.9 to ~0.1 W/m^2) compared to the counter-flow mode (from ~0.6 to ~0.3 W/m^2). However, this model adopted a fairly long residence time (60 s) of the fluid. With shorter residence time, the difference between co-flow and counter-flow is marginal. In the case of counter-flow, there is a possibility of internal deformation in the stack due to the pressure differences over the LCC and HCC compartments which might could result in an increase of hydrodynamic losses [240]. The co-flow configuration mitigates the risk of leakage in the manifolds and allows the use of thin, low resistance membrane materials [240]. On the other hand, the counter-flow mode was proven to increase energy efficiency.

Other designs of RED involve segmented electrodes, i.e. electrode used in layered stack units [70, 240]. Theoretically, the use of segmented electrodes improves the energy efficiency of RED. In fact, this concept is not well covered in the RED research so far. However, some promising outcomes have been verified using experiments and modeling. Veerman *et al.* [240] adopted a triple segmentation of electrodes in RED, reporting up to 11% higher power output compared to a single electrode. Vermaas *et al.* [70] compared the energy extraction effi ciency when using the three flow modes both with single and multiple electrodes pairs (segmentation). It was observed that energy efficiency in counter-flow mode is higher than that in cross-flow, whereas the co-flow mode was found to be less efficient (2-fold lower). It was estimated

that up to 95 % of the theoretically available energy can be extracted in counter-flow mode (saltwater fraction of 0.13) using a single electrode segment. The counter-flow mode allows non-zero local electromotive force along the flow channels as the outflow positions are aligned oppositely, thus enabling efficient utilization of the salinity difference.
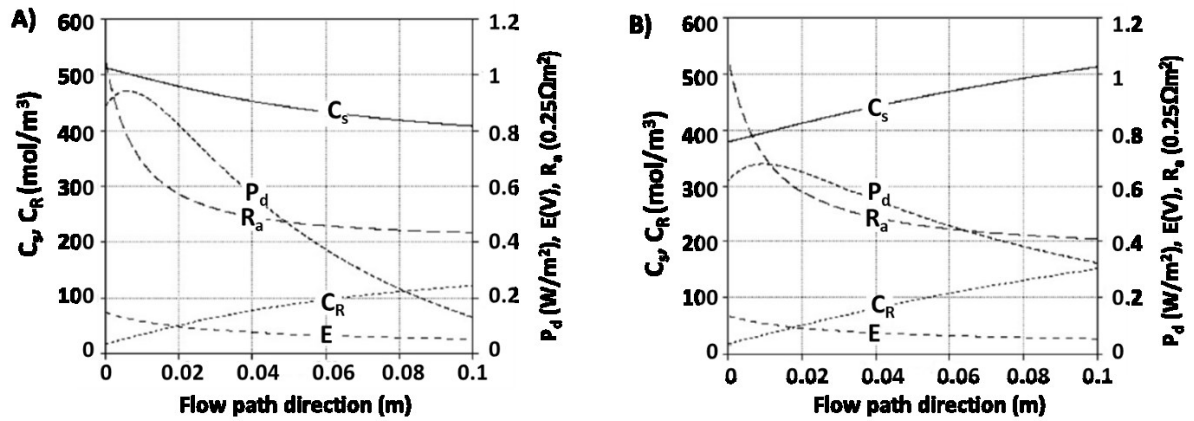
Fig. 23 Model predictions for a RED stack operated under: A) co-current feed and B) counter-current feed. Fumasep membranes, 10 cm × 10 cm, undivided electrodes, spacer thickness of 200 μm; residence time of 60s. In each diagram, the following local values are shown: concentration of seawater (C_S), river water (C_R), power density (P_d), open circuit voltage (E), area resistance (R_a). Reproduced with permission [89]. Copyright 2011 Elsevier.

A novel RED design based on radial-axial feed flow has also been suggested [273]. As shown in Figure 24, the radial flow allows a relatively small inflow manifold for LCC solution (river water), and the axial flow of the HCC (sea water) in round pipes is subject to low hydraulic friction. It is expected that power density increases at a lower intermembrane distance; however, the high axial length of channels for high

concentration compartment may require a larger intermembrane distance to reduce pumping losses [273].
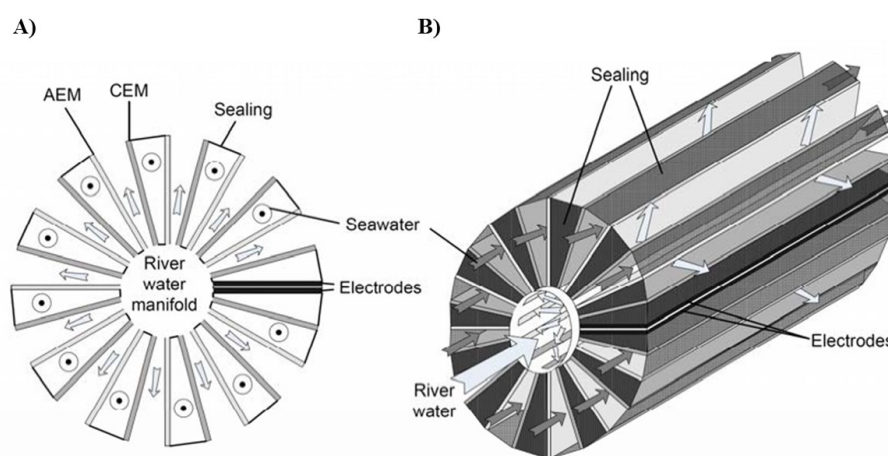
Fig. 24 RED design with radial river water flow and axial seawater flow: A) cross-sectional view and B) three-dimensional view [273].

4.4.5. Electrode systems

Electrode and electrolyte materials play an essential role in energy storage and conversion devices [154, 265, 274-285]. Consequently, systematic investigations on the design and selection of the suitable electrode have been carried out for RED [109, 240, 286]. Electrode systems with opposite electrode reactions and recirculating electrode rinse are not accompanied by a net chemical reaction and have a zero equilibrium voltage. Typical examples of such electrodes include copper gauze electrodes in $CuSO_4$ solution [287], Zn electrodes in $ZnSO_4$ solution [18], Ag/AgCl electrodes in NaCl solution [18]: Some of the electrode system, and the reaction schemes, used so far for RED applications are summarized in Table 5. In such redox systems, one electrode grows while the other dissolves; consequently, feed solutions need to be reversed periodically to invert the direction of the electrical flow, thus limiting the stack design to identical HCCs and LCCs [108]. Flow reversal can be prevented by using a homogeneous redox couple with inert electrodes like platinized titanium and coated titanium mesh. Currently, a Ru-Ir coated Ti mesh electrode with an electrode rinse solution of $K_4Fe(CN)_6$ and $K_3Fe(CN)_6$ in NaCl is extensively used as an electrode system in RED [23, 35, 41, 70, 71, 74, 288]. The redox couple $[Fe(CN)_6]^{3-}\backslash[Fe(CN)_6]^{4-}$ is sufficiently stable at a pH of 7, although there is a has a risk of toxicity under a strongly acidic condition or in the presence of light [109, 240, 286].

Table 5. Electrode systems used for RED.

Electrodes	Electrolyte solution	Electrode reaction	Ref.
Cu metal	$CuSO_4$	$Cu^{2+} + 2e \rightarrow Cu$ $Cu \rightarrow Cu^{2+} + 2e$	[16, 287]
Zn foil	0.015 M $ZnCl_2$	$Zn^{2+} + 2e \rightarrow Zn$ $Zn \rightarrow Zn^{2+} + 2e$	[289]
Ag-AgCl plates	NaCl	$AgCl + e \rightarrow Ag + Cl^-$ $Ag + Cl^- \rightarrow AgCl + e$	[18]
Ti-Pt metal	0.035 M Na_2SO_4	$2H_2O + 2e \rightarrow H_2 + 2OH^-$ $H_2O \rightarrow \frac{1}{2}O_2 + 2H^+ + 2e$	[75]
C plates	~0.5 M NaCl	$2H_2O + 2e \rightarrow H_2 + 2OH^-$ $H_2O \rightarrow \frac{1}{2}O_2 + 2H^+ + 2e$	[290]*
Ti-Ru/ Ir mesh	0.05 M $FeCl_2$, 0.05 M $FeCl_3$ in 0.5 M NaCl	$Fe^{3+} + 3e \rightarrow Fe$ $Fe \rightarrow Fe^{3+} + 3e$	[240]
Ti-Ru/ Ir mesh	0.05-0.3 $K_4Fe(CN)_6$, 0.3 M $K_3Fe(CN)_6$ in 0.25-2.5 M NaCl	$[Fe(CN_6)]^{3-} + e \rightarrow [Fe(CN)_6]^{4-}$ $[Fe(CN)_6]^{4-} \rightarrow [Fe(CN)_6]^{3-} + e$	[23, 29, 30, 35, 39, 41, 71, 82, 240, 241]
Ti-Ru/ Ir mesh	0.26 M NaCl	$2H_2O + 2e \rightarrow H_2 + 2OH^-$ $H_2O \rightarrow \frac{1}{2}O_2 + 2H^+ + 2e$	[74]*
Ti-Pt with C-PVDF layer**	0.25 M NaCl	$2H_2O + 2e \rightarrow H_2 + 2OH^-$ $H_2O \rightarrow \frac{1}{2}O_2 + 2H^+ + 2e$	[78]*

* Possibility of Cl_2 formation at anode ($Cl^- \rightarrow \frac{1}{2}Cl_2 + e$): the generated Cl_2 can be prevented from passing into RED channels by applying external CEMs at the end of the membrane pile. **Capacitive electrode.

4.4.5.1. Capacitive Electrodes in RED

This capacitive reverse electrodialysis (CRED) system synergistically combines capacitive mixing and RED [240, 291]. In the CRED system, AEMs and CEMs are aligned alternatively to create two compartments similar to the RED system. A capacitive electrode consisting of a current collector like Ti/Pt mesh or glassy carbon along with a layer of activated carbon can be used in CRED. Since capacitive electrodes do not require redox reactions, NaCl solution can be used as an electrode rinse solution. Thus, the selective transport of ions driven by the concentration gradient induces a potential difference over each membrane, hence an electrical current in the external circuit. CRED can be operated in cyclic stages where electricity is generated during mixing of the saltwater and freshwater. The system generally allows energy generation under safe operating conditions (no redox reaction or no use of hazardous electrode rinse solutions).

4.5. Fouling

So far, the performance of RED has mostly been studied and optimized using model NaCl solutions. However, the goal of RED for sustainable power generation critically depends on the possibility to exploit the salinity differences between natural

water bodies (such as oceans, seas, rivers, lakes, etc.) or industrial waste streams. In comparison to artificial NaCl solutions, such solutions exhibit a variable and rich composition of different ions, minerals, organic matter and living organisms. Thus, the different fouling phenomena are also expected during operation of RED with natural feed streams.

The binding of organic compounds to membrane charges has similar effects (mainly in terms of reduced permselectivity and increased electric resistance) [32, 33, 292] to the binding of divalent ions as previously described. The majority of organic compounds, such as humic acids, are negatively charged, thus being preferentially deposited/adsorbed on AEMs [293, 294]. Humic acids can be also transported from LCCs to HCCs [295]. In addition, scale formation due to minerals and other particulate matters i.e. scaling fouling could also occur in RED [32].

4.5.1. Fouling studies in RED

Vermaas *et al.* [32] were the first to operate RED units with natural feeds. A stack with flat IEMs and 240 μm thick spacers, a stack with profiled membranes (an intermembrane distance of 240 μm), and a stack with profiled non-conductive plastic sheets (200 μm thick inter-membrane distance) were operated over a period of 25 days. RED devices were fed with fresh water (~2.2 g/L NaCl$_{equivalent}$) from canal (Van Harinxmakanaal) and salt water (~16 g/L NaCl$_{equivalent}$) from the Wadden Sea. Figure 25 illustrates SEM micrographs of fouled membranes in each of the three stacks tested, and respective pressure drops and output power. All samples except the profiled plastic in seawater were covered with solid deposits (Figure 25A-B), mainly composed of diatoms, which are mostly attracted to AEMs because of the negative charge on their silica skeleton [296-298]. On the other hand, scaling was more pronounced on CEMs because of the higher concentration of multivalent ions like calcium and phosphate that precipitated as calcium phosphates. The precipitation of calcium as carbonate and sulphate, causing scaling problems in many membrane operations [296-298], is also possible.

The pressure drop in the stack with spacers increased rapidly (5 days) up to ~1.5 bar during first 5 days, whereas in the stack with profiled membranes the same pressure drop was observed only after 20 days (Figure 25C). The increase in pressure drop was associated with channel clogging by minerals and organic matter. One of the spots where foulants may preferentially accumulate is upstream to the spacer

filaments and knits due to lower fluid mixing and lower linear flow velocity in such spots. Slower channel clogging when ridge profiled membranes were used was attributed to the reduced adhesion of colloids and particulates on smooth and parallel channels compared to woven spacers [268]. The decrease in power density (Figure 25D) was faster than the pressure drop due to additional overlapping effects such as the enhancement of Ohmic losses because of the partial coverage of IEMs by organic and particulate foulants, and the reduced effective surface charge of the membranes and consequent reduction of perm-selectivity.
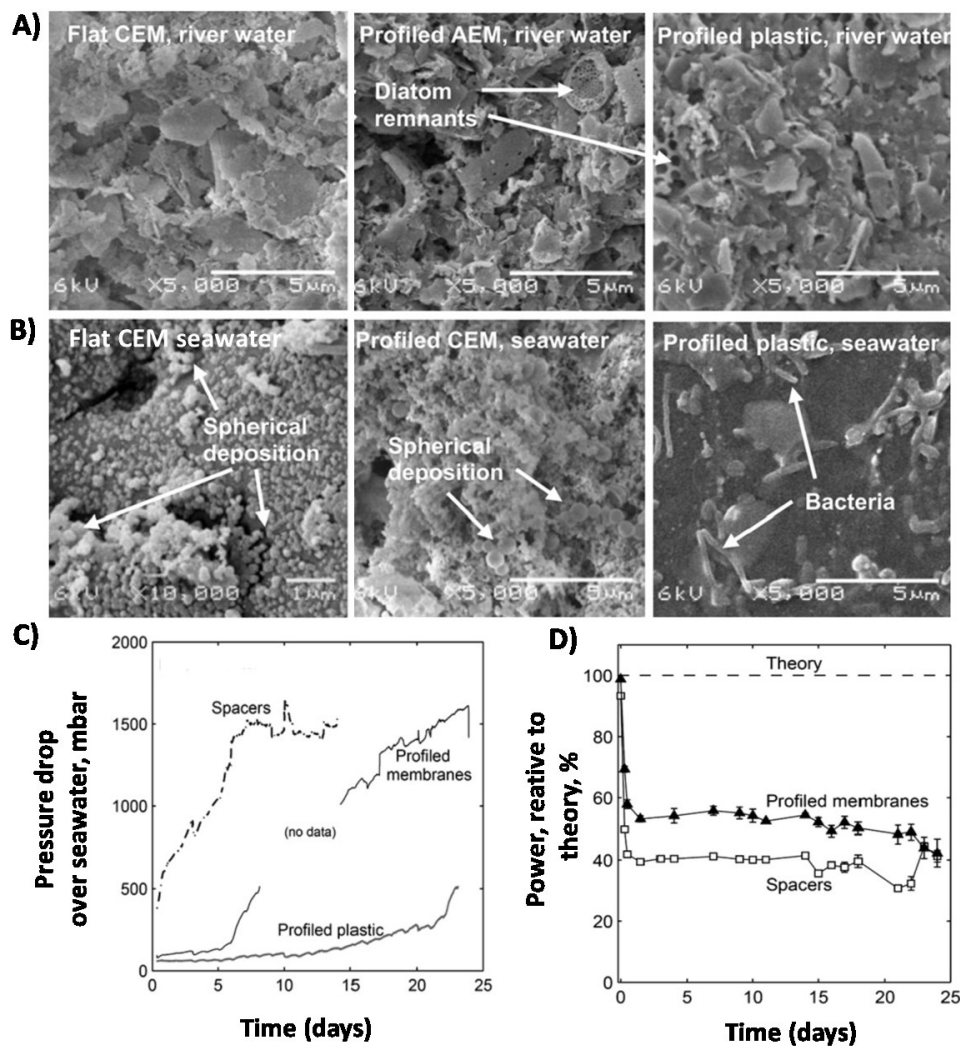

Fig. 25 SEM micrographs of membranes (CEM, AEM) and profiled plastics contacted with: A) river water B) seawater. Arrows indicate the presence of diatoms, bacteria and spherical deposition. Time-dependent profile of: C) pressure drop over the seawater compartments; D) power density. Reproduced with permission [32]. Copyright 2013 Elsevier.

Pawlowski *et al.* [31, 295] used a RED stack with relatively thick spacers (800 μm), fed with natural river water (Lisandro River, ~ 0.4 g/L NaCl$_{equivalent}$) and seawater (Atlantic Ocean, Portuguese coast, ~ 32 g/L NaCl$_{equivalent}$). A net power density in the range of 0.027-0.14 W/m^2 was obtained during one month, depending on daily salinity and flow rates, while the electric resistance increased by 11% [31]. Utilization of thick channels avoided their clogging, and the increase in pressure drop was, on average, 6 times slower than in the work of Vermaas *et al.* [32]. The initial pressure drop value was around 30 times lower since the pressure drop in a channel depends inversely on thickness by a power of 3 [264]. Although increasing thickness of the channels leads to an increase in electric resistance in the compartments (Eqs. 9-11), it was a necessary step when feeding natural saline streams without any pre-treatment. In this study, fouling development, efficiency of membrane cleaning and levels of humic compounds in saline streams and their transport from river to seawater compartments were monitored by 2D fluorescence spectroscopy. 2D fluorescence spectroscopy measurements resulted in excitation-emission matrices (EEMs), where each value of fluorescence emission intensity corresponds to a pair of excitation/emission wavelengths. Multivariate statistical analysis of EEMs of the membranes surfaces showed that the main variations occurred in AEMs exposed to the river water compartment due to the deposition of humic compounds (Figure 26). Thus, it was concluded that the main bottleneck in using natural streams resides in the dilute compartment. It was also observed that, with respect to artificial saline streams, the evolution/degradation of the membranes is much faster when natural feeds are used [295]. The incorporation of an optical fiber bundle probe in a membrane fouling simulator device with an optical window [299] may enable a more precise in-depth study and modeling of fouling based on data captured by 2D fluorescence spectroscopy [31, 295, 300, 301]. Such captured information has already proved to be essential to the development of robust multivariate statistical models for the prediction of pressure drop, electric resistance and net power density in a RED stack [31].

Tedesco *et al.* [30] used natural brackish water (~1.74 g/L NaCl$_{equivalent}$) and saline brine (~232-290 g/L NaCl$_{equivalent}$) from Ettore-Infersa Saltworks (Marsala, Italy), filtered through a 5 μm membrane, as feed to RED unit equipped with 280 μm thick spacers. Additionally, twice a week (during 3 months of stack operation), a shock treatment with NaClO solution was applied on the LCC stream to avoid the formation

of bio-film. This pre-treatment enabled an almost constant pressure drop in the stack and a value of net power density in the range of 0.21-0.62 W/m^2 / 0.03-0.06 kWh/m^3 (depending on variations in temperature, salinity and flow rate) [30]. Although the pre-treatment used avoided the formation of organic fouling, this did not prevent the nefarious effects of divalent ions present in the used saline streams. When model NaCl solutions (with conductivities comparable to those of natural saline streams) were used, the obtained power output was 30-70% higher in comparison to values obtained when natural saline streams were used [30]. The energy required by this specific pre-treatment was not accounted for the determination of net power density, thus this point still needs further investigation. Besides the elimination of organic fouling, two other factors contributed to the highest power generation by Tedesco *et al.* [30] when natural saline streams were used compared to other studies [31, 32, 295]; the ion-exchange membranes used had almost 5 times lower electric resistance and utilization of highly concentrated saline brines allowed for a much higher salinity ratio between concentrated and dilute streams: ~150 [30], ~80 [31, 295] and ~7 [32]. The utilization of highly concentrated brines, however, incurs an additional challenge as the efficiency of power extraction decreases with an increase in concentrated stream salinity since the membrane permselectivity (especially that of the anion-exchange membrane) decreases due to the weakening of the Donnan exclusion of co-ions. So far, utilization of natural saline streams in RED has resulted in lower stack performance in comparison to model NaCl solution [29-32, 268, 295]. Table 6 summarizes fouling studies in RED reported so far.
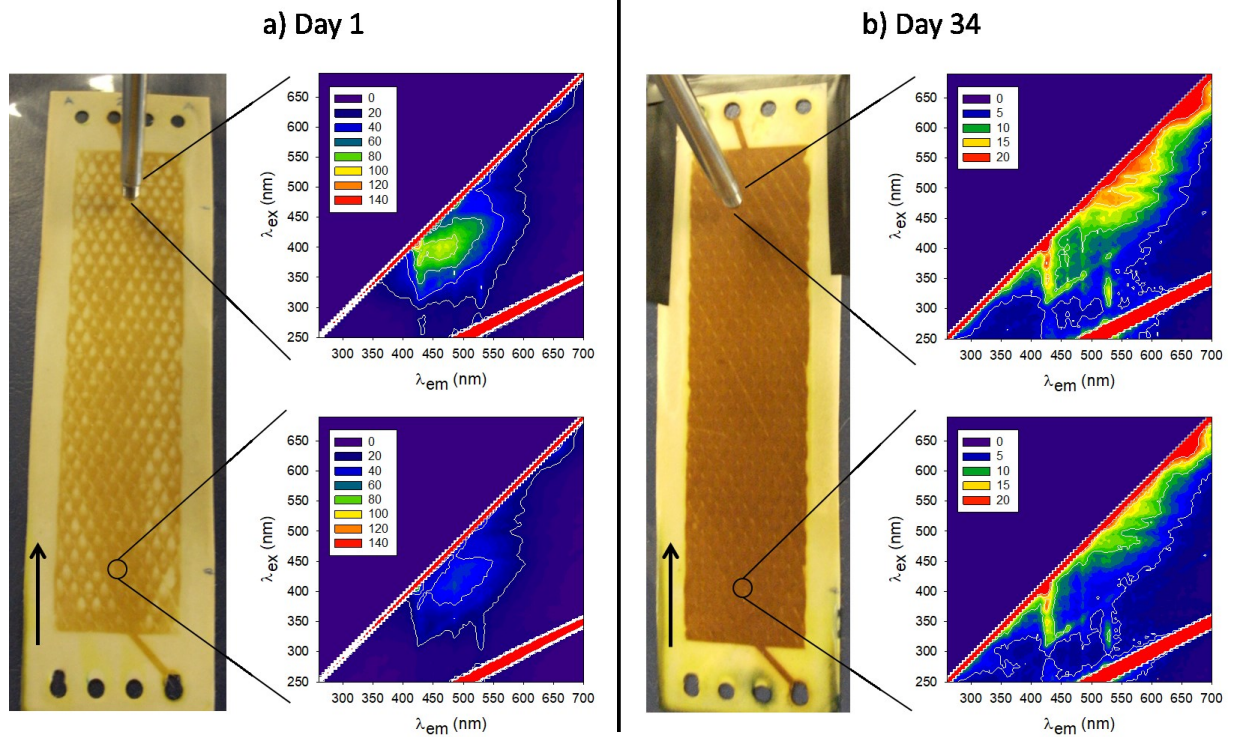
Fig. 26 AEM surface in contact with natural river water after: a) 1 day; b) 34 days of RED stack operation. The brownish color is due to adsorption of humic compounds. The arrow indicates the flow direction. The fluorescence excitation-emission matrices and the regions of their acquisition are shown next to photos. Reproduced with permission [295]. Copyright 2015 Elsevier.

Table 6. RED conditions and power density reported in fouling studies.

Membranes				Spacers	Electrode compartment			v	$P_{d,\,max}$	Ref.
Type	A (cm^2)	δ (μm)	N	(δ, μm)	Electrolyte	Electrode	Feeds solutions	(cm/s)	(W/m^2)	
Ralex CMH/AMH(MEGA AS, Czech Republic)	10x10	700-714	5	Woven (245)	0.05 M K$_3$Fe(CN)$_6$, 0.05 M, K$_4$Fe(CN)$_6$ and 0.25 M NaCl	Ti/Pt mesh	Natural seawater/river water	7.6	0.05-0.08[a]	[32]
Profiled Ralex CMH/AMH (MEGA AS, Czech Republic)	10x10	477±15	5	Spacerless	0.05 M K$_3$Fe(CN)$_6$, 0.05 M, K$_4$Fe(CN)$_6$ and 0.25 M NaCl	Ti/Pt mesh	Natural seawater/river water	7.6	0.11-0.14	[32]
Neosepta CMX/ACS (Tokuyama Co., Japan)	104	140-200	4	Non-conductive (500)	0.25 M NaCl	Ti-Ru/Ir mesh	Artificial seawater (0.5 M NaCl)/artificial river water (0.017 NaCl) dosed with biodegradable compounds and inoculates	~2	-[b]	[86]
Profiled Ralex CMH/AMH, (MEGA AS, Czech Republic)	10x10	477±15	10	Spacerless	0.25 M NaCl	Ti/Pt mesh	Natural seawater/river water	1.7	-[c]	[268]
Neosepta CMX, Modified/ Neosepta AMX (Astom Corp., Tokyo, Japan)	4.5x4.5	120-200	2	Non-conductive (300)	0.05 M K$_3$Fe(CN)$_6$, 0.05 M K$_4$Fe(CN)$_6$ and 0.25 M NaCl	Ti/Ir-Rb mesh	Artificial seawater (bacteria)/seawater	37	-[e]	[302]

Table 6 *(continued)*

Membrane		A	N	Spacer (δ)	Electrolyte	Electrode	Feed water	v	$P_{d,max}$	Ref.
Profiled Ralex CMH/AMH, (MEGA AS, Czech Republic)	10x10	477±15	5	Spacerless	0.05 M $K_3Fe(CN)_6$, 0.05 M $K_4Fe(CN)_6$ and 0.25 M NaCl	Ti/Pt mesh	Artificial seawater (0.508 M NaCl)/artificial river water (0.017 NaCl)	20.8	0.62	[125]
Ralex CMH/AMH, (MEGA AS, Czech Republic)	4x16	700-714	3	Non-conductive (800)	0.1 M $K_4Fe(CN)_6$, 0.1 M $K_3Fe(CN)_6$ and 0.27 M NaCl	Ti/Pt mesh	Natural ocean water/natural river water	1-3.6	0.08-0.16[d]	[31, 295]
Neosepta CMX/AMX (Tokuyama Co., Japan)	-	140-200	5	Non-conductive (480)	0.05 M $K_3Fe(CN)_6$, 0.05 M $K_4Fe(CN)_6$ and 0.25 M NaCl	Ti/Ir-Rb mesh	Natural seawater/natural river water	1	0.18	[303]
PC-SK and PC-SA (PCCell, Germany)	11x11	90-130	10	Non-conductive (500)	0.5 M NaCl	Ti coated with Pt	RO brine/brackish ground water	1	0.59	[33]

A: Active membrane area; N: Number of cell pairs; δ: thickness; $P_{d,max}$: Maximum power density; *v*: Flow velocity. [a]Gross power density decreased by 60% on the first day, fast increase of pressure drop (channel clogging), 90% reduction of flow rate after 5 days, occurrence of organic fouling and scaling, lower fouling incidence using profiled membranes. [b]OCV in the range of 0.55-0.65 V. [c]Electric resistance increased by 11%, almost no channel clogging (due to thick spacers), observed transport of humic compounds from LCC to HCC. [d]Up to 40% decrease in power density with respect to theoretical power density in the first 4.5 h using natural feed waters. [e]Up to 8% reduction in voltage during biofouling experiments over 20 h.

4.5.2. Antifouling strategies

Antifouling strategies are necessary to control fouling and to maintain a consistent performance of RED. Veerman *et al.* (2014) proposed a periodical reversal of feed streams by changing the polarity of the stack [268], a strategy largely used in ED. This was demonstrated by an increase of the time interval (14 days) before the rise of pressure-drop in a stack with a periodic reversal of 24 hours [86]. The operational period can be further increased up to 17 days using a shorter reversal time (every hour).

Periodic reversal also accounts for the stability of OCV and for the decrease in Ohmic losses. Moreover, the periodic reversal of flow direction can further increase the performance due to the difference in the distribution of biofilm near the inlet and the outlet of the stack. However, the periodic feed reversal is less effective in reducing colloidal fouling [268], and it is also associated with preferential channeling [125, 268]. Periodic air sparging (Figure 27) avoided channels clogging and led to ~50% higher power densities than in an untreated stack; however, after 10 days, the power consumed by applying this anti-fouling strategy overcame the power generated in the RED stack [268]. A viable alternative may be to clean channels with CO_2-saturated water, during which the bubbles are released uniformly, contrary to the preferential bubbles channeling when air is directly sparkled [303, 304]. Recently, Moreno *et al.* [303] demonstrated the merit of using of CO_2-saturated water as an anti-fouling strategy in RED by a comparison with an air sparging technique. RED stacks operated with CO_2-saturated water displayed a higher net power density (0.18 W/m^2) compared to the stacks with the air sparging technique (0.04 W/m^2) during operation over 30 days under natural conditions. The overall low performance of the stack using the air sparging technique was attributed to an increase in Ohmic resistance as a result of the formation of stagnant bubbles and an increase in pressure drop as a result of excessive fouling and channel blockage [303].

Addition of poly(ethylene imine) (PEI) to the feed stream has been investigated in order to impair deposition of humic compounds on ion-exchange membrane surfaces [305]. PEI is a positively charged, water-soluble polymer which, in correct proportions, leads to the formation of a neutral complex with humic compounds. The addition of adsorbents, such as mesoporous adsorbent resin and/or powdered activated carbon proved to be effective in removing of organic pollutants in drinking water production as well [306, 307].
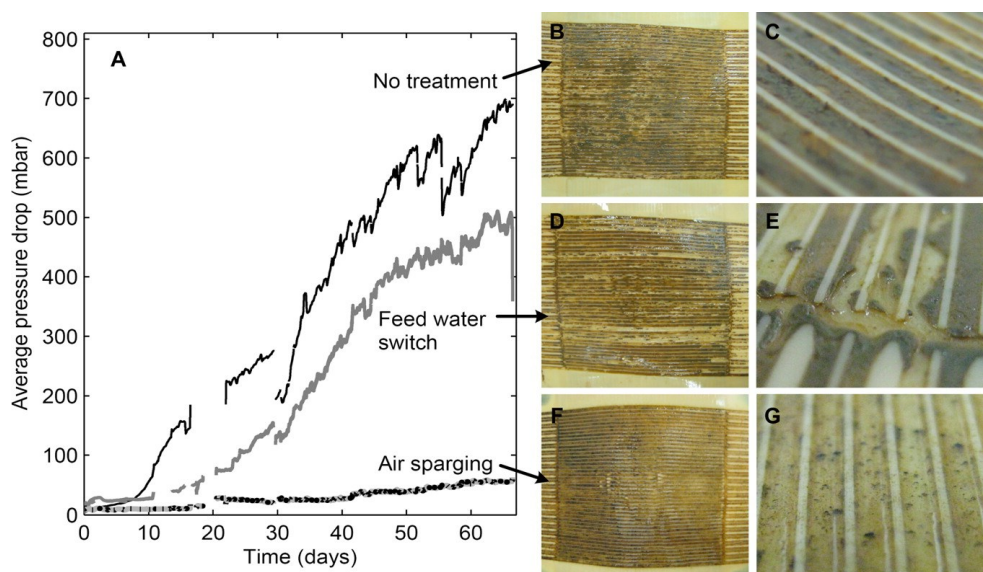
Fig. 27 Average pressure drop as a function of time for RED stack operated without pre-treatment, periodic feed reversal or air sparing (A), and full area (10×10 cm^2) photos (B, D, and F) and zoomed (1x1 cm^2) photos (C, E, and G) of profiled cation exchange membranes after fouling experiments. The original color of the membrane is beige. Reproduced with permission [268]. Copyright 2014 American Chemical Society.

Since organic fouling is mainly activated by electrostatic and hydrophobic interactions [308], increasing membrane hydrophilicity as well as surface smoothness (slip conditions) could improve membrane antifouling properties. The addition of a thin layer of opposite charge at the IEM surface creates an electrostatic repulsion between organic foulants and the thin layer [309]. Polyelectrolytes/zwitterions with poly(sodium 4-styrene sulfonate) (PSS) or poly(vinylsulfonic acid, sodium salt) (PVS) or poly(sodium acrylate) (PAAS) or polydopamine (PDA) groups can prevent adsorption of organic compounds on surface of AEMs [224, 309-311]. Utilization of such a strategy requires that the coating layer should not significantly increase membrane resistance. The nature of AEMs also influences the interactions with organic foulants. The lower number of benzene rings in aliphatic AEMs reduces the number of possible aromatic (π-π) interactions between the membrane and foulants compared with an aromatic AEM, while increasing the cross-linker content reduces the mobility of foulants in the membrane though at the cost of higher membrane electrical resistance [312]. However, since the price of the membrane is the key limiting factor in RED [81], additional

reflection about utilization of cheap/disposable membranes, like those from paper material [313], could be of interest.

The chemical cleaning procedures used in classical ED, consisting in flushing NaOH and citric acid solutions through the channels, allowed to remove clogging from the channels caused by sands and minerals, but were inefficient to remove organic fouling (TOC was nearly zero in the recovered solutions) [295]. Additionally, chemical cleaning may induce undesirable membrane structural changes consisting in the break of the chemical bonds, which increase its electrical resistance [295, 314, 315]. Such structural changes, and consequently the efficiency of the cleaning strategy, can be detected/evaluated by measuring the intensity of the natural fluorescence of a membrane (Figure 28) which results from the presence of aromatic groups and/or planar or cyclic molecules with several π bonds in their structure. When such bonds are broken, the intensity of the emitted fluorescence decrease, as can be compared between Figure 28c and Figure 28d.
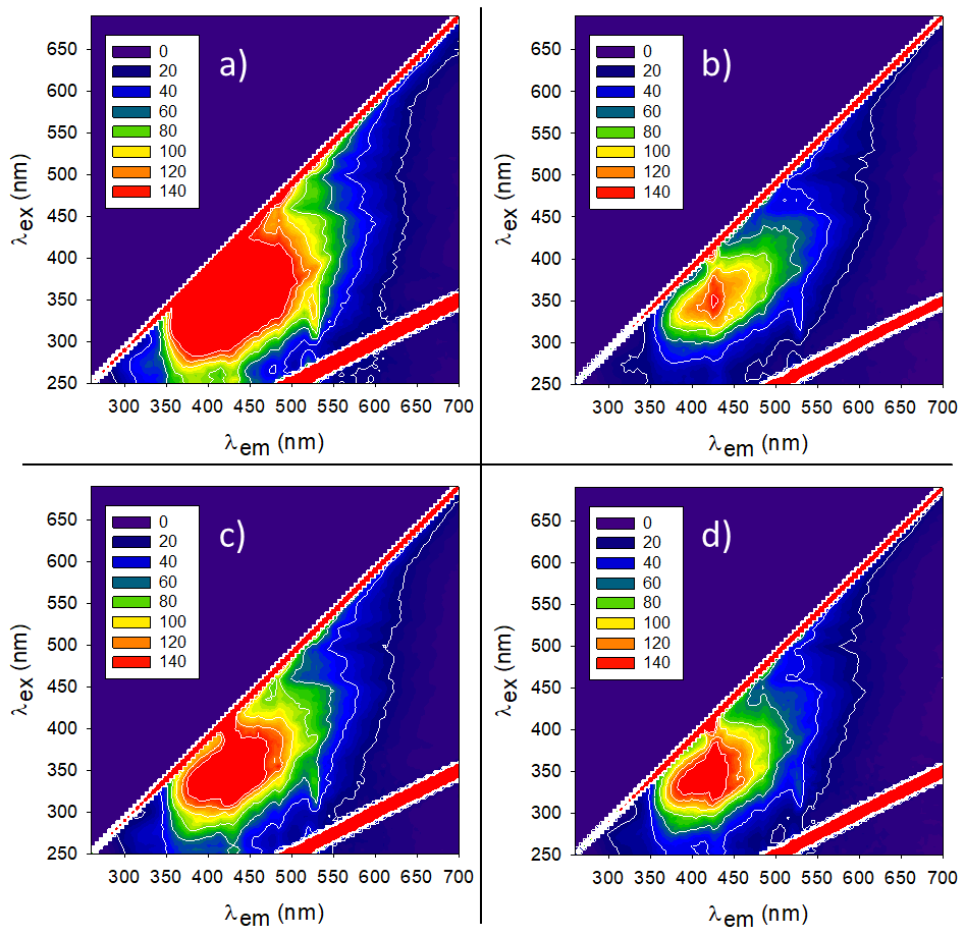

Fig. 28 Timeline of sequential fluorescence spectra of CEM surface in contact with natural seawater (a) in day 0, (b) after 32 days of RED stack operation, (c) after washing

the membrane with water, (d) after chemical cleaning. Reproduced with permission [295]. Copyright 2015 Elsevier.

The cleaning strategies and the validity of antifouling strategies so far tested in lab-scale require further investigation and validation in pilot/industrial installations. Saline streams, in function of their composition, and stack design, in function of granting an efficient fluid mixing, are anticipated to strongly influence choice/frequency of antifouling strategies and water pretreatment. An economic study considering costs of such steps has not yet been developed, despite being crucial to evaluate the practical viability of RED technology.

5. Advances in power density

The maximum P_d is a crucial parameter determining the commercial feasibility of RED. Progressive improvements in power density have been reported from the time of early investigations till now (Figure 29). Very low power density (up to 0.17 W/m^2) was reported at the early stage of RED research activity by Weinstein and Leitz [9], who carried out experiments with seawater and river water. Driven by improvement in membrane materials and manufacturing, significant enhancement has emerged since 2009. Veerman *et al*. [74] reported a P_d value of up to 1.2 W/m^2 for a RED stack equipped with Fumasep (FAD and FDK) and Selemion (AMV and CMV) commercial membranes using seawater/river water feed solutions. A power density of 2.2 W/m^2 was obtained for 0.5 M NaCl//0.017 M NaCl feed solutions using modified commercial IEMs (Fumatech, Germany) [72] which was the highest power density reported so far for river water and seawater at ambient temperature. A model prediction by Tedesco *et al*. [87] based on RED technology using thin (<20μm) and highly selective ionic exchange membranes (>85 %) indicates the possibility of achieving a power density of 4.2 W/m^2 at ambient conditions. The same authors also reported a power density of 6 W/m^2 at 40 ºC by mixing brine (5 M NaCl) and brackish water (0.1 M NaCl) [34], whereas Daniilidis *et al*. [239] achieved 6.7 W/m^2 at 60 ºC when mixing brine (5 M NaCl) and river water (0.01 M NaCl). Moreover, theoretical calculation indicated the possibility to obtain a power density as high as 20 W/m^2 by using membranes with significantly low resistance (below 0.1 Ω.cm^2) and a cell length of 1 mm[316].
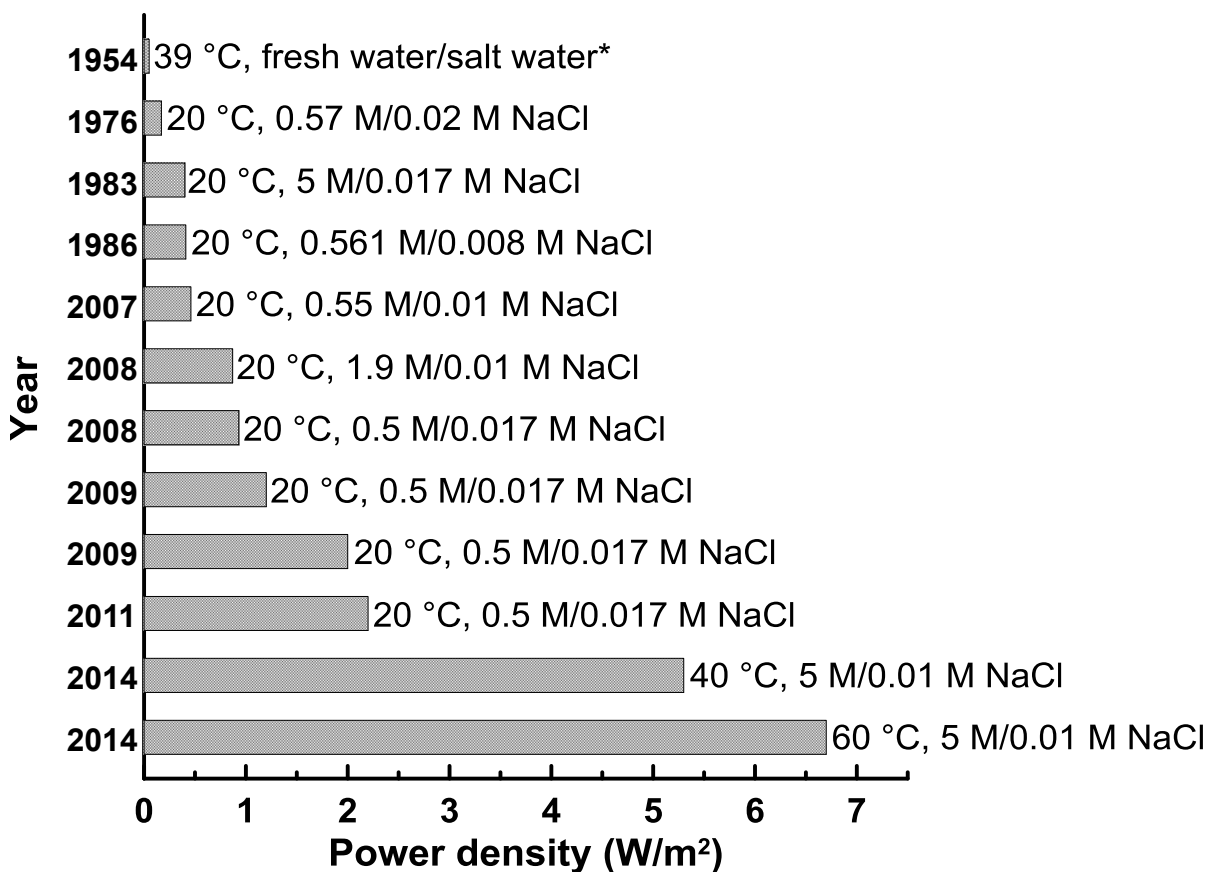
Fig. 29 Progressive increase of RED power density as reported in literature [9, 16, 18, 39, 72-75, 239, 289, 317];*Concentrations are not specified in [16].

6. Advanced applications of RED

RED systems integrated with other technologies are emerging as an attractive option in the production of key resources like water and hydrogen, in addition to electrical energy generation. RED technology can be integrated with different technologies in desalination [35, 38, 47, 99, 100, 107, 318-322], bio-electrochemical systems [51, 53, 107, 278, 323, 324] and water electrolysis [23, 106, 278] (Table 7).

Table 7. Relevant literature on hybrid (integrated) RED applications.

Description of the integration system	Membranes				Spacers (δ, µm)	Electrode compartment		v (cm/s)	$P_{max,d}$ W/m² (OCV, V)	Ref.
	Type	A (cm²)	δ (µm)	N		Electrolyte	Electrode			
RED operating on MD brine (5 M NaCl) and seawater (0.5 M NaCl) combined with RO/MD for water purification and power generation	Fuji AEM/CEM (Fujifilm Europe B.V., The Netherlands)	10x10	109-170	25	Woven (270)	0.3 M K$_3$Fe(CN)$_6$, 0.3 0.3 M K$_4$Fe(CN)$_6$ and 2.5 M NaCl	Ti-Ru/Ir mesh	1.1	1.2	[35]
RED operating on RO brine (1.2 M NaCl) and river water (0.1 M NaCl) for power generation	Neosepta AMX/ CMX (Tokuyama, Japan)	7x7	134-164	5	Woven (280)	0.05 M K$_3$Fe(CN)$_6$, 0.05 M K$_4$Fe(CN)6, 0.3 M NaCl	Ti-Ir/Ru	1.2	1.48	[99]
RED operating on NaHCO$_3$ (HCC concentration: 1.4 M, LCC concentration: 0-0.000175 M) combined with microbial electrolysis cell for hydrogen production	Selemion CMV/AMV (Asashi glass, Japan)	4x2	110-150	5	Polyethylene mesh (1300)	Catholyte: 1 M NaHCO$_3$, Anolyte: 1.0 g/L of CH$_3$COONa in NaHCO$_3$ buffer with vitamins and minerals	Anode: graphite fiber brushes, Cathode: stainless steel mesh	~0.025	(0.21-0.348)	[53]

Table 7. (*Continued*)

RED operating on NaHCO₃ (HCC concentration: 1.4 M, LCC solution: distilled water) combined with microbial electrolysis cell for hydrogen production	PC-SK and PC-SA (PCCell, Germany)	195	500	5-10	-	Catholyte: 1 M $NaHCO_3$, Anolyte: 1.0 g/L of CH_3COONa in $NaHCO_3$ buffer with vitamins and minerals	Cathode: Stainless steel mesh, Anode: carbon fiber brush	~40	(0.6-0.75)	[324]
RED operating on NaCl (HCC concentration: 0.6 M , LCC concentration: 0.06 M) combined with microbial electrolysis cell for hydrogen production and CO₂ sequestration	Selemion CMV/AMV (Asahi glass, Japan)	4x2	110-150	7	Polyethylene mesh (1300)	Catholyte: 0.35 g/L NaCl, Anolyte: 0.82 g/L CH_3COONa in a 50 mM phosphate-buffered nutrient medium	Cathode: Stainless steel mesh, Anode: graphite fiber brush	0.06	0.37±0.023	[325]
RED operating on seawater (0.6 M NaCl) and river water (0.006 M NaCl) combined with microbial fuel cell for enhanced power generation	Selemion CMV/AMV (Asahi glass, Japan)	4x2	110-150	10	Polyethylene mesh (1300)	Catholyte: synthetic seawater; Anolyte: 1.0 g/L CH_3COONa in a phosphate buffer with minerals and vitamins	Stainless steel mesh cathode, graphite fiber brush anode	0.05	4.3	[326]

Table 7. (*Continued*)

RED operating on seawater (0.6 M NaCl) and river water (0.01 M NaCl) combined with microbial fuel cell for enhanced power generation and chemical production	Selemion CMV/AMV (Asahi glass, Japan)	4x2	110-150	5	Polyethylene mesh (1300)	Anolyte: 1 g/L CH_3COONa in a 50 mM phosphate buffered nutrient medium, Catholyte: 0.7 g/L NaCl	Cathode: carbon cloth containing four polytetrafluoroethylene (PTFE) diffusion layers, Anodes: graphite fiber brush	0.05	0.9	[327]
RED operating on NH_4HCO_3 solutions (1.0 M) and LC (0.01 M) combined with microbial fuel cell for enhanced power production	Selemion CMV/AMV (Asahi glass, Japan)	4x2	110-150	1	Silicon gaskets (500)	Anolyte: 2 g/L of CH_3COONa in the 50 mM phosphate buffered nutrient medium, Catholyte:1 M NH_4HCO_3	Cathode: carbon-cloth, Anode: graphite fiber brushes	0.08	1.7-3.1	[328]

Table 7. (*Continued*)

RED operating on MD brine (5 M NaCl) and brackish water (0.1 M NaCl) combined alkaline water electrolysis for hydrogen production	Fuji AEM/CEM (Fujifilm Europe B.V., The Netherlands)	10x10	109-170	27	Woven (270)	0.3 M $K_3Fe(CN)_6$, 0.3 0.3 M $K_4Fe(CN)_6$ and 2.5 M NaCl	Ti-Ru/Ir mesh	0.7	1.6 (3.7)	[23]
RED operating on ground water (2.67 M NaCl) and seawater (0.79 M NaCl) (5 M NaCl) combined with a sustainable green house system	Fuji AEM/CEM (Fujifilm Europe B.V., The Netherlands)	10x10	109-170	19	Woven (270)	0.3 M $K_3Fe(CN)_6$, 0.3 0.3 M $K_4Fe(CN)_6$ and 2.5 M NaCl	Ti-Ru/Ir mesh	1	0.17 (0.91)	[102]

A: Active membrane area; N: Number of cell pairs; δ: thickness; $P_{d,max}$: Maximum power density; OCV: open circuit voltage; *v*: flow velocity; *flow rate: 400 mL min^{-1}

6.1. Applications in desalination technologies

One of the most interesting applications of the RED concept in hybrid systems is the simultaneous generation of renewable energy and drinking water. The requirement of a concentrated solution as an input to the RED system creates a beneficial opportunity for integrated application with membrane-based seawater desalination technologies like MD, RO, ED and capacitive deionization [35, 329-336].

Cumulative global contracted desalination capacity reached 99.8 million m^3/d in 2017 [337]. The estimated 6 % annual cumulative growth from 2016-2020 is expected to result in a total installed capacity of 117.3 million m^3/day by 2021 [338]. Mixing RO brine (assuming ~1 M in NaCl) with feed seawater (~0.5 M NaCl) has a significant potential for SGP (see Figure 2). The consequent dilution effect is not only favorable in terms of energy generation but also allows the mitigation of environmental problems associated with brine discharge [35, 339-341].

The integrated application of RED in desalination technologies involves the feeding of brine discharged into the HCC [38, 100, 319]. Figure 30 shows a conceptual illustration of the integrated application of RED with RO and/or MD systems as well as solar evaporation systems (ponds). The RO retentate can be directly fed into the RED system or further concentrated by MD (or other evaporative technologies, such as thermal vapour compression, mechanical vapour compression, etc.) before entering the RED system [35, 38, 100]. Additionally, the use of solar energy is particularly important in hybrid systems as it is abundantly available, for example, with a potential above 1000 W/m² during daytime in the Middle East region [38]. Moreover, solar heaters applied to raise the temperature of feed solutions may result in higher RED power density.

Li *et al*. [47] proposed different configurations for coupling RED with RO systems. In one of them, the RED effluent (seawater with reduced salinity) can be fed directly to RO as a low saline solution, thus allowing lower energy consumption. In another configuration, the retentate from RO can be used as a feed solution for RED thereby enhancing the potential of SGP with simultaneous reduction of environmental threat from brine discharge. Stages can be cascaded to take advantage of the synergetic benefits from the combined application of RO and RED units (see Figure 30). The HCC and LCC solutions are recycled in batch-wise operations. Considering a RED stack (50 cells and active membrane area of 600 cm^2) in 20 parallel branches (5 RED stacks in each branch), model predictions indicated the possibility of 56% reduction in RO energy

consumption when using RED effluent as RO feed (initial solution concentrations: 0.57 M HCC and 0.005 M LCC) [47]. Despite the expected low energy density, we tested salinity gradient energy from seawater and brine in our previous work and observed that advantage can be gained by heating feed streams [35], which is also a possible solution to the utilization of waste heat. The use of seawater with brine is also beneficial from an environmental point.
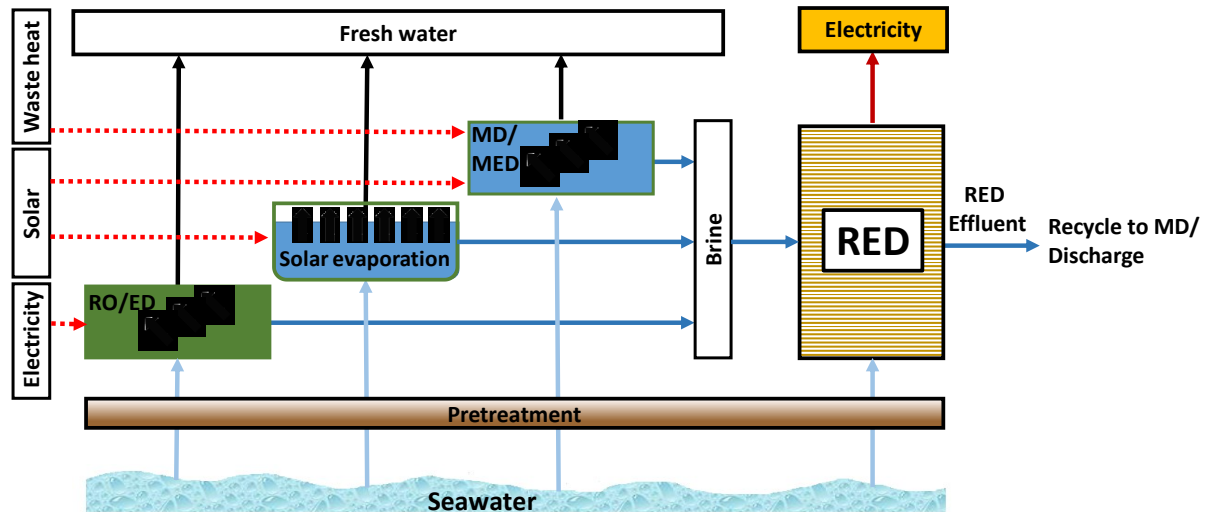

Fig. 30 Conceptual illustration of the integrated application of RED in desalination technologies.

Tufa *et al*. [35] presented an innovative approach combining RED and MD for simultaneous production of blue energy and drinking water in the logic of Near-Zero Liquid Discharge (N-ZLD) and low energy consumption in seawater RO desalination. The ability of MD to attain a significant volume reduction factor of up to 83.6% and to increase the concentration of NaCl solution up to saturation level (5.4 M NaCl) has been demonstrated [35]. A maximum P_d of 2.4 W/m^2 was achieved when mixing brine (5.4 M) and seawater (0.5 M). In general, the advantages of RED application in desalination technologies include: a significant reduction in Ohmic losses due to the highly saline brine, the use of salinity gradient power generated by RED to decrease the energy consumption of RO, no extra-pump energy to recirculate seawater and brine through RED, no additional pre-treatment against fouling with respect to that implemented in a desalination train, reduction of the environmental impact related to brine disposal as a consequence of the dilution effect from mixing seawater and brine.

Hybrid applications of RED systems with ED could also enable low-energy desalination, and such a system have recently been investigated using theoretical and experimental approaches [322, 342]. ED produces pure water by desalination of salt water [343, 344] leaving a concentrated solution that can be used as a HCC solution of RED [322, 342].

6.2. *Applications in bio-electrochemical systems*

Bioelectrochemical systems like microbial fuel cell (MFC) (Figure 31A) allow the production of electrical power with simultaneous treatment of wastewater [278, 345-356]. In air cathode MFCs, exoelectrogenic bacteria oxidize substrate and transfer electrons through the anode, thereby reducing oxygen at the air cathode with a corresponding theoretical maximum voltage of 1.1 V, an OCV of ~0.8 V and operational voltages in the range of ~0.5 - 0.3 V. Up to 2.4 W/m^2, P_d can be obtained by an air cathode MFC under well-optimized solution conditions [356]. One of the limitations of MFCs is that they cannot be simply linked in series to boost the overall potential since cells in a stacked MFC undergo voltage reversal leading to an OCV equal to (or less than) that of a single cell [357]. One means to overcome this limitation is the use of an integrated approach combining MFC and RED, creating a new system termed as 'Microbial RED Cell (MRC)' [50, 51, 53, 101, 323, 324]. Figure 31B and C presents MRCs with 1-cell pair and 2-cell pair configurations, respectively.
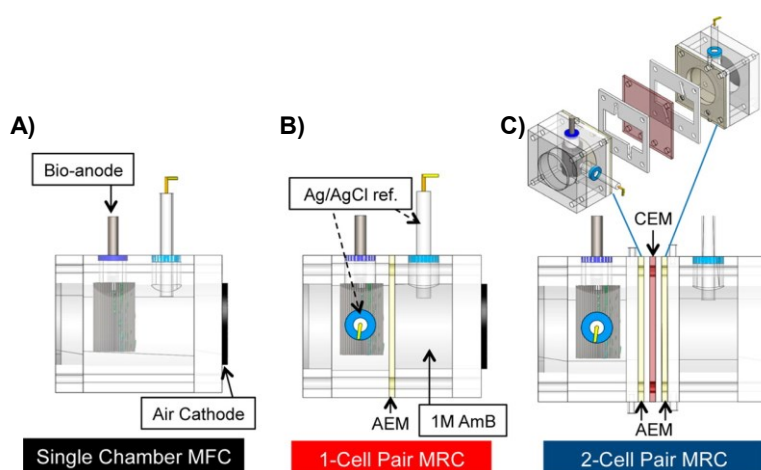
Fig. 31 Illustration of A) single chamber microbial fuel cell and the different microbial Reverse Electrodialysis configurations with B) one cell pair (1-CP), and C) two cell pairs (2-CPs).

In general, the integration of RED with MFCs has a synergetic advantage in terms of power and efficiency enhancement, overcoming the individual process limitations. The use of RED enables the low voltage produced by MFCs to be increased.

With the aim to optimize the MRC, Kim and Logan [51] investigated the effects of solution flow rate and salinity on power production. The MRC contained RED with 5 cell pairs, an air cathode prepared from a platinum catalyst and a Nafion binder, and an inoculated anode made of graphite fiber brush. A P_d of about 3.6 W/m^2 and voltage of 1.2 - 1.3V were recorded in the MFC fed with 0.6 M and 0.012 M NaCl solutions at a flow rate of 0.85 mL/min. The P_d was enhanced by about 19% (from 3.6 to 4.3 W/m^2) on increasing the flow rate to 1.55 mL/min [51]. Further work by Cusick et al. [328] indicated a substantial improvement in P_d by using ammonium bicarbonate (AmB) solutions in multiple RED cell pairs. Unlike electrolytes containing Na$^+$, the use of AmB allows for buffering pH changes and improves cathode kinetics in MRC. With a two-cells RED stack, a further reduction of anode charge transfer resistance and production of P_d up to 4.2 W/m^2 were reported.

The application of RED in the bio-electrochemical system includes hydrogen production by the integrated application with microbial electrolysis cell (MEC) [53, 323-325, 358-363]. In the MREC, H$_2$ production is achieved by a thermodynamically favorable oxidation of organic matter by exo-electrogens on the anode, and energy derived from the salinity gradient. The external power source required for the MEC is supplied by the added salinity energy using only a few number of RED cell pairs when using seawater and river water. Kim and Logan [323] demonstrated this concept using a five-cell RED unit sandwiched between an anode, containing exo-electrogenic bacteria, and a cathode. The system yielded an H$_2$ production rate of 0.8 - 1.6 m^3 H$_2$/m^3-anolyte/d by mixing river water/seawater at flow rates in the range of 0.1 - 0.8 mL/min [323]. Nam et al. [358] employed ammonium bicarbonate as the electrolyte for efficient voltage and hydrogen gas generation in the MREC, obtaining a maximum hydrogen production rate of 1.6 m^3 H$_2$/m^3/d at a flow rate of 0.8 mL/min. Using MRECs with 10 cell pairs, Watson et al. [324] produced H$_2$ from fermentation wastewater, recording a hydrogen production rate of 0.9 ± 0.1 m^3 H$_2$/m^3/d. Recently, the use of substrate without buffer solution in a MREC has been demonstrated Song et al. [363]. However, the MREC exhibited a low H$_2$ production rate and low coulombic efficiency as well as pH instability and low conductivity in the anolyte.

6.3. Applications in water electrolysis

Water electrolysis is a mature technology for hydrogen production through the use of direct electric current to split water [148, 364-372]: high purity (up to 99.9 %v/v) H_2 is achieved. Three main types of technologies are commonly used for this process: alkaline water electrolysis, proton exchange membrane water electrolysis and high temperature water electrolysis. Electrolysis suffers from high energy consumption, determining production costs in the range of 3-5 euros/kg of hydrogen depending on the plant size. Therefore, for sustainable hydrogen production, the primary energy used for water splitting should come from renewable energy resources. This approach is currently gaining a lot of attention driven by the projected exhaustion of fossil fuel and the rise in environmental concerns related to greenhouse gas emissions [373-377]. Although the wind and sun have been widely investigated to power water electrolysis, such energy sources are associated with stability issues caused by daily fluctuations [378]. On the other hand, non-intermittent SGP is a viable alternative to sustainable hydrogen production [23, 106, 379]. In an integrated RED-water electrolysis energy system, the required electrical power to fuel a water electrolyzer can be supplied by a separate RED system.

Hatzell *et al.* [106] investigated different scenarios involving oxygen reduction or hydrogen evolution reactions using NH_4HCO_3 feed solutions. A RED stack consisting of 20 cell pairs and a total active membrane area of 0.87 m^2, tested for indirect hydrogen production by coupling with an external electrolysis system, resulted in a power potential of ~1.5 Whm^{-3} (corresponding to a hydrogen production rate of 0.2x10^{-5} mol H_2 $h^{-1}cm^{-2}$-electrode) : the performance of RED with NH_4HCO_3 is generally limited due to the low ionic activities [252] and the poor performance of ion exchange membranes in NH_4HCO_3 [138]. The direct production of hydrogen by RED over cathode compartment is also possible, for example, by using HCl as a catholyte solution. In such a scenario, a hydrogen production rate of 0.55 mL h^{-1} cm^{-2}, corresponding to 2.7x10^{-5} mol H_2 $h^{-1}cm^{-2}$-electrode, of electrode area was obtained, however, with only 2.1% of hydrogen energy recovery [380].

Tufa *et al.* [23] explored the potential of an alkaline polymer electrolyte water electrolysis (APEWE) system driven by a RED generator for hydrogen production. Figure 32A shows a schematic representation of an integrated RED-APEWE system. The RED system consisted of 27 cells and a total active membrane area of 0.27 m^2; the

single-cell APEWE system was equipped with a highly conductive anion selective membrane composed of inert low-density polyethylene, non-platinum catalysts ($NiCo_2O_4$ and $NiFe_2O_4$) and electrodes based on nickel foam with an area of 4 cm^2. For a catalyst loading of 10 mg cm^{-2}, polymer binder loading of 15 wt% and temperature of 65 °C, a maximum hydrogen production rate of 44 $cm^3h^{-1}cm^{-2}$-electrode area, corresponding to 1.8×10^{-3} mol H_2 $h^{-1}cm^{-2}$-electrode, was recorded (Figure 32B), which was much higher than the aforementioned hydrogen production technologies.
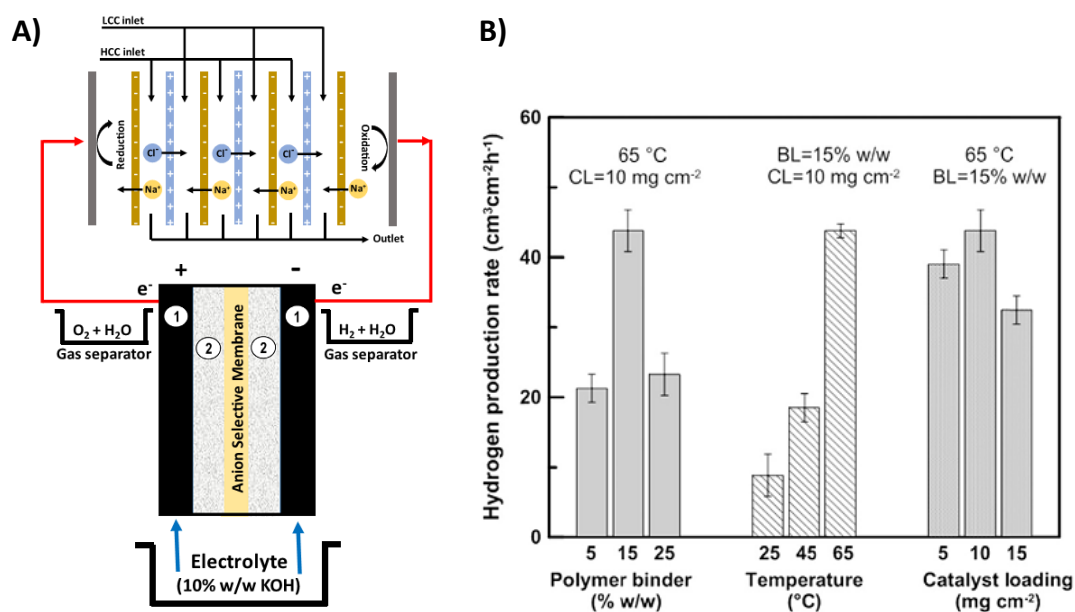
Fig. 32 A) Schematic illustration of RED integrated with an Alkaline Polymer Electrolyte Water Electrolysis (APEWE) system; B) Performance of RED-APEWE at different experimental conditions. Reproduced with permission [23]. Copyright 2016 Elsevier.

Moreover, with the aim to overcome the intrinsically low photovoltage associated with the narrow bandgap of Si in photoelectrochemical (PEC) water splitting, an integrated RED-PEC system (Figure 33) was implemented for hydrogen production. The integrated system, employing RED with 24 cells and a PEC system equipped with a Ni-Mo/Si photocathode and Ni foam anode, attained a constant current density of about 20mA/cm^2 with sufficient stability over 25h [381].
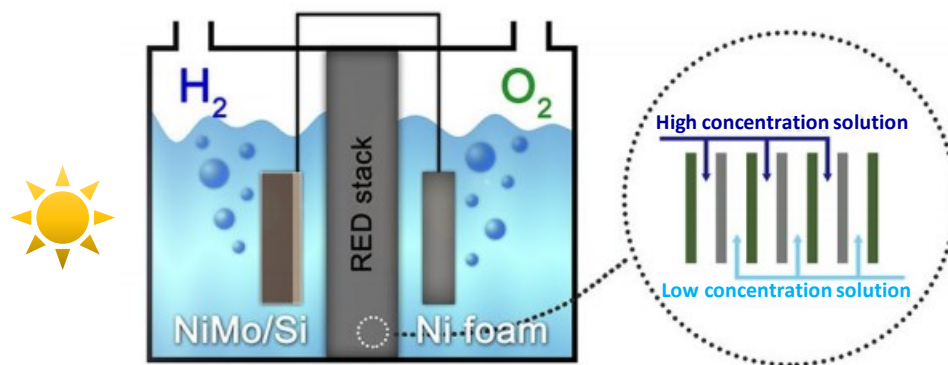
Fig. 33 Schematic illustration of an integrated RED-photoelectrochemical (PEC) water splitting system for hydrogen production.

7. Other designs and applications of RED

7.1. Closed-loop RED system

Operation of RED in open-loop with natural water or wastewater streams has some drawbacks, such as the requirement of extensive pretreatment and fouling-control strategies. Additionally, there could be an environmental impact due to the withdrawal of natural water from ecosystems and to some extent the discharge of outlet effluents into natural waters [7, 8, 382].

During the RED process, the mixing of the HCC and LCC occurs in the stack as a result of ion transport, as well as water transport to a limited extent. Therefore, there is a difference in concentration between the inlet and the outlet solutions. The concentration of the HCC solution at the outlet decreases whereas the concentration of the LCC solutions at the outlet increases. Interestingly, it is possible to concentrate or dilute the outlet solutions or regenerate the feed streams by a post-RED treatment process. Such design allows for the implementation of a closed-loop RED system. Regeneration can be achieved by two approaches: solvent removal or salt recovery from the outlet solutions. The solvent removal approach follows the separation of the solvent from the salt by different strategies involving evaporative processes like MED and MD, Liquid-Liquid extraction process or Azeotropic mixture separation, whereas the salt recovery approach follows the extraction of the salt by thermolysis or precipitation [43]. Such closed-loop approach generally has the advantage both from energy and environmental point of view [7, 43].

The salt recovery approach particularly using thermolytic solutions like solutions like NH_4HCO_3 [43, 50, 358] is recently attracting a huge attention among the scientific communities. Essentially, such system also allows for recovery of low-grade waste heat and conversion into electricity. Figure 34 presents a conceptual utilization of RED in closed-loop for converting low-grade waste heat to electricity. Such process typically involves thermal regeneration of the mixed RED effluents into low and high concentration streams, which are then recycled back into the system. The regeneration stage could involve extraction of either the solvent or the salt from the RED effluent [43]. The RED heat engine can be economically viable as it enables the use of low-grade waste heat ($\geq 60°C$) which is freely available from industrial or geothermal sources.
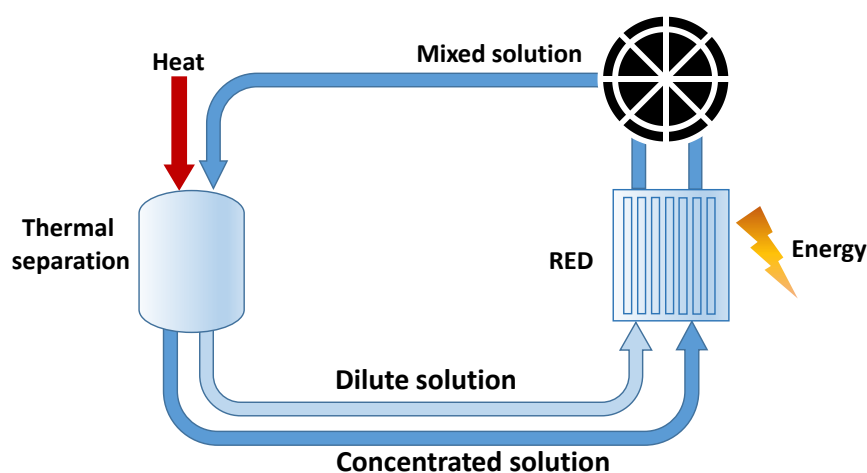
Fig. 34 Schematic illustration of a closed system in which a concentrated solution and dilute solution pass through a RED system to generate electrical power. Thermal energy (*e.g.* low-grade waste heat) is used to regenerate the original salinity gradient in a closed loop.

Studies on RED operating with thermolytic solutions, in particular, with NH_4HCO_3 has rapidly grown in the past few years [40, 43, 106, 252, 272, 358]. A recent study by Tamburini *et al*. provides a detailed theory and modelling of the potential applicability of RED as a heat engine operating on several salt solutions [43]. Model calculations depicted that a high power density can be achieved by using aqueous salt solutions based on lithium ions, such as LiBr and LiCl. Moreover, different designs of RED heat engine, following solvent extraction (NaCl solution) and salt extraction (NH_4HCO_3 solution) techniques, were evaluated in terms of power density and efficiency. Multiple Effect Distillation (MED) was employed as thermal regeneration

stage based on solvent extraction (NaCl solution) technique. As shown in Figure 35, the RED system integrated with MED operating on NaCl (MED-RED) (Figure 35a) and RED operating on NH_4HCO_3 (NH_4HCO_3-RED) (Figure 35b) displayed a comparable maximum power density of 7.5 W/m^2 and 7.7 W/m^2 , respectively, at 25 ^{o}C and flow velocity of 1 cm/s [43]. Similarly, comparable energetic efficiencies of 5 % and 5.4 % were recorded for RED-MED and NH_4HCO_3-RED, respectively. The closed-loop system attained an exergetic efficiency of about 85% implying that it is a promising strategy to convert low-grade waste heat to electricity. Generally, it was observed that the case of RED-MED operating on NaCl solution using optimal IEMs (low resistance and high permselectivity) outperforms NH_4HCO_3-RED system. However, the possibility of using low-grade waste heat at 60 °C by NH_4HCO_3-RED system favors the advantage of utilizing a much wider range of waste heat sources.
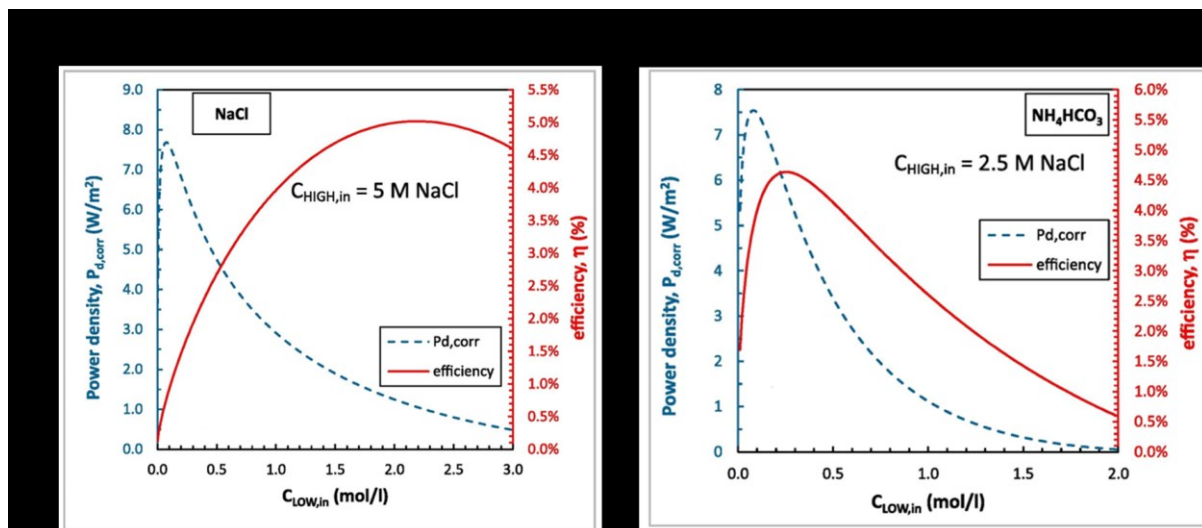
Fig. 35 Effect of solution concentration on (a) MED-RED system; variation of corrected power density ($P_d corr$, i.e corrected for black resistance [30]) and efficiency (η) vs with concentration of HCC solution at fixed HCC solution concentration of 5 M. Regeneration requirements of 40 kWh$_{th}$/m^3 of extracted solvent; (b) NH_4HCO_3-RED system; variation of $P_{d,corr}$ and efficiency (η) vs with a concentration of HCC solution at fixed HCC solution concentration of 2.5 M. Regeneration requirements of 100 kJ/mol of extracted salt and 4 °C thermal heating of dilute stream. Simulations of a RED unit (10×10 cm^2, 10 cell pairs) at 25 °C and flow velocity of 1 cm/s. Reproduced with permission [43]. Copyright 2016 Elsevier.

The performance of RED operated with NH_4HCO_3 is expected to be lower than of NaCl feed streams. A lower power output was measured in a RED stack operated

with NH_4HCO_3 solution (0.32 W/m^2) compared to NaCl solution (0.36 W/m^2) for HCC 0.6 M and LCC 0.006 M. The lower power output was mainly attributed to the lower conductivity of aqueous NH_4HCO_3 solutions compared to NaCl solutions [252] and, to a lesser extent, to the lower permselectivities of membranes in NH_4HCO_3 solutions [138].

Integrated MD and RED [7, 8, 318] can also function as closed-loop system following a thermal regeneration stage based on solvent extraction technique [318]. The separation step could involve MD which allows for desalination of the effluent from RED leaving a concentrated brine that can be recycled back to RED. In this perspective, an integrated MD-RED system was evaluated for potential conversion of low-grade waste heat into electricity. Results from theoretical modeling indicated the possibility to obtain an electrical efficiency of up to 1.15% by operating on MD feed solution (5 molal NaCl) at 20 - 60 °C [318].

7.2. *Concentration battery*

The design of a RED unit can be modified to work as a battery for energy storage, termed as a 'concentration battery'. The system produces power during the RED mode (discharging) from mixing the feed solutions. Regeneration of the chemical potential is performed during the ED mode (charging), using a higher potential than the membrane potential. Concentration battery offers several advantages including the use of non-toxic salts solutions, flexibility and the possibility of independent optimization of RED and ED for diverse applications. Figure 36 shows a CGFB (i.e. a closed-loop RED-ED system) able to store energy in the form of chemical potential of the two electrolyte solutions.
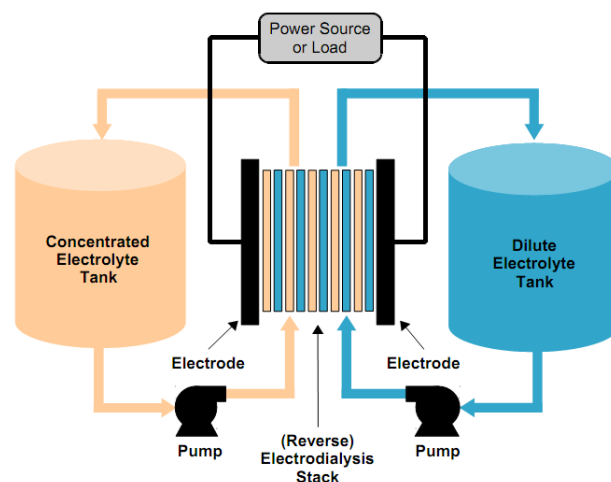
Fig. 36 Illustration of a Concentration Gradient Flow Battery (CGFB) [103].

Kingsbury *et al.* [103] obtained an energy efficiency of 62-77% for concentration battery. An average power density of 0.07 - 0.44 W/m^2 was delivered during the discharge stage. The results from the model calculations indicated that faradaic losses in the battery were mainly due to osmosis which also inhibits the system from returning to its initial state after charging-discharging cycles. With the aim to reduce undesirable osmotic water flux, a non-charged solute (referred to as 'Osmotic Ballast') was added to the dilute electrolyte solution to balance the osmotic pressure between the dilute and concentrated feed solutions [383]. The use of non-charged ballast resulted in a more than 50 % increase in the faradaic energy efficiency of the close-loop concentration battery compared to ballast-free battery operation.

Van Egmond *et al.* showed that the thermodynamic efficiency of CGFB increases with increasing current density and decreases with increasing HCC concentration: a maximum value of 75 % was recorded at 0.5 mol kg^{-1} [104]. A power density of up to 0.6 W/m^2 was attained during discharging. Further studies (Figure 37) revealed that power losses due to co-ion transport were relatively stable across the investigated range of concentration (0-1 M) and increased with temperature. The highest (dis)charge efficiency (up to 72 %) was recorded when working at molality difference of ~0.5-0.75.
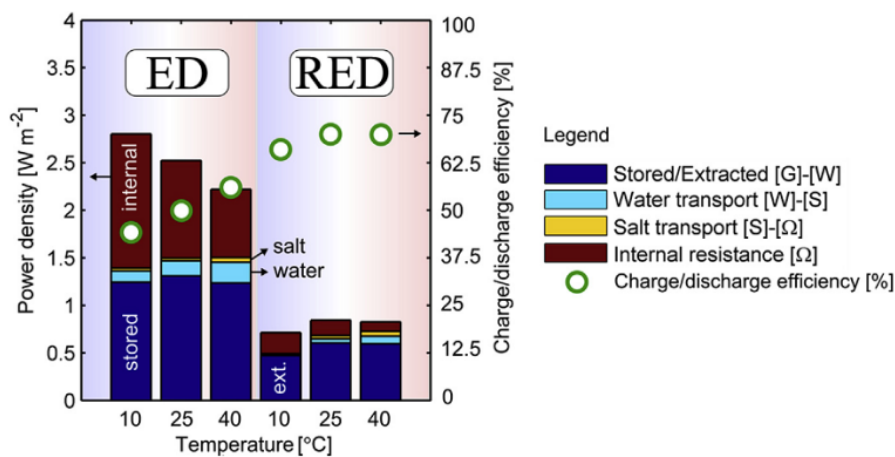
Fig. 37 Power dissipation and (dis)charge efficiency of a CGFB at different temperatures (10-40 °C). Charge experiments were performed at a current density of -32.5 A/m^2(ED) and discharge at 15 A/m^2 (RED). Reproduced with permission [384]. Copyright 2016 Elsevier.

7.3. Nanofluidic Reverse Electrodialysis system

Energy conversion by RED based on functional nanostructured materials has recently attracted attention as alternative energy sources using miniaturized electrical devices [385-387]. Kim and Duan [387] demonstrated the possibility of harnessing salinity gradient energy by a system consisting of silica nanochannels fabricated by a standard semiconductor manufacturing process and placed between two potassium chloride solutions with varying concentrations. Such a system is called a 'Nanofluidic Reverse Electrodialysis System (NFRED)' (Figure 38A). A maximum P_d of about 7.7 W/m², a channel length of 0.14 mm and channel height of 4 nm was reported. Cao *et al*. [386] fabricated and utilized solid-state nanofluidic channels or nanopores, which exhibit high ionic flux and lower fluidic resistance, for applications in NFRED. The performance of the nanopores was investigated for three representative monovalent inorganic electrolytes (KCl, NaCl and LiCl). As shown in Figure 38B, a maximum power of 45 pW was generated using cation-selective nanopores with a concentration gradient of 1000 (defined as the ratio of KCL solution concentration in HCC and LCC) for KCl solution, while only 17 pW was obtained for LiCl solution. For the anion-selective nanopores, the highest power (22 pW) was obtained with the LiCl solution and the lowest power (6 pW) with the KCl solution (Figure 38C). The difference in electrical power for the different electrolytes was attributed to the difference in ionic transport within the charged nanopores. For example, for the cation-selective nanopores, the power generated increased by increasing the diffusion coefficients of the respective cations ($D_K^+ = 1.957 \times 10^{-5}$ cm² s⁻¹ $> D_{Na}^+ = 1.334 \times 10^{-5}$ cm² s⁻¹, $D_{Li}^+ = 1.029 \times 10^{-5}$ cm² s⁻¹). A reverse trend was observed in the case of the anion-selective nanopores, implying that the electrolyte type and the nanopore charge selectivity mutually influence the output power [386].
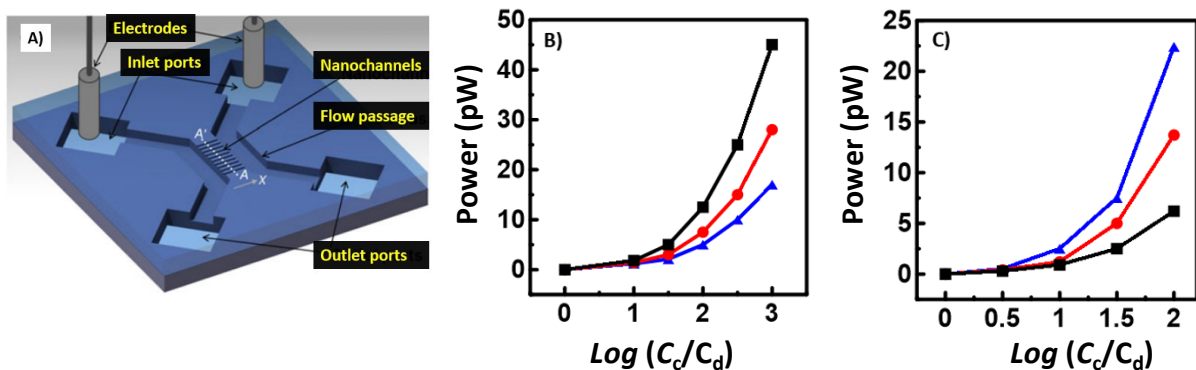
Fig. 38 A) Schematic illustration of Nanofluidic Reverse Electrodialysis System. Reproduced (adapted) with permission [387]. Copyright 2010 Springer. Power generation as a function of concentration gradient (C_c: HCC concentration; C_d: LCC concentration) from: B) cation-selective single-nanopore fluidic system; C anion-selective single-nanopore fluidic system Electrolytes: KCl (black square), NaCl (red circle), LiCl (blue triangle). Reproduced with permission [386]. Copyright 2011 Royal Society of Chemistry.

8. Pilot-scale Reverse Electrodialysis developments

Significant contributions and improvement in performance of RED have been recorded at lab scale in the past. Conversely, large-scale RED advances and scale-up is limited. In fact, some research on industrial-scale development of RED were recently foreseen in R&D projects [28, 29, 161]. REDstack BV (The Netherlands) is the company which operated the first 5 kW RED pilot plant together with Frisia Zout BV (a European salt company)[388]. On October 2013, REDstack BV, Fujifilm Manufacturing BV (The Netherlands) and Wetsus, Centre of Excellence for Sustainable Water Technology (The Netherlands) started to build this first real-world RED pilot plant with a capacity of 50 kW at Breezanddijk on the Afsluitdijk (The Netherlands) [28, 388]. The installed RED pilot plant generates electricity by mixing salt water (~28 g/L NaCl) from the Wadden Sea/North Sea and fresh water (0.2 - 0.5 g/L NaCl) from Lake Issel [28]. The goal of the pilot installation is to investigate RED performance under natural conditions, to advance RED technology and upscale to 1 MW by 2020 [388].

In 2014, a pilot-scale RED system was developed and demonstrated under an EU-FP7 REAPower project [29, 30, 34]. A RED pilot plant equipped with 125 cell pairs and IEMs with an active area of 50 m^2 (44x44 cm^2) was installed at Ettore-Infersa

Saltworks in Marsala (Trapani, Italy). Figure 39a shows the RED prototype together with the equivalent resistance (Figure 39b) of the external circuit adopted during the experimental tests. First tests with artificial brackish water (0.03 M NaCl) and saturated brine (4 - 5 M NaCl) resulted in a maximum output power of 65 W [30]. In 2016, the system was further scaled-up to RED units consisting of 500 cell pairs with over 400 m^2 of total membrane area [29]. A nominal power capacity of 1 kW was planned, and ~700W of power capacity was extracted when using artificial solutions, whereas 50% decrease in power density was observed when using real solutions. The system is under further investigation, focusing on improvement of the stack design and development of optimal materials including IEMs.
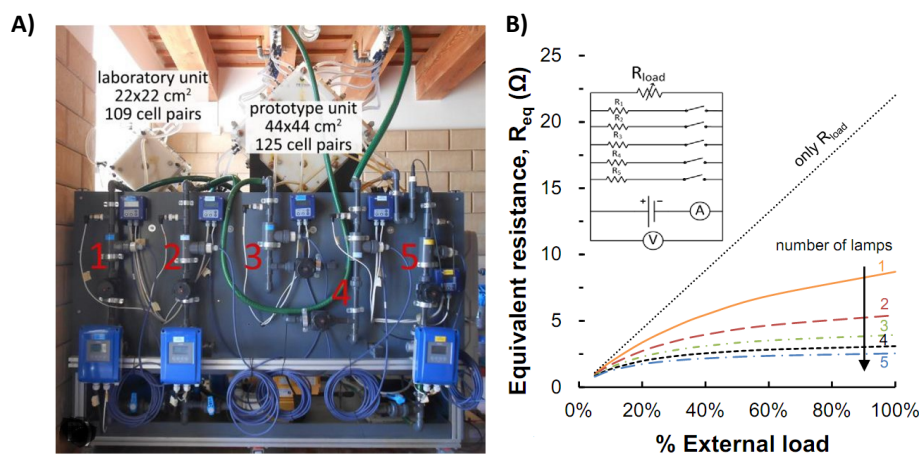
Fig. 39 A) RED pilot plant installed at Ettore-Infersa Saltworks in Marsala (Trapani, Italy) with 125 cells and 44x44 cm^2 single membrane area; B) The equivalent resistance of the external circuit used during RED tests. Reproduced with permission [30]. Copyright 2016 Elsevier.

9. Economic aspects

The economic and financial feasibility of RED has been preliminarily investigated for different scenarios in comparison with other renewable energy resources [81, 273]. It was observed that the current membrane price of 50 €/m^2 makes RED energy more expensive than other energy sources, such as solar and wind power [81]. However, if the membrane price could be reduced to 4.3 €/m^2 by using cheap raw materials and manufacturing procedures in the near future, the cost of produced electricity might drop to 0.18 €/kWh [81].

Post *et al.* [131] presented a conceptual design of a RED power plant with 200 kW capacity. A modular design with frames containing six RED stacks having a total effective membrane area of 100,000 m^2 was considered, assuming an installed membrane price of 2 €/m^2. The estimated cost of electricity was 0.08 €/kWh when mixing seawater and river water feed solutions. Low resistance IEMs generally have high prices (above 80 €/m^2) [131] which account for about 50 - 80% of total capital costs [388].

Daniilidis *et al.* performed a simulation of a RED power plant to evaluate the technical and financial feasibility of a large-scale RED system for different scenarios combining river water, seawater, and brines from 5 M levels can be found in salt mining sites [81, 239]. The boundaries for feed flowrate were fixed depending on feed types, along with the variation of power density depending on the feed pairs used for model calculations. Results depicted that the application of RED with brine feed seems more economical than river water/seawater, showing an upscale potential of 1 MW.

An electricity cost of 0.17 €/kWh was predicted for a membrane price of 4.3 €/m^2 when operating with seawater/river water [81]; this is indicative of a scenario in which RED could compete with solar, wind, and other conventional power generation systems with a cost reaching up to 0.14 €/kWh [389].

Economic evaluations of RED in hybrid applications with RO and MD are more complex. RO system can generate a large volume of brine that can be further concentration by MD to be used in RED. The operating costs of MD can be mitigated by the use of low-grade waste heat [10, 390]. In this context, a promising application from an economic point of view can be envisaged. An exemplary case study has been reported under an EU-FP7 REAPower project [161, 391]: Considering an RO system that disposes 250,000 m³ of brine at a salinity of 60 g/kg, it was predicted an MD system can convert this discharge into a potable water and brine (300 g/kg) at a rate of 10,411 m³/h and 12,500 m³/h, respectively. Assuming six years payback period of the extra revenue generated by the additional potable water produced by MD system using waste heat, a LCOE for an RO-MD-RED system was estimated to be 10.5 cents/kWh [161, 391].

In the case of a RED system working with heat-regenerative solutions like ammonium bicarbonate, the use of cost-free low-grade waste heat will have a significant impact on the economy of the system. A preliminary analysis estimates a levelized cost

of electricity (LCOE) of fewer than 0.07 €/kWh for a RED unit operating with low-grade waste heat [161].

An economic breakthrough might be achieved by developing high performance IEM materials, and by the use of a low-grade waste heat source to increase the RED output power; based on this hypothesis, a price of ~85 €/MW and levelized costs of electricity of ~0.10-0.19 €/kWh are predicted for RED in 2020 [388].

10. Concluding remarks and future prospects

The major limitation of RED at the current state-of-the-art is the availability of low resistance ion-conductive membrane materials at a low cost (<4 €/m^2) and with high permselectivity (>95 %) for operation under real conditions. Addressing these issues by the design of novel, high performance IEM materials at an affordable cost highly impacts the possible commercial implementation of RED technology. Prospective, low cost hydrocarbons to be further investigated could be polyolefin, polyaryletherketones, halogenated polyethers, polyethylene and poly(arylene ether sulfone). Potential membranes for applications in other electrochemical systems like ED [392], water electrolyzes [133, 148, 393], fuel cells [394, 395] and batteries [396] can also be adapted for RED applications.

Utilization of natural saline streams as a source for RED resulted in positive net power generation [29-31], but to a lesser extent when compared to artificial NaCl solutions. The presence of organic compounds and divalent ions in natural streams reduces (in some cases by more than - 50%) the obtained power due to overlapping electrochemical and fouling phenomena [29-32, 268, 295].

The negative impact of divalent ions on the performance of RED is one of the major challenges when working with natural streams. In particular, the relatively high abundance of magnesium ions in feed solutions leads to a drastic reduction in P_d, suppressing the Nernst potential drop across IEMs for reasons related to the alteration of electrochemical membrane properties and transport phenomena within the SGP-RED system [41, 46, 71, 203, 241]. In this framework, pre-treatment strategies based on chemical softening and/or membrane treatment could be envisaged. Pressure-driven membrane operations such as nanofiltration, today extensively used as pre-treatment to reverse osmosis, can easily be adapted to RED.

The use of monovalent selective IEMs could also be a strategic approach to alleviate the influence of multivalent ions [83]. Different strategies can be followed to design a new generation monovalent selective CEMs able to exclude multivalent ions effectively, for example, coating with a thin layer of conducting polymers, polyanaline or pyrrole [150, 156]. The difficulty in preparing highly selective membranes is most practice is due to the trade-off between resistance and permselectivty. The use of conducting polymers would reduce such increase of membrane resistance. In line with this, other strategies like crosslinking and layer by layer modification would also be promising strategies given the electrical resistance of membranes are controlled.

Moreover, further research on design and fabrication of antifouling membranes is required, since the long-term stability of IEMs, particularly in highly concentrated brine solutions, is crucial for process reliability.

Optimization of stack design also impacts positively in terms of efficient mixing of feed solutions, reduction of hydrodynamic losses and decrease of internal stack resistance. In particular, the use of profiled IEMs with optimal geometries could be a promising strategy to improve the overall fluid dynamics and, consequently, the power generated by RED [52, 77, 83, 92, 261, 266]. Compared to spacers, profiled membranes mitigate fouling, limit the deposition of colloidal materials and hence may limit pressure drop increase during stack operation.

RED can be regarded as a promising technology for renewable energy generation both in its standalone and integrated applications. Novel approaches based on the integration of RED into current membrane desalination processes is expected to minimize both energy input and brine disposal impact, simultaneously increasing the yield of desalted water [35]. In the logic of process intensification [330], this approach may well represent a step towards low-energy desalination and Near-Zero Liquid Discharge paradigm [329, 330, 397]. Moreover, the benefits, in terms of the reduction of adverse effects of brine discharge on aquatic life and minimization of greenhouse gas emissions, can already be envisaged [35, 382, 398, 399]. The implementation of MD-RED on an industrial level requires accurate thermo-economic analysis in order to optimize CAPEX and OPEX.

The practical applicability of RED technology as an energy supplier to water electrolysis for hydrogen production requires intensive material and process optimization, the development of highly conductive and stable membranes separators,

highly active and durable electrodes and low-cost catalyst materials are required for successful implementation of APEWE.

The use of a closed-loop RED system is currently emerging as a promising option for electricity generation from low-grade waste heat. The concept is based on coupling an RED unit with a thermally-driven regenerative process such as the use of thermolytic solutions like NH_4HCO_3 (which decompose at a temperature of 40-45°C) following a salt recovery approach and the use of combined MED-RED or MD-RED following a solvent removal approach. Further R&D is required in order to implement this concept in real applications [162].

The application of RED can potentially be extended to several other scenarios since brine solutions (eventually at high temperatures) can be obtained from a number of industrial activities. Several other applications are also emerging, such as the treatment of wastewater with simultaneous generation of electricity [400]. Overall, this represents a promising perspective for RED as a reliable power source once the technology challenges have been overcomed.

References

[1] U.S. Energy Information Administration , International Energy Outlook, U.S. Department of Energy. May 2016.

[2] Organization for Economic Co-operation and Development, Energy: The Next Fifty Years. 1999.

[3] Chu S, Majumdar A. Opportunities and challenges for a sustainable energy future. Nature. 2012;488:294-303.

[4] Annual energy outlook 2013. US Energy Information Administration, International Energy Outlook 2013, US Department of Energy. July 2013.

[5] Elimelech M, Phillip WA. The Future of Seawater Desalination: Energy, Technology, and the Environment. Science. 2011;333:712-7.

[6] Yip NY, Brogioli D, Hamelers HVM, Nijmeijer K. Salinity Gradients for Sustainable Energy: Primer, Progress, and Prospects. Environmental Science & Technology. 2016;50:12072-94.

[7] Logan BE, Elimelech M. Membrane-based processes for sustainable power generation using water. Nature. 2012;488:313-9.

[8] Ramon GZ, Feinberg BJ, Hoek EMV. Membrane-based production of salinity-gradient power. Energy & Environmental Science. 2011;4:4423-34.

[9] Weinstein JN, Leitz FB. Electric Power from Differences in Salinity: The Dialytic Battery. Science. 1976;191:557-9.

[10] Jia Z, Wang B, Song S, Fan Y. Blue energy: Current technologies for sustainable power generation from water salinity gradient. Renewable and Sustainable Energy Reviews. 2014;31:91-100.

[11] Helfer F, Lemckert C. The power of salinity gradients: An Australian example. Renewable and Sustainable Energy Reviews. 2015;50:1-16.

[12] Hussain A, Arif SM, Aslam M. Emerging renewable and sustainable energy technologies: State of the art. Renewable and Sustainable Energy Reviews. 2017;71:12-28.

[13] Kangas MT, Lund PD. Dynamic effects in a salinity-gradient solar-pond heating system. Applied Energy. 1985;20:189-205.

[14] Tsilingiris PT. Effect of salinity-concentration gradient on radiation transmission in salt-gradient ponds. Applied Energy. 1990;35:125-33.

[15] Beniwal RS, Singh RV, Chaudhary DR. Heat losses from a salt-gradient solar pond. Applied Energy. 1985;19:273-85.

[16] Pattle RE. Production of Electric Power by mixing Fresh and Salt Water in the Hydroelectric Pile. Nature. 1954;174:660-.

[17] Loeb S. Method and apparatus for generating power utilizing reverse electrodialysis. (1979) Patent US4171409, Method and apparatus for generating power utilizing reverse electrodialysis.

[18] Audinos R. Electrodialyse inverse. Etude de l'energie electrique obtenue a partir de deux solutions de salinites differentes. Journal of Power Sources. 1983;10:203-17.

[19] Lacey RE. Energy by reverse electrodialysis. Ocean Engineering. 1980;7:1-47.

[20] Jones A, Finley W. Recent development in salinity gradient power. OCEANS 2003 Proceedings: IEEE; 2003 *in Proceeding of Oceans 2003*. p. 2284-7.

[21] Post JW, Hamelers HVM, Buisman CJN. Energy recovery from controlled mixing salt and fresh water with a reverse electrodialysis system. Environmental Science and Technology. 2008;42:5785-90.

[22] Alvarez-Silva OA, Osorio AF, Winter C. Practical global salinity gradient energy potential. Renewable and Sustainable Energy Reviews. 2016;60:1387-95.

[23] Tufa RA, Rugiero E, Chanda D, Hnàt J, van Baak W, Veerman J, et al. Salinity gradient power-reverse electrodialysis and alkaline polymer electrolyte water electrolysis for hydrogen production. Journal of Membrane Science. 2016;514:155-64.

[24] Rattner AS, Garimella S. Energy harvesting, reuse and upgrade to reduce primary energy usage in the USA. Energy. 2011;36:6172-83.

[25] Jacobson MZ. Review of solutions to global warming, air pollution, and energy security. Energy & Environmental Science. 2009;2:148-73.

[26] Segura E, Morales R, Somolinos JA. A strategic analysis of tidal current energy conversion systems in the European Union. Applied Energy. 2018;212:527-51.

[27] Pacheco A, Ferreira Ó. Hydrodynamic changes imposed by tidal energy converters on extracting energy on a real case scenario. Applied Energy. 2016;180:369-85.

[28] REDstack. http://www.redstack.nl/.

[29] Tedesco M, Cipollina A, Tamburini A, Micale G. Towards 1 kW power production in a reverse electrodialysis pilot plant with saline waters and concentrated brines. Journal of Membrane Science. 2017;522:226-36.

[30] Tedesco M, Scalici C, Vaccari D, Cipollina A, Tamburini A, Micale G. Performance of the first reverse electrodialysis pilot plant for power production from saline waters and concentrated brines. Journal of Membrane Science. 2016;500:33-45.

[31] Pawlowski S, Galinha CF, Crespo JG, Velizarov S. Prediction of reverse electrodialysis performance by inclusion of 2D fluorescence spectroscopy data into multivariate statistical models. Separation and Purification Technology. 2015;150:159-69.

[32] Vermaas DA, Kunteng D, Saakes M, Nijmeijer K. Fouling in reverse electrodialysis under natural conditions. Water Research. 2013;47:1289-98.

[33] Kingsbury RS, Liu F, Zhu S, Boggs C, Armstrong MD, Call DF, et al. Impact of natural organic matter and inorganic solutes on energy recovery from five real salinity gradients using reverse electrodialysis. Journal of Membrane Science. 2017;541:621-32.

[34] Tedesco M, Brauns E, Cipollina A, Micale G, Modica P, Russo G, et al. Reverse Electrodialysis with saline waters and concentrated brines: a laboratory investigation towards technology scale-up. Journal of Membrane Science. 2015;492:9-20.

[35] Tufa RA, Curcio E, Brauns E, van Baak W, Fontananova E, Di Profio G. Membrane distillation and Reverse Electrodialysis for Near-zero liquid discharge and low energy seawater desalination. Journal of Membrane Science. 2015;496:325-33.

[36] Klotz IM, Rosenberg RM. Chemical thermodynamics: basic concepts and methods: Wiley Online Library; 2008.

[37] Post JW, Veerman J, Hamelers HVM, Euverink GJW, Metz SJ, Nymeijer K, et al. Salinity-gradient power: Evaluation of pressure-retarded osmosis and reverse electrodialysis. Journal of Membrane Science. 2007;288:218-30.

[38] Brauns E. Towards a worldwide sustainable and simultaneous large-scale production of renewable energy and potable water through salinity gradient power by combining reversed electrodialysis and solar power? Desalination. 2008;219:312-23.

[39] Veerman J, Saakes M, Metz SJ, Harmsen GJ. Reverse electrodialysis: Performance of a stack with 50 cells on the mixing of sea and river water. Journal of Membrane Science. 2009;327:136-44.

[40] Luo X, Cao X, Mo Y, Xiao K, Zhang X, Liang P, et al. Power generation by coupling reverse electrodialysis and ammonium bicarbonate: Implication for recovery of waste heat. Electrochem Commun. 2012;19:25.

[41] Vermaas DA, Veerman J, Saakes M, Nijmeijer K. Influence of multivalent ions on renewable energy generation in reverse electrodialysis. Energy & Environmental Science. 2014;7:1434-45.

[42] Veerman J, Vermaas DA. 4 - Reverse electrodialysis: Fundamentals A2 - Cipollina, Andrea. In: Micale G, editor. Sustainable Energy from Salinity Gradients: Woodhead Publishing; 2016. p. 77-133.

[43] Tamburini A, Tedesco M, Cipollina A, Micale G, Ciofalo M, Papapetrou M, et al. Reverse electrodialysis heat engine for sustainable power production. Applied Energy. 2017;206:1334-53.

[44] Nijmeijer K, Metz S. Chapter 5 Salinity Gradient Energy. In: Escobar IC, Schäfer AI, editors. Sustainability Science and Engineering: Elsevier; 2010. p. 95-139.

[45] Gao X, Chen M, Andreasen SJ, Kaer SK. Potential Usage of Thermoelectric Devices in a High-Temperature Polymer Electrolyte Membrane (PEM) Fuel Cell System: Two Case Studies. J Electron Mater. 2012;41:1838-44.

[46] Hong JG, Zhang W, Luo J, Chen Y. Modeling of power generation from the mixing of simulated saline and freshwater with a reverse electrodialysis system: The effect of monovalent and multivalent ions. Applied Energy. 2013;110:244-51.

[47] Li W, Krantz WB, Cornelissen ER, Post JW, Verliefde ARD, Tang CY. A novel hybrid process of reverse electrodialysis and reverse osmosis for low energy seawater desalination and brine management. Applied Energy. 2013;104:592-602.

[48] Veerman J, Vermaas D. Reverse electrodialysis: fundamentals. Sustainable Energy from Salinity Gradients: Elsevier; 2016. p. 77-133.

[49] Tufa RA, Curcio E, Fontananova E, Di Profio G. 3.8 Membrane-Based Processes for Sustainable Power Generation Using Water: Pressure-Retarded Osmosis (PRO), Reverse Electrodialysis (RED), and Capacitive Mixing (CAPMIX). Comprehensive Membrane Science and Engineering (Second Edition). Oxford: Elsevier; 2017. p. 206-48.

[50] Cusick RD, Kim Y, Logan BE. Energy Capture from Thermolytic Solutions in Microbial Reverse-Electrodialysis Cells. Science. 2012;335:1474-7.

[51] Kim Y, Logan BE. Microbial reverse electrodialysis cells for synergistically enhanced power production. Environmental Science & Technology. 2011;45:5834-9.

[52] Liu J, Geise GM, Luo X, Hou H, Zhang F, Feng Y, et al. Patterned ion exchange membranes for improved power production in microbial reverse-electrodialysis cells. Journal of Power Sources. 2014;271:437-43.

[53] Nam JY, Cusick RD, Kim Y, Logan BE. Hydrogen generation in microbial reverse-electrodialysis electrolysis cells using a heat-regenerated salt solution. Environmental Science and Technology. 2012;46:5240-6.

[54] Liu F, Schaetzle O, Sales BB, Saakes M, Buisman CJN, Hamelers HVM. Effect of additional charging and current density on the performance of Capacitive energy extraction based on Donnan Potential. Energy & Environmental Science. 2012;5:8642-50.

[55] Brogioli D, Zhao R, Biesheuvel PM. A prototype cell for extracting energy from a water salinity difference by means of double layer expansion in nanoporous carbon electrodes. Energy & Environmental Science. 2011;4:772-7.

[56] La Mantia F, Pasta M, Deshazer HD, Logan BE, Cui Y. Batteries for Efficient Energy Extraction from a Water Salinity Difference. Nano Letters. 2011;11:1810-3.

[57] Klaysom C, Cath TY, Depuydt T, Vankelecom IFJ. Forward and pressure retarded osmosis: potential solutions for global challenges in energy and water supply. Chemical Society Reviews. 2013;42:6959-89.

[58] Achilli A, Childress AE. Pressure retarded osmosis: From the vision of Sidney Loeb to the first prototype installation — Review. Desalination. 2010;261:205-11.

[59] Straub AP, Deshmukh A, Elimelech M. Pressure-retarded osmosis for power generation from salinity gradients: is it viable? Energy & Environmental Science. 2016;9:31-48.

[60] Lin S, Straub AP, Elimelech M. Thermodynamic limits of extractable energy by pressure retarded osmosis. Energy & Environmental Science. 2014;7:2706-14.

[61] Maisonneuve J, Laflamme CB, Pillay P. Experimental investigation of pressure retarded osmosis for renewable energy conversion: Towards increased net power. Applied Energy. 2016;164:425-35.

[62] Prante JL, Ruskowitz JA, Childress AE, Achilli A. RO-PRO desalination: An integrated low-energy approach to seawater desalination. Applied Energy. 2014;120:104-14.

[63] Wan CF, Chung T-S. Energy recovery by pressure retarded osmosis (PRO) in SWRO–PRO integrated processes. Applied Energy. 2016;162:687-98.

[64] Altaee A, Zhou J, Alhathal Alanezi A, Zaragoza G. Pressure retarded osmosis process for power generation: Feasibility, energy balance and controlling parameters. Applied Energy. 2017;206:303-11.

[65] Altaee A, Zaragoza G, Drioli E, Zhou J. Evaluation the potential and energy efficiency of dual stage pressure retarded osmosis process. Applied Energy. 2017;199:359-69.

[66] Han G, Ge Q, Chung T-S. Conceptual demonstration of novel closed-loop pressure retarded osmosis process for sustainable osmotic energy generation. Applied Energy. 2014;132:383-93.

[67] Altaee A, Palenzuela P, Zaragoza G, AlAnezi AA. Single and dual stage closed-loop pressure retarded osmosis for power generation: Feasibility and performance. Applied Energy. 2017;191:328-45.

[68] He W, Wang Y, Shaheed MH. Maximum power point tracking (MPPT) of a scale-up pressure retarded osmosis (PRO) osmotic power plant. Applied Energy. 2015;158:584-96.

[69] Olsson M, Wick GL, Isaacs JD. Salinity Gradient Power: Utilizing Vapor Pressure Differences. Science. 1979;206:452-4.

[70] Vermaas DA, Veerman J, Yip NY, Elimelech M, Saakes M, Nijmeijer K. High Efficiency in Energy Generation from Salinity Gradients with Reverse Electrodialysis. ACS Sustainable Chemistry & Engineering. 2013;1:1295-302.

[71] Tufa RA, Curcio E, van Baak W, Veerman J, Grasman S, Fontananova E, et al. Potential of brackish water and brine for energy generation by salinity gradient power-reverse electrodialysis (SGP-RE). RSC Advances. 2014;4:42617-23.

[72] Vermaas DA, Saakes M, Nijmeijer K. Doubled Power Density from Salinity Gradients at Reduced Intermembrane Distance. Environmental Science & Technology. 2011;45:7089-95.

[73] Długołęcki P, Gambier A, Nijmeijer K, Wessling M. Practical potential of reverse electrodialysis as process for sustainable energy generation. Environmental Science and Technology. 2009;43:6888-94.

[74] Veerman J, de Jong RM, Saakes M, Metz SJ, Harmsen GJ. Reverse electrodialysis: Comparison of six commercial membrane pairs on the thermodynamic efficiency and power density. Journal of Membrane Science. 2009;343:7-15.

[75] Turek M, Bandura B. Renewable energy by reverse electrodialysis. Desalination. 2007;205:67-74.

[76] Zhu X, He W, Logan BE. Reducing pumping energy by using different flow rates of high and low concentration solutions in reverse electrodialysis cells. Journal of Membrane Science. 2015;486:215-21.

[77] Vermaas DA, Saakes M, Nijmeijer K. Power generation using profiled membranes in reverse electrodialysis. Journal of Membrane Science. 2011;385-386:234-42.

[78] Vermaas DA, Bajracharya S, Sales BB, Saakes M, Hamelers B, Nijmeijer K. Clean energy generation using capacitive electrodes in reverse electrodialysis. Energy and Environmental Science. 2013;6:643-51.

[79] Długołecki P, Dabrowska J, Nijmeijer K, Wessling M. Ion conductive spacers for increased power generation in reverse electrodialysis. Journal of Membrane Science. 2010;347:101-7.

[80] Veerman J, Post JW, Saakes M, Metz SJ, Harmsen GJ. Reducing power losses caused by ionic shortcut currents in reverse electrodialysis stacks by a validated model. Journal of Membrane Science. 2008;310:418-30.

[81] Daniilidis A, Herber R, Vermaas DA. Upscale potential and financial feasibility of a reverse electrodialysis power plant. Applied Energy. 2014;119:257-65.

[82] Guler E, Zhang Y, Saakes M, Nijmeijer K. Tailor-Made Anion-Exchange Membranes for Salinity Gradient Power Generation Using Reverse Electrodialysis. ChemSusChem. 2012;5:2262-70.

[83] Güler E, Elizen R, Saakes M, Nijmeijer K. Micro-structured membranes for electricity generation by reverse electrodialysis. Journal of Membrane Science. 2014;458:136-48.

[84] Hong JG, Chen Y. Nanocomposite reverse electrodialysis (RED) ion-exchange membranes for salinity gradient power generation. Journal of Membrane Science. 2014;460:139-47.

[85] Gi Hong J, Chen Y. Evaluation of electrochemical properties and reverse electrodialysis performance for porous cation exchange membranes with sulfate-functionalized iron oxide. Journal of Membrane Science. 2015;473:210-7.

[86] Post JW. Blue Energy: electricity production from salinity gradients by reverse electrodialysis, PhD thesis: Wageningen University, The Netherlands; 2009.

[87] Tedesco M, Cipollina A, Tamburini A, van Baak W, Micale G. Modelling the Reverse ElectroDialysis process with seawater and concentrated brines. Desalination and Water Treatment. 2012;49:404-24.

[88] Tedesco M, Mazzola P, Tamburini A, Micale G, Bogle IDL, Papapetrou M, et al. Analysis and simulation of scale-up potentials in reverse electrodialysis. Desalination and Water Treatment. 2015;55:3391-403.

[89] Veerman J, Saakes M, Metz SJ, Harmsen GJ. Reverse electrodialysis: A validated process model for design and optimization. Chemical Engineering Journal. 2011;166:256-68.

[90] Yip NY, Vermaas DA, Nijmeijer K, Elimelech M. Thermodynamic, Energy Efficiency, and Power Density Analysis of Reverse Electrodialysis Power Generation with Natural Salinity Gradients. Environmental Science & Technology. 2014;48:4925-36.

[91] Tedesco M, Hamelers HVM, Biesheuvel PM. Nernst-Planck transport theory for (reverse) electrodialysis: I. Effect of co-ion transport through the membranes. Journal of Membrane Science. 2016;510:370-81.

[92] Gurreri L, Ciofalo M, Cipollina A, Tamburini A, Van Baak W, Micale G. CFD modelling of profiled-membrane channels for reverse electrodialysis. Desalination and Water Treatment. 2015;55:3404-23.

[93] Gurreri L, Tamburini A, Cipollina A, Micale G. CFD analysis of the fluid flow behavior in a reverse electrodialysis stack. Desalination and Water Treatment. 2012;48:390-403.

[94] Gurreri L, Tamburini A, Cipollina A, Micale G, Ciofalo M. CFD prediction of concentration polarization phenomena in spacer-filled channels for reverse electrodialysis. Journal of Membrane Science. 2014;468:133-48.

[95] Gurreri L, Tamburini A, Cipollina A, Micale G, Ciofalo M. Flow and mass transfer in spacer-filled channels for reverse electrodialysis: a CFD parametrical study. Journal of Membrane Science. 2016;497:300-17.

[96] Tamburini A, La Barbera G, Cipollina A, Micale G, Ciofalo M. CFD prediction of scalar transport in thin channels for reverse electrodialysis. Desalination and Water Treatment. 2015;55:3424-45.

[97] Cerva ML, Liberto MD, Gurreri L, Tamburini A, Cipollina A, Micale G, et al. Coupling CFD with a one-dimensional model to predict the performance of reverse electrodialysis stacks. Journal of Membrane Science. 2017;541:595-610.

[98] Gurreri L, Battaglia G, Tamburini A, Cipollina A, Micale G, Ciofalo M. Multi-physical modelling of reverse electrodialysis. Desalination. 2017;423:52-64.

[99] Kwon K, Han J, Park BH, Shin Y, Kim D. Brine recovery using reverse electrodialysis in membrane-based desalination processes. Desalination. 2015;362:1-10.

[100] Brauns E. An alternative hybrid concept combining seawater desalination, solar energy and reverse electrodialysis for a sustainable production of sweet water and electrical energy. Desalination and Water Treatment. 2010;13:53-62.

[101] Kim Y, Logan BE. Hydrogen production from inexhaustible supplies of fresh and salt water using microbial reverse-electrodialysis electrolysis cells. Proceedings of the National Academy of Sciences. 2011;108:16176-81.

[102] Farrell E, Hassan MI, Tufa RA, Tuomiranta A, Avci AH, Politano A, et al. Reverse electrodialysis powered greenhouse concept for water- and energy-self-sufficient agriculture. Applied Energy. 2017;187:390-409.

[103] Kingsbury RS, Chu K, Coronell O. Energy storage by reversible electrodialysis: The concentration battery. Journal of Membrane Science. 2015;495:502-16.

[104] van Egmond WJ, Saakes M, Porada S, Meuwissen T, Buisman CJN, Hamelers HVM. The concentration gradient flow battery as electricity storage system: Technology potential and energy dissipation. Journal of Power Sources. 2016;325:129-39.

[105] Luo X, Cao X, Mo Y, Xiao K, Zhang X, Liang P, et al. Power generation by coupling reverse electrodialysis and ammonium bicarbonate: Implication for recovery of waste heat. Electrochemistry Communications. 2012;19:25-8.

[106] Hatzell MC, Ivanov I, D. Cusick R, Zhu X, Logan BE. Comparison of hydrogen production and electrical power generation for energy capture in closed-loop ammonium bicarbonate reverse electrodialysis systems. Physical Chemistry Chemical Physics. 2014;16:1632-8.

[107] Cipollina A, Micale G, Tamburini A, Tedesco M, Gurreri L, Veerman J, et al. 5 - Reverse electrodialysis: Applications. Sustainable Energy from Salinity Gradients: Woodhead Publishing; 2016. p. 135-80.

[108] Veerman J, Saakes M, Metz SJ, Harmsen GJ. Reverse electrodialysis: evaluation of suitable electrode systems. J Appl Electrochem. 2010;40:1461-74.

[109] Scialdone O, Guarisco C, Grispo S, D' Angelo A, Galia A. Investigation of electrode material – Redox couple systems for reverse electrodialysis processes. Part I: Iron redox couples. Journal of Electroanalytical Chemistry. 2012;681:66-75.

[110] Chen K, Xue D. Materials chemistry toward electrochemical energy storage. Journal of Materials Chemistry A. 2016;4:7522-37.

[111] Li CW, Kanan MW. CO2 reduction at low overpotential on Cu electrodes resulting from the reduction of thick Cu2O films. Journal of the American Chemical Society. 2012;134:7231-4.

[112] Yu XQ, He Y, Sun JP, Tang K, Li H, Chen LQ, et al. Nanocrystalline MnO thin film anode for lithium ion batteries with low overpotential. Electrochemistry Communications. 2009;11:791-4.

[113] Zhou W, Wu X-J, Cao X, Huang X, Tan C, Tian J, et al. Ni 3 S 2 nanorods/Ni foam composite electrode with low overpotential for electrocatalytic oxygen evolution. Energy & Environmental Science. 2013;6:2921-4.

[114] Geise GM, Hickner MA, Logan BE. Ionic Resistance and Permselectivity Tradeoffs in Anion Exchange Membranes. ACS Applied Materials & Interfaces. 2013;5:10294-301.

[115] Strathmann H. Ion-exchange membrane separation processes: Elsevier; 2004.

[116] Strathmann H. 2.14 - Electromembrane Processes: Basic Aspects and Applications. Comprehensive Membrane Science and Engineering. Oxford: Elsevier; 2010. p. 391-429.

[117] Sata T. Studies on ion exchange membranes with permselectivity for specific ions in electrodialysis. Journal of membrane science. 1994;93:117-35.

[118] Manzanares JA, Murphy WD, Mafe S, Reiss H. Numerical simulation of the nonequilibrium diffuse double layer in ion-exchange membranes. The Journal of Physical Chemistry. 1993;97:8524-30.

[119] Larchet C, Nouri S, Auclair B, Dammak L, Nikonenko V. Application of chronopotentiometry to determine the thickness of diffusion layer adjacent to an ion-exchange membrane under natural convection. Advances in Colloid and Interface Science. 2008;139:45-61.

[120] Moya AA, Sistat P. Chronoamperometric response of ion-exchange membrane systems. Journal of Membrane Science. 2013;444:412-9.

[121] Balster J, Yildirim MH, Stamatialis DF, Ibanez R, Lammertink RGH, Jordan V, et al. Morphology and Microtopology of Cation-Exchange Polymers and the Origin of the Overlimiting Current. The Journal of Physical Chemistry B. 2007;111:2152-65.

[122] Długołęcki P, Ogonowski P, Metz SJ, Saakes M, Nijmeijer K, Wessling M. On the resistances of membrane, diffusion boundary layer and double layer in ion exchange membrane transport. Journal of Membrane Science. 2010;349:369-79.

[123] Fontananova E, Zhang W, Nicotera I, Simari C, van Baak W, Di Profio G, et al. Probing membrane and interface properties in concentrated electrolyte solutions. Journal of Membrane Science. 2014;459:177-89.

[124] Fontananova E, Messana D, Tufa RA, Nicotera I, Kosma V, Curcio E, et al. Effect of solution concentration and composition on the electrochemical properties of ion exchange membranes for energy conversion. Journal of Power Sources. 2017;340:282-93.

[125] Vermaas DA, Saakes M, Nijmeijer K. Early detection of preferential channeling in reverse electrodialysis. Electrochimica Acta. 2014;117:9-17.

[126] Pawlowski S, Sistat P, Crespo JG, Velizarov S. Mass transfer in reverse electrodialysis: Flow entrance effects and diffusion boundary layer thickness. Journal of Membrane Science. 2014;471:72-83.

[127] Bohinc K, Kralj-Iglič V, Iglič A. Thickness of electrical double layer. Effect of ion size. Electrochimica Acta. 2001;46:3033-40.

[128] Tedesco M, Hamelers HVM, Biesheuvel PM. Nernst-Planck transport theory for (reverse) electrodialysis: II. Effect of water transport through ion-exchange membranes. Journal of Membrane Science. 2017;531:172-82.

[129] Galama AH, Vermaas DA, Veerman J, Saakes M, Rijnaarts HHM, Post JW, et al. Membrane resistance: The effect of salinity gradients over a cation exchange membrane. Journal of Membrane Science. 2014;467:279-91.

[130] Higa M, Tanioka A, Kira A. A novel measurement method of Donnan potential at an interface between a charged membrane and mixed salt solution. Journal of Membrane Science. 1998;140:213-20.

[131] Post JW, Goeting CH, Valk J, Goinga S, Veerman J, Hamelers HVM, et al. Towards implementation of reverse electrodialysis for power generation from salinity gradients. Desalination and Water Treatment. 2010;16:182-93.

[132] Güler E, Elizen R, Vermaas DA, Saakes M, Nijmeijer K. Performance-determining membrane properties in reverse electrodialysis. Journal of Membrane Science. 2013;446:266-76.

[133] Varcoe JR, Atanassov P, Dekel DR, Herring AM, Hickner MA, Kohl PA, et al. Anion-exchange membranes in electrochemical energy systems. Energy & Environmental Science. 2014;7:3135-91.

[134] Devanathan R. Recent developments in proton exchange membranes for fuel cells. Energy & Environmental Science. 2008;1:101-19.

[135] Smitha B, Sridhar S, Khan A. Solid polymer electrolyte membranes for fuel cell applications—a review. Journal of Membrane Science. 2005;259:10-26.

[136] Spurgeon JM, Walter MG, Zhou J, Kohl PA, Lewis NS. Electrical conductivity, ionic conductivity, optical absorption, and gas separation properties of ionically conductive polymer membranes embedded with Si microwire arrays. Energy & Environmental Science. 2011;4:1772-80.

[137] Cassady HJ, Cimino EC, Kumar M, Hickner MA. Specific ion effects on the permselectivity of sulfonated poly(ether sulfone) cation exchange membranes. Journal of Membrane Science. 2016;508:146-52.

[138] Geise GM, Cassady HJ, Paul DR, Logan BE, Hickner MA. Specific ion effects on membrane potential and the permselectivity of ion exchange membranes. Physical Chemistry Chemical Physics. 2014;16:21673-81.

[139] Kristensen MB, Haldrup S, Christensen JR, Catalano J, Bentien A. Sulfonated poly(arylene thioether sulfone) cation exchange membranes with improved permselectivity/ion conductivity trade-off. Journal of Membrane Science. 2016;520:731-9.

[140] Zlotorowicz A, Strand RV, Burheim OS, Wilhelmsen Ø, Kjelstrup S. The permselectivity and water transference number of ion exchange membranes in reverse electrodialysis. Journal of Membrane Science. 2017;523:402-8.

[141] Ponce-Gonzalez J, Whelligan DK, Wang L, Bance-Soualhi R, Wang Y, Peng Y, et al. High performance aliphatic-heterocyclic benzyl-quaternary ammonium radiation-grafted anion-exchange membranes. Energy & Environmental Science. 2016;9:3724-35.

[142] Wright AG, Fan J, Britton B, Weissbach T, Lee H-F, Kitching EA, et al. Hexamethyl-p-terphenyl poly(benzimidazolium): a universal hydroxide-conducting polymer for energy conversion devices. Energy & Environmental Science. 2016;9:2130-42.

[143] Baek JD, Yoon Y-J, Lee W, Su P-C. A circular membrane for nano thin film micro solid oxide fuel cells with enhanced mechanical stability. Energy & Environmental Science. 2015;8:3374-80.

[144] Zeng L, Zhao TS, An L, Zhao G, Yan XH. A high-performance sandwiched-porous polybenzimidazole membrane with enhanced alkaline retention for anion exchange membrane fuel cells. Energy & Environmental Science. 2015;8:2768-74.

[145] Hsiao M-C, Liao S-H, Lin Y-F, Weng C-C, Tsai HM, Ma C-CM, et al. Polypropylene-grafted multi-walled carbon nanotube reinforced polypropylene composite bipolar plates in polymer electrolyte membrane fuel cells. Energy & Environmental Science. 2011;4:543-50.

[146] Li L, Shang F, Wang L, Pei S, Zhang Y. Transport properties of PFSA membranes with various ion exchange capacities for direct methanol fuel cell application. Energy & Environmental Science. 2010;3:114-6.

[147] Wu D, Paddison SJ, Elliott JA. A comparative study of the hydrated morphologies of perfluorosulfonic acid fuel cell membranes with mesoscopic simulations. Energy & Environmental Science. 2008;1:284-93.

[148] Xiao L, Zhang S, Pan J, Yang C, He M, Zhuang L, et al. First implementation of alkaline polymer electrolyte water electrolysis working only with pure water. Energy & Environmental Science. 2012;5:7869-71.

[149] Deavin OI, Murphy S, Ong AL, Poynton SD, Zeng R, Herman H, et al. Anion-exchange membranes for alkaline polymer electrolyte fuel cells: comparison of pendent benzyltrimethylammonium- and benzylmethylimidazolium-head-groups. Energy & Environmental Science. 2012;5:8584-97.

[150] Peron J, Shi Z, Holdcroft S. Hydrocarbon proton conducting polymers for fuel cell catalyst layers. Energy & Environmental Science. 2011;4:1575-91.

[151] Yu EH, Wang X, Krewer U, Li L, Scott K. Direct oxidation alkaline fuel cells: from materials to systems. Energy & Environmental Science. 2012;5:5668-80.

[152] Søndergaard T, Cleemann LN, Becker H, Aili D, Steenberg T, Hjuler HA, et al. Long-term durability of HT-PEM fuel cells based on thermally cross-linked polybenzimidazole. Journal of Power Sources. 2017;342:570-8.

[153] Hnát J, Paidar M, Schauer J, Žitka J, Bouzek K. Polymer anion-selective membranes for electrolytic splitting of water. Part II: Enhancement of ionic conductivity and performance under conditions of alkaline water electrolysis. J Appl Electrochem. 2012;42:545-54.

[154] Diaz LA, Hnát J, Heredia N, Bruno MM, Viva FA, Paidar M, et al. Alkali doped poly (2, 5-benzimidazole) membrane for alkaline water electrolysis: Characterization and performance. Journal of Power Sources. 2016;312:128-36.

[155] Marsh N, Fujii S, Takeichi K, Higa M. Euromembrane Conference 2012Optimization of RED Test Cell for PVA Based Ion-Exchange Membranes. Procedia Engineering. 2012;44:1300-2.

[156] Li N, Lee SY, Liu Y-L, Lee YM, Guiver MD. A new class of highly-conducting polymer electrolyte membranes: Aromatic ABA triblock copolymers. Energy & Environmental Science. 2012;5:5346-55.

[157] Gao H, Lian K. Proton-conducting polymer electrolytes and their applications in solid supercapacitors: a review. RSC Advances. 2014;4:33091-113.

[158] Munakata H, Yamamoto D, Kanamura K. Properties of composite proton-conducting membranes prepared from three-dimensionally ordered macroporous polyimide matrix and polyelectrolyte. Chemical Communications. 2005:3986-8.

[159] Nasef MM. Radiation-Grafted Membranes for Polymer Electrolyte Fuel Cells: Current Trends and Future Directions. Chemical Reviews. 2014;114:12278-329.

[160] Hong JG, Zhang B, Glabman S, Uzal N, Dou X, Zhang H, et al. Potential ion exchange membranes and system performance in reverse electrodialysis for power generation: A review. Journal of Membrane Science. 2015;486:71-88.

[161] Tedesco M, Cipollina A, Tamburini A, Micale G, Helsen J, Papapetrou M. REAPower: use of desalination brine for power production through reverse electrodialysis. Desalination and Water Treatment. 2015;53:3161-9.

[162] RED-Heat-to-Power. 2016.

[163] Długołęcki P, Nymeijer K, Metz S, Wessling M. Current status of ion exchange membranes for power generation from salinity gradients. Journal of Membrane Science. 2008;319:214-22.

[164] Xu T. Ion exchange membranes: State of their development and perspective. Journal of Membrane Science. 2005;263:1-29.

[165] Nagarale RK, Gohil GS, Shahi VK. Recent developments on ion-exchange membranes and electro-membrane processes. Advances in Colloid and Interface Science. 2006;119:97-130.

[166] Cho DH, Lee KH, Kim YM, Park SH, Lee WH, Lee SM, et al. Effect of cationic groups in poly(arylene ether sulfone) membranes on reverse electrodialysis performance. Chemical Communications. 2017;53:2323-6.

[167] Zhang H, Jiang D, Zhang B, Hong JG, Chen Y. A Novel Hybrid Poly (vinyl alcohol) (PVA)/Poly (2,6-dimethyl-1,4-phenylene oxide) (PPO) Membranes for Reverse Electrodialysis Power System. Electrochimica Acta. 2017;239:65-73.

[168] Kim H-K, Lee M-S, Lee S-Y, Choi Y-W, Jeong N-J, Kim C-S. High power density of reverse electrodialysis with pore-filling ion exchange membranes and a high-open-area spacer. Journal of Materials Chemistry A. 2015;3:16302-6.

[169] Moreno J, Díez V, Saakes M, Nijmeijer K. Mitigation of the effects of multivalent ion transport in reverse electrodialysis. Journal of Membrane Science. 2018;550:155-62.

[170] Sata T. Ion exchange membranes: preparation, characterization, modification and application: Royal Society of chemistry; 2004.

[171] Koneshan S, Rasaiah JC, Lynden-Bell RM, Lee SH. Solvent Structure, Dynamics, and Ion Mobility in Aqueous Solutions at 25 °C. The Journal of Physical Chemistry B. 1998;102:4193-204.

[172] Rijnaarts T, Huerta E, van Baak W, Nijmeijer K. Effect of Divalent Cations on RED Performance and Cation Exchange Membrane Selection to Enhance Power Densities. Environmental Science & Technology. 2017;51:13028-35.

[173] Mikhailenko SD, Wang K, Kaliaguine S, Xing P, Robertson GP, Guiver MD. Proton conducting membranes based on cross-linked sulfonated poly (ether ether ketone)(SPEEK). Journal of membrane science. 2004;233:93-9.

[174] Sambandam S, Ramani V. SPEEK/functionalized silica composite membranes for polymer electrolyte fuel cells. Journal of power sources. 2007;170:259-67.

[175] Xu D, Zhang G, Zhang N, Li H, Zhang Y, Shao K, et al. Surface modification of heteropoly acid/SPEEK membranes by polypyrrole with a sandwich structure for direct methanol fuel cells. Journal of Materials Chemistry. 2010;20:9239-45.

[176] Xing P, Robertson GP, Guiver MD, Mikhailenko SD, Wang K, Kaliaguine S. Synthesis and characterization of sulfonated poly(ether ether ketone) for proton exchange membranes. Journal of Membrane Science. 2004;229:95-106.

[177] Bolto B, Tran T, Hoang M, Xie Z. Crosslinked poly (vinyl alcohol) membranes. Progress in Polymer Science. 2009;34:969-81.

[178] Xu F, Zhang W, Zhang S, Li L, Li J, Zhang Y. Preparation and characterization of poly (vinyl alcohol) and 1, 2, 3-propanetriol diglycidyl ether incorporated soy protein isolate-based films. Journal of Applied Polymer Science. 2015;132:42578.

[179] Zhang QG, Liu QL, Huang SP, Hu WW, Zhu AM. Microstructure-related performances of poly (vinyl alcohol)-silica hybrid membranes: a molecular dynamics simulation study. Journal of Materials Chemistry. 2012;22:10860-6.

[180] Dai W, Shen Y, Li Z, Yu L, Xi J, Qiu X. SPEEK/Graphene oxide nanocomposite membranes with superior cyclability for highly efficient vanadium redox flow battery. Journal of Materials Chemistry A. 2014;2:12423-32.

[181] Wu Y, Wu C, Xu T, Yu F, Fu Y. Novel anion-exchange organic–inorganic hybrid membranes: preparation and characterizations for potential use in fuel cells. Journal of Membrane Science. 2008;321:299-308.

[182] Watanabe M, Uchida H, Emori M. Analyses of Self-Humidification and Suppression of Gas Crossover in Pt-Dispersed Polymer Electrolyte Membranes for Fuel Cells. Journal of The Electrochemical Society. 1998;145:1137-41.

[183] Baglio V, Di Blasi A, Aricò AS, Antonucci V, Antonucci PL, Fiory FS, et al. Influence of TiO2 nanometric filler on the behaviour of a composite membrane for applications in direct methanol fuel cells. Journal of New Materials for Electrochemical Systems. 2004;7:275-80.

[184] Pandey RP, Thakur AK, Shahi VK. Sulfonated Polyimide/Acid-Functionalized Graphene Oxide Composite Polymer Electrolyte Membranes with Improved Proton Conductivity and Water-Retention Properties. ACS Applied Materials & Interfaces. 2014;6:16993-7002.

[185] Burnat D, Schlupp M, Wichser A, Lothenbach B, Gorbar M, Züttel A, et al. Composite membranes for alkaline electrolysis based on polysulfone and mineral fillers. Journal of Power Sources. 2015;291:163-72.

[186] Jang I-Y, Kweon O-H, Kim K-E, Hwang G-J, Moon S-B, Kang A-S. Covalently cross-linked sulfonated poly (ether ether ketone)/tungstophosphoric acid composite membranes for water electrolysis application. Journal of Power Sources. 2008;181:127-34.

[187] Aili D, Hansen MK, Pan C, Li Q, Christensen E, Jensen JO, et al. Phosphoric acid doped membranes based on Nafion®, PBI and their blends–Membrane preparation, characterization and steam electrolysis testing. International journal of hydrogen energy. 2011;36:6985-93.

[188] Hansen MK, Aili D, Christensen E, Pan C, Eriksen S, Jensen JO, et al. PEM steam electrolysis at 130° C using a phosphoric acid doped short side chain PFSA membrane. International journal of hydrogen energy. 2012;37:10992-1000.

[189] Tian B, Yan CW, Wang FH. Proton conducting composite membrane from Daramic/Nafion for vanadium redox flow battery. Journal of membrane science. 2004;234:51-4.

[190] Mohammadi T, Skyllas-Kazacos M. Use of polyelectrolyte for incorporation of ion-exchange groups in composite membranes for vanadium redox flow battery applications. Journal of power sources. 1995;56:91-6.

[191] Teng X, Zhao Y, Xi J, Wu Z, Qiu X, Chen L. Nafion/organic silica modified TiO 2 composite membrane for vanadium redox flow battery via in situ sol–gel reactions. Journal of Membrane Science. 2009;341:149-54.

[192] Raghavan P, Choi J-W, Ahn J-H, Cheruvally G, Chauhan GS, Ahn H-J, et al. Novel electrospun poly (vinylidene fluoride-co-hexafluoropropylene)–in situ SiO 2 composite membrane-based polymer electrolyte for lithium batteries. Journal of Power Sources. 2008;184:437-43.

[193] Lee H-J, Lim J-M, Kim H-W, Jeong S-H, Eom S-W, Hong YT, et al. Electrospun polyetherimide nanofiber mat-reinforced, permselective polyvinyl alcohol composite separator membranes: A membrane-driven step closer toward rechargeable zinc–air batteries. Journal of Membrane Science. 2016;499:526-37.

[194] Gi Hong J, Glabman S, Chen Y. Effect of inorganic filler size on electrochemical performance of nanocomposite cation exchange membranes for salinity gradient power generation. Journal of Membrane Science. 2015;482:33-41.

[195] Yamaguchi T, Miyata F, Nakao S-i. Pore-filling type polymer electrolyte membranes for a direct methanol fuel cell. Journal of Membrane Science. 2003;214:283-92.

[196] Yamaguchi T, Kuroki H, Miyata F. DMFC performances using a pore-filling polymer electrolyte membrane for portable usages. Electrochemistry communications. 2005;7:730-4.

[197] Jung H, Fujii K, Tamaki T, Ohashi H, Ito T, Yamaguchi T. Low fuel crossover anion exchange pore-filling membrane for solid-state alkaline fuel cells. Journal of membrane science. 2011;373:107-11.

[198] Hara N, Ohashi H, Ito T, Yamaguchi T. Rapid proton conduction through unfreezable and bound water in a wholly aromatic pore-filling electrolyte membrane. The Journal of Physical Chemistry B. 2009;113:4656-63.

[199] Adrus N, Ulbricht M. Novel hydrogel pore-filled composite membranes with tunable and temperature-responsive size-selectivity. Journal of Materials Chemistry. 2012;22:3088-98.

[200] Lee J-Y, Kim J-H, Lee J-H, Kim S, Moon S-H. Morphologically Aligned Cation-Exchange Membranes by a Pulsed Electric Field for Reverse Electrodialysis. Environmental Science & Technology. 2015;49:8872-7.

[201] Safronova EY, Golubenko DV, Shevlyakova NV, D'yakova MG, Tverskoi VA, Dammak L, et al. New cation-exchange membranes based on cross-linked sulfonated polystyrene and polyethylene for power generation systems. Journal of Membrane Science. 2016;515:196-203.

[202] Lee KH, Cho DH, Kim YM, Moon SJ, Kim JF, Lee YM. Isomeric influences of naphthalene based sulfonated poly(arylene ether sulfone) membranes for energy generation using reverse electrodialysis and polymer electrolyte membrane fuel cell. Journal of Membrane Science. 2017;535:35-44.

[203] Post JW, Hamelers HVM, Buisman CJN. Influence of multivalent ions on power production from mixing salt and fresh water with a reverse electrodialysis system. Journal of Membrane Science. 2009;330:65-72.

[204] Ran J, Wu L, He Y, Yang Z, Wang Y, Jiang C, et al. Ion exchange membranes: New developments and applications. Journal of Membrane Science. 2017;522:267-91.

[205] Sata T, Yamaguchi T, Matsusaki K. Interaction between anionic polyelectrolytes and anion exchange membranes and change in membrane properties. Journal of Membrane Science. 1995;100:229-38.

[206] Wang XL, Wang M, Jia YX, Wang BB. Surface Modification of Anion Exchange Membrane by Covalent Grafting for Imparting Permselectivity between Specific Anions. Electrochimica Acta. 2015;174:1113-21.

[207] Sata T. Studies on anion exchange membranes having permselectivity for specific anions in electrodialysis — effect of hydrophilicity of anion exchange membranes on permselectivity of anions. Journal of Membrane Science. 2000;167:1-31.

[208] Sata T, Mine K, Matsusaki K. Change in Transport Properties of Anion-Exchange Membranes in the Presence of Ethylene Glycols in Electrodialysis. Journal of Colloid and Interface Science. 1998;202:348-58.

[209] Sata T, Yamaguchi T, Matsusaki K. Effect of Hydrophobicity of Ion Exchange Groups of Anion Exchange Membranes on Permselectivity between Two Anions. The Journal of Physical Chemistry. 1995;99:12875-82.

[210] Li J, Xu Y, Hu M, Shen J, Gao C, van der Bruggen B. Enhanced conductivity of monovalent cation exchange membranes with chitosan/PANI composite modification. RSC Advances. 2015;5:90969-75.

[211] Andrés LJ, Riera FA, Alvarez R, Audinos R. Separation of strong acids by electrodialysis with membranes selective to monovalent ions. An approach to modelling the process. The Canadian Journal of Chemical Engineering. 1994;72:848-53.

[212] Balster J, Krupenko O, Pünt I, Stamatialis DF, Wessling M. Preparation and characterisation of monovalent ion selective cation exchange membranes based on sulphonated poly(ether ether ketone). Journal of Membrane Science. 2005;263:137-45.

[213] Güler E, van Baak W, Saakes M, Nijmeijer K. Monovalent-ion-selective membranes for reverse electrodialysis. Journal of Membrane Science. 2014;455:254-70.

[214] Hosseini SM, Madaeni SS, Asiani H, Heidari AR. Preparation and Electrochemical Characterization of Monovalent Ion Selective Poly (Vinyl Chloride)-Blend-Poly (Styrene-Co-Butadiene) Heterogeneous Cation Exchange Membrane Coated with Poly (Methyl Methacrylate). Separation Science and Technology 2012;47:1443-54.

[215] Lambert J, Avila-Rodriguez M, Durand G, Rakib M. Separation of sodium ions from trivalent chromium by electrodialysis using monovalent cation selective membranes. Journal of Membrane Science. 2006;280:219-25.

[216] Nie XY, Sun SY, Sun Z, Song X, Yu JG. Ion-fractionation of lithium ions from magnesium ions by electrodialysis using monovalent selective ion-exchange membranes. Desalination. 2017;403:128-35.

[217] Tas S, Miedema H, Nijmeijer K. Ion exchange membranes for the selective separation of monovalent cation. Procedia Engineering *Procedia Engineering,* 2012. p. 1101-2.

[218] Zhang Y, Van der Bruggen B, Pinoy L, Meesschaert B. Separation of nutrient ions and organic compounds from salts in RO concentrates by standard and monovalent selective ion-exchange membranes used in electrodialysis. Journal of Membrane Science. 2009;332:104-12.

[219] Le XT, Viel P, Jégou P, Garcia A, Berthelot T, Bui TH, et al. Diazonium-induced anchoring process: an application to improve the monovalent selectivity of cation exchange membranes. Journal of Materials Chemistry. 2010;20:3750-7.

[220] Amara M, Kerdjoudj H. Electro-adsorption of polyethyleneimine on the anion exchange membrane: Application to the nitrate removal from loaded solutions. Analytica Chimica Acta. 2005;547:50-2.

[221] Guesmi F, Hannachi C, Hamrouni B. Selectivity of anion exchange membrane modified with polyethyleneimine. Ionics. 2012;18:711-7.

[222] Hong SU, Malaisamy R, Bruening ML. Optimization of flux and selectivity in Cl−/SO42− separations with multilayer polyelectrolyte membranes. Journal of Membrane Science. 2006;283:366-72.

[223] White N, Misovich M, Yaroshchuk A, Bruening ML. Coating of nafion membranes with polyelectrolyte multilayers to achieve high monovalent/divalent cation electrodialysis selectivities. ACS applied materials & interfaces. 2015;7:6620-8.

[224] Mulyati S, Takagi R, Fujii A, Ohmukai Y, Matsuyama H. Simultaneous improvement of the monovalent anion selectivity and antifouling properties of an anion exchange membrane in an electrodialysis process, using polyelectrolyte multilayer deposition. Journal of Membrane Science. 2013;431:113-20.

[225] Li J, Zhou ML, Lin JY, Ye WY, Xu YQ, Shen JN, et al. Mono-valent cation selective membranes for electrodialysis by introducing polyquaternium-7 in a commercial cation exchange membrane. Journal of Membrane Science. 2015;486:89-96.

[226] Kumar M, Khan MA, AlOthman ZA, Siddiqui MR. Polyaniline modified organic–inorganic hybrid cation-exchange membranes for the separation of monovalent and multivalent ions. Desalination. 2013;325:95-103.

[227] Tas S, Zoetebier B, Hempenius MA, Vancso GJ, Nijmeijer K. Monovalent cation selective crown ether containing poly(arylene ether ketone)/SPEEK blend membranes. RSC Advances. 2016;6:55635-42.

[228] Tas S, Miedema H, Nijmeijer K. Ion Exchange Membranes for the Selective Separation of Monovalent Cation. Procedia Engineering. 2012;44:1101-2.

[229] White N, Misovich M, Alemayehu E, Yaroshchuk A, Bruening ML. Highly selective separations of multivalent and monovalent cations in electrodialysis through Nafion membranes coated with polyelectrolyte multilayers. Polymer. 2016;103:478-85.

[230] Li J, Zhou M-l, Lin J-y, Ye W-y, Xu Y-q, Shen J-n, et al. Mono-valent cation selective membranes for electrodialysis by introducing polyquaternium-7 in a commercial cation exchange membrane. Journal of Membrane Science. 2015;486:89-96.

[231] Chu D, Jiang R. Effect of operating conditions on energy efficiency for a small passive direct methanol fuel cell. Electrochimica Acta. 2006;51:5829-35.

[232] Belt JR, Ho CD, Miller TJ, Habib MA, Duong TQ. The effect of temperature on capacity and power in cycled lithium ion batteries. Journal of power sources. 2005;142:354-60.

[233] Liu H, Cheng S, Logan BE. Power generation in fed-batch microbial fuel cells as a function of ionic strength, temperature, and reactor configuration. Environmental Science & Technology. 2005;39:5488-93.

[234] Khandelwal M, Mench MM. Direct measurement of through-plane thermal conductivity and contact resistance in fuel cell materials. Journal of Power Sources. 2006;161:1106-15.

[235] Zhang Z, Huang X, Jiang J, Wu B. An improved dynamic model considering effects of temperature and equivalent internal resistance for PEM fuel cell power modules. Journal of Power Sources. 2006;161:1062-8.

[236] Park J, Li X. Effect of flow and temperature distribution on the performance of a PEM fuel cell stack. Journal of Power Sources. 2006;162:444-59.

[237] Amphlett JC, Peppley BA, Halliop E, Sadiq A. The effect of anode flow characteristics and temperature on the performance of a direct methanol fuel cell. Journal of Power Sources. 2001;96:204-13.

[238] Ferng YM, Su A. A three-dimensional full-cell CFD model used to investigate the effects of different flow channel designs on PEMFC performance. International Journal of Hydrogen Energy. 2007;32:4466-76.

[239] Daniilidis A, Vermaas DA, Herber R, Nijmeijer K. Experimentally obtainable energy from mixing river water, seawater or brines with reverse electrodialysis. Renewable Energy. 2014;64:123-31.

[240] Veerman J, Saakes M, Metz SJ, Harmsen GJ. Electrical power from sea and river water by reverse electrodialysis: A first step from the laboratory to a real power plant. Environmental Science and Technology. 2010;44:9207-12.

[241] Avci AH, Sarkar P, Tufa RA, Messana D, Argurio P, Fontananova E, et al. Effect of Mg2+ ions on energy generation by Reverse Electrodialysis. Journal of Membrane Science. 2016;520:499-506.

[242] Zhang B, Gao H, Chen Y. Enhanced Ionic Conductivity and Power Generation Using Ion-Exchange Resin Beads in a Reverse-Electrodialysis Stack. Environmental Science & Technology. 2015;49:14717-24.

[243] Vermaas DA, Saakes M, Nijmeijer K. Enhanced mixing in the diffusive boundary layer for energy generation in reverse electrodialysis. Journal of Membrane Science. 2014;453:312-9.

[244] Weiner AM, McGovern RK, Lienhard V JH. A new reverse electrodialysis design strategy which significantly reduces the levelized cost of electricity. Journal of Membrane Science. 2015;493:605-14.

[245] Benneker AM, Rijnaarts T, Lammertink RGH, Wood JA. Effect of Temperature Gradients in (Reverse) Electrodialysis in the Ohmic Regime. Journal of Membrane Science. 2017.

[246] Alberti G, Casciola M, Massinelli L, Bauer B. Polymeric proton conducting membranes for medium temperature fuel cells (110–160 C). Journal of Membrane Science. 2001;185:73-81.

[247] Riedel I, Parisi J, Dyakonov V, Lutsen L, Vanderzande D, Hummelen JC. Effect of Temperature and Illumination on the Electrical Characteristics of Polymer–Fullerene Bulk-Heterojunction Solar Cells. Advanced Functional Materials. 2004;14:38-44.

[248] Karpas Z, Berant Z, Shahal O. Effect of temperature on the mobility of ions. Journal of the American Chemical Society. 1989;111:6015-8.

[249] Mahmoud T, Fereshteh R. Comparing the effect of pressure and temperature on ion mobilities. Journal of Physics D: Applied Physics. 2005;38:857-62.

[250] Długołęcki P, Anet B, Metz SJ, Nijmeijer K, Wessling M. Transport limitations in ion exchange membranes at low salt concentrations. Journal of Membrane Science. 2010;346:163-71.

[251] Weiner AM, McGovern RK. Increasing the power density and reducing the levelized cost of electricity of a reverse electrodialysis stack through blending. Desalination. 2015;369:140-8.

[252] Zhu X, He W, Logan BE. Influence of solution concentration and salt types on the performance of reverse electrodialysis cells. Journal of Membrane Science. 2015;494:154-60.

[253] Geise GM, Curtis AJ, Hatzell MC, Hickner MA, Logan BE. Salt Concentration Differences Alter Membrane Resistance in Reverse Electrodialysis Stacks. Environmental Science & Technology Letters. 2014;1:36-9.

[254] Kreuer KD. On the development of proton conducting polymer membranes for hydrogen and methanol fuel cells. Journal of Membrane Science. 2001;185:29-39.

[255] Pawlowski S, Crespo J, Velizarov S. Sustainable Power Generation from Salinity Gradient Energy by Reverse Electrodialysis. In: Ribeiro AB, Mateus EP, Couto N, editors. Electrokinetics Across Disciplines and Continents: New Strategies for Sustainable Development. Cham: Springer International Publishing; 2016. p. 57-80.

[256] Rijnaarts T, Huerta E, van Baak W, Nijmeijer K. Effect of divalent cations on RED performance and cation exchange membrane selection to enhance power densities. Environmental Science & Technology. 2017.

[257] Sata T. Ion exchange membranes: preparation, characterization, modification and application: Royal Society of chemistry; 2007.

[258] Van der Bruggen B, Koninckx A, Vandecasteele C. Separation of monovalent and divalent ions from aqueous solution by electrodialysis and nanofiltration. Water Research. 2004;38:1347-53.

[259] Zhang Y-F, Liu L, Du J, Fu R, Van der Bruggen B, Zhang Y. Fracsis: Ion fractionation and metathesis by a NF-ED integrated system to improve water recovery. Journal of Membrane Science. 2017;523:385-93.

[260] Vanoppen M, Stoffels G, Demuytere C, Bleyaert W, Verliefde ARD. Increasing RO efficiency by chemical-free ion-exchange and Donnan dialysis: Principles and practical implications. Water Research. 2015;80:59-70.

[261] Pawlowski S, Geraldes V, Crespo JG, Velizarov S. Computational fluid dynamics (CFD) assisted analysis of profiled membranes performance in reverse electrodialysis. Journal of Membrane Science. 2016;502:179-90.

[262] Li F, Meindersma W, de Haan AB, Reith T. Novel spacers for mass transfer enhancement in membrane separations. Journal of Membrane Science. 2005;253:1-12.

[263] Balster J, Pünt I, Stamatialis DF, Wessling M. Multi-layer spacer geometries with improved mass transport. Journal of Membrane Science. 2006;282:351-61.

[264] Pawlowski S, Crespo JG, Velizarov S. Pressure drop in reverse electrodialysis: Experimental and modeling studies for stacks with variable number of cell pairs. Journal of Membrane Science. 2014;462:96-111.

[265] Pánek P, Kodým R, Šnita D, Bouzek K. Spatially two-dimensional mathematical model of the flow hydrodynamics in a spacer-filled channel – The effect of inertial forces. Journal of Membrane Science. 2015;492:588-99.

[266] Pawlowski S, Rijnaarts T, Saakes M, Nijmeijer K, Crespo JG, Velizarov S. Improved fluid mixing and power density in reverse electrodialysis stacks with chevron-profiled membranes. Journal of Membrane Science. 2017;531:111-21.

[267] Moreno J, Slouwerhof E, Vermaas DA, Saakes M, Nijmeijer K. The Breathing Cell: Cyclic Intermembrane Distance Variation in Reverse Electrodialysis. Environmental Science & Technology. 2016;50:11386-93.

[268] Vermaas DA, Kunteng D, Veerman J, Saakes M, Nijmeijer K. Periodic Feedwater Reversal and Air Sparging As Antifouling Strategies in Reverse Electrodialysis. Environmental Science & Technology. 2014;48:3065-73.

[269] Ngene IS, Lammertink RGH, Wessling M, Van der Meer WGJ. Particle deposition and biofilm formation on microstructured membranes. Journal of Membrane Science. 2010;364:43-51.

[270] Seo J, Kushner DI, Hickner MA. 3D Printing of Micropatterned Anion Exchange Membranes. ACS Applied Materials & Interfaces. 2016;8:16656-63.

[271] Tamburini A, La Barbera G, Cipollina A, Ciofalo M, Micale G. CFD simulation of channels for direct and reverse electrodialysis. Desalination and Water Treatment. 2012;48:370-89.

[272] Hatzell MC, Logan BE. Evaluation of flow fields on bubble removal and system performance in an ammonium bicarbonate reverse electrodialysis stack. Journal of membrane science. 2013;446:449-55.

[273] Vermaas DA. Energy generation from mixing salt water and fresh water: Smart flow strategies for reverse electrodialysis: Universiteit Twente; 2014.

[274] Ponrouch A, Goni AR, Sougrati MT, Ati M, Tarascon J-M, Nava-Avendano J, et al. A new room temperature and solvent free carbon coating procedure for battery electrode materials. Energy & Environmental Science. 2013;6:3363-71.

[275] Ponrouch A, Marchante E, Courty M, Tarascon J-M, Palacin MR. In search of an optimized electrolyte for Na-ion batteries. Energy & Environmental Science. 2012;5:8572-83.

[276] Mahmoud L, Lalia BS, Hashaikeh R. Carbon nanostructures modified LiFePO4 cathodes for lithium ion battery applications: optimized porosity and composition. Materials Research Express. 2016;3:125008.

[277] Haregewoin AM, Wotango AS, Hwang B-J. Electrolyte additives for lithium ion battery electrodes: progress and perspectives. Energy & Environmental Science. 2016;9:1955-88.

[278] Xie X, Criddle C, Cui Y. Design and fabrication of bioelectrodes for microbial bioelectrochemical systems. Energy & Environmental Science. 2015;8:3418-41.

[279] Walter M, Kravchyk KV, Ibáñez M, Kovalenko MV. Efficient and Inexpensive Sodium–Magnesium Hybrid Battery. Chemistry of Materials. 2015;27:7452-8.

[280] Dunn B, Kamath H, Tarascon J-M. Electrical energy storage for the grid: a battery of choices. Science. 2011;334:928-35.

[281] Arico AS, Bruce P, Scrosati B, Tarascon J-M, Van Schalkwijk W. Nanostructured materials for advanced energy conversion and storage devices. Nature materials. 2005;4:366-77.

[282] Liu C, Li F, Ma LP, Cheng HM. Advanced materials for energy storage. Advanced materials. 2010;22:28-62.

[283] Kraglund MR, Aili D, Jankova K, Christensen E, Li Q, Jensen JO. Zero-gap alkaline water electrolysis using ion-solvating polymer electrolyte membranes at reduced KOH concentrations. Journal of The Electrochemical Society. 2016;163:F3125-F31.

[284] Lubitz W, Tumas W. Hydrogen: An Overview. Chemical Reviews. 2007;107:3900-3.

[285] Yang Z, Zhang J, Kintner-Meyer MCW, Lu X, Choi D, Lemmon JP, et al. Electrochemical Energy Storage for Green Grid. Chemical Reviews. 2011;111:3577-613.

[286] Scialdone O, Albanese A, D' Angelo A, Galia A, Guarisco C. Investigation of electrode material–redox couple systems for reverse electrodialysis processes. Part II: Experiments in a stack with 10–50 cell pairs. Journal of electroanalytical chemistry. 2013;704:1-9.

[287] Pattle RE. Electricity from fresh and salt water—without fuel

Chem Proc Eng. 1955;35:351-4.

[288] Veerman J, Saakes M, Metz SJ, Harmsen GJ. Electrical Power from Sea and River Water by Reverse Electrodialysis: A First Step from the Laboratory to a Real Power Plant. Environmental Science & Technology. 2010;44:9207-12.

[289] Jagur-Grodzinski J, Kramer R. Novel process for direct conversion of free energy of mixing into electric power. Industrial & Engineering Chemistry Process Design and Development. 1986;25:443-9.

[290] Suda F, Matsuo T, Ushioda D. Transient changes in the power output from the concentration difference cell (dialytic battery) between seawater and river water. Energy. 2007;32:165-73.

[291] Vermaas DA, Saakes M, Nijmeijer K. Capacitive Electrodes for Energy Generation by Reverse Electrodialysis. Procedia Engineering. 2012;44:496-7.

[292] Lee H-J, Hong M-K, Han S-D, Cho S-H, Moon S-H. Fouling of an anion exchange membrane in the electrodialysis desalination process in the presence of organic foulants. Desalination. 2009;238:60-9.

[293] Tanaka N, Nagase M, Higa M. Organic fouling behavior of commercially available hydrocarbon-based anion-exchange membranes by various organic-fouling substances. Desalination. 2012;296:81-6.

[294] Lindstrand V, Sundström G, Jönsson A-S. Fouling of electrodialysis membranes by organic substances. Desalination. 2000;128:91-102.

[295] Pawlowski S, Galinha CF, Crespo JG, Velizarov S. 2D fluorescence spectroscopy for monitoring ion-exchange membrane based technologies – Reverse electrodialysis (RED). Water Research. 2016;88:184-98.

[296] Pendergast MM, Hoek EMV. A review of water treatment membrane nanotechnologies. Energy & Environmental Science. 2011;4:1946-71.

[297] Cohen-Tanugi D, McGovern RK, Dave SH, Lienhard JH, Grossman JC. Quantifying the potential of ultra-permeable membranes for water desalination. Energy & Environmental Science. 2014;7:1134-41.

[298] Curcio E, Ji X, Di Profio G, Fontananova E, Drioli E. Membrane distillation operated at high seawater concentration factors: role of the membrane on CaCO 3 scaling in presence of humic acid. Journal of Membrane Science. 2010;346:263-9.

[299] Vrouwenvelder JS, van Paassen JAM, Wessels LP, van Dam AF, Bakker SM. The Membrane Fouling Simulator: A practical tool for fouling prediction and control. Journal of Membrane Science. 2006;281:316-24.

[300] Galinha CF, Carvalho G, Portugal CAM, Guglielmi G, Reis MAM, Crespo JG. Two-dimensional fluorescence as a fingerprinting tool for monitoring wastewater treatment systems. Journal of Chemical Technology & Biotechnology. 2011;86:985-92.

[301] Marose S, Lindemann C, Scheper T. Two-Dimensional Fluorescence Spectroscopy: A New Tool for On-Line Bioprocess Monitoring. Biotechnology Progress. 1998;14:63-74.

[302] Vaselbehagh M, Karkhanechi H, Takagi R, Matsuyama H. Biofouling phenomena on anion exchange membranes under the reverse electrodialysis process. Journal of Membrane Science. 2017;530:232-9.

[303] Moreno J, de Hart N, Saakes M, Nijmeijer K. CO2 saturated water as two-phase flow for fouling control in reverse electrodialysis. Water Research. 2017;125:23-31.

[304] Ngene IS, Lammertink RGH, Kemperman AJB, van de Ven WJC, Wessels LP, Wessling M, et al. CO2 Nucleation in Membrane Spacer Channels Remove Biofilms and Fouling Deposits. Industrial & Engineering Chemistry Research. 2010;49:10034-9.

[305] Park J-S, Lee H-J, Choi S-J, Geckeler KE, Cho J, Moon S-H. Fouling mitigation of anion exchange membrane by zeta potential control. Journal of Colloid and Interface Science. 2003;259:293-300.

[306] Pramanik BK, Roddick FA, Fan L. Long-term operation of biological activated carbon pre-treatment for microfiltration of secondary effluent: Correlation between the organic foulants and fouling potential. Water Research. 2016;90:405-14.

[307] Sagbo O, Sun Y, Hao A, Gu P. Effect of PAC addition on MBR process for drinking water treatment. Separation and Purification Technology. 2008;58:320-7.

[308] Mikhaylin S, Bazinet L. Fouling on ion-exchange membranes: Classification, characterization and strategies of prevention and control. Advances in Colloid and Interface Science. 2016;229:34-56.

[309] Zhao Z, Cao H, Shi S, Li Y, Yao L. Characterization of anion exchange membrane modified by electrodeposition of polyelectrolyte containing different functional groups. Desalination. 2016;386:58-66.

[310] Mulyati S, Takagi R, Fujii A, Ohmukai Y, Maruyama T, Matsuyama H. Improvement of the antifouling potential of an anion exchange membrane by surface modification with a polyelectrolyte for an electrodialysis process. Journal of Membrane Science. 2012;417–418:137-43.

[311] Vaselbehagh M, Karkhanechi H, Mulyati S, Takagi R, Matsuyama H. Improved antifouling of anion-exchange membrane by polydopamine coating in electrodialysis process. Desalination. 2014;332:126-33.

[312] Tanaka N, Nagase M, Higa M. Preparation of aliphatic-hydrocarbon-based anion-exchange membranes and their anti-organic-fouling properties. Journal of Membrane Science. 2011;384:27-36.

[313] Chang H-K, Choi E, Park J. Paper-based energy harvesting from salinity gradients. Lab on a Chip. 2016;16:700-8.

[314] Garcia-Vasquez W, Ghalloussi R, Dammak L, Larchet C, Nikonenko V, Grande D. Structure and properties of heterogeneous and homogeneous ion-exchange membranes subjected to ageing in sodium hypochlorite. Journal of Membrane Science. 2014;452:104-16.

[315] Garcia-Vasquez W, Dammak L, Larchet C, Nikonenko V, Grande D. Effects of acid–base cleaning procedure on structure and properties of anion-exchange membranes used in electrodialysis. Journal of Membrane Science. 2016;507:12-23.

[316] Vermaas DA, Guler E, Saakes M, Nijmeijer K. Theoretical power density from salinity gradients using reverse electrodialysis. Energy Procedia. 2012;20:170-84.

[317] Turek M, Bandura B, Dydo P. Power production from coal-mine brine utilizing reversed electrodialysis. Desalination. 2008;221:462-6.

[318] Long R, Li B, Liu Z, Liu W. Hybrid membrane distillation-reverse electrodialysis electricity generation system to harvest low-grade thermal energy. Journal of Membrane Science. 2017;525:107-15.

[319] Brauns E. (2012) US20080230376A1, Combination of desalination plant and salinity gradient power reverse electrodialysis plant and usethereof.

[320] Giwa A, Dufour V, Al Marzooqi F, Al Kaabi M, Hasan SW. Brine management methods: Recent innovations and current status. Desalination. 2017;407:1-23.

[321] Kwon K, Han J, Park BH, Shin Y, Kim D. Brine recovery using reverse electrodialysis in membrane-based desalination processes. Desalination. 2015;362:1-10.

[322] Luo F, Wang Y, Jiang C, Wu B, Feng H, Xu T. A power free electrodialysis (PFED) for desalination. Desalination. 2017;404:138-46.

[323] Kim Y, Logan BE. Hydrogen production from inexhaustible supplies of fresh and salt water using microbial reverse-electrodialysis electrolysis cells. Proceedings of the National Academy of Sciences of the United States of America. 2011;108:16176-81.

[324] Watson VJ, Hatzell M, Logan BE. Hydrogen production from continuous flow, microbial reverse-electrodialysis electrolysis cells treating fermentation wastewater. Bioresource Technology. 2015;195:51-6.

[325] Zhu X, Hatzell MC, Logan BE. Microbial reverse-electrodialysis electrolysis and chemical-production cell for H2 production and CO2 sequestration. Environmental science & technology letters. 2014;1:231-5.

[326] Kim Y, Logan BE. Microbial reverse electrodialysis cells for synergistically enhanced power production. Environmental Science and Technology. 2011;45:5834-9.

[327] Zhu X, Hatzell MC, Cusick RD, Logan BE. Microbial reverse-electrodialysis chemical-production cell for acid and alkali production. Electrochemistry Communications. 2013;31:52-5.

[328] Cusick RD, Hatzell M, Zhang F, Logan BE. Minimal RED cell pairs markedly improve electrode kinetics and power production in microbial reverse electrodialysis cells. Environmental science & technology. 2013;47:14518-24.

[329] Drioli E, Criscuoli A, Curcio E. Integrated membrane operations for seawater desalination. Desalination. 2002;147:77-81.

[330] Macedonio F, Curcio E, Drioli E. Integrated membrane systems for seawater desalination: energetic and exergetic analysis, economic evaluation, experimental study. Desalination. 2007;203:260-76.

[331] Ali A, Tufa RA, Macedonio F, Curcio E, Drioli E. Membrane technology in renewable-energy-driven desalination. Renewable and Sustainable Energy Reviews. 2018;81:1-21.

[332] Mei Y, Tang CY. Co-locating reverse electrodialysis with reverse osmosis desalination: Synergies and implications. Journal of Membrane Science. 2017;539:305-12.

[333] Saleem MW, Jande YAC, Kim W-S. Performance optimization of integrated electrochemical capacitive deionization and reverse electrodialysis model through a series pass desorption process. Journal of Electroanalytical Chemistry. 2017;795:41-50.

[334] Buonomenna MG, Bae J. Membrane processes and renewable energies. Renewable and Sustainable Energy Reviews. 2015;43:1343-98.

[335] Eltawil MA, Zhengming Z, Yuan L. A review of renewable energy technologies integrated with desalination systems. Renewable and Sustainable Energy Reviews. 2009;13:2245-62.

[336] Ghaffour N, Lattemann S, Missimer T, Ng KC, Sinha S, Amy G. Renewable energy-driven innovative energy-efficient desalination technologies. Applied Energy. 2014;136:1155-65.

[337] Global Water Intelligence, IDA Desalination Yearbook 2017-2018. October 9th, 2017.

[338] Caldera U, Bogdanov D, Breyer C. Chapter 8 - Desalination Costs Using Renewable Energy Technologies A2 - Gude, Veera Gnaneswar. Renewable Energy Powered Desalination Handbook: Butterworth-Heinemann; 2018. p. 287-329.

[339] Liu Z, Bai H, Lee J, Sun DD. A low-energy forward osmosis process to produce drinking water. Energy & Environmental Science. 2011;4:2582-5.

[340] Zhou J, Chang VWC, Fane AG. Environmental life cycle assessment of brackish water reverse osmosis desalination for different electricity production models. Energy & Environmental Science. 2011;4:2267-78.

[341] Roberts DA, Johnston EL, Knott NA. Impacts of desalination plant discharges on the marine environment: A critical review of published studies. Water research. 2010;44:5117-28.

[342] Wang Q, Gao X, Zhang Y, He Z, Ji Z, Wang X, et al. Hybrid RED/ED system: Simultaneous osmotic energy recovery and desalination of high-salinity wastewater. Desalination. 2017;405:59-67.

[343] Gonzalez A, Grágeda M, Ushak S. Assessment of pilot-scale water purification module with electrodialysis technology and solar energy. Applied Energy. 2017;206:1643-52.

[344] McGovern RK, Weiner AM, Sun L, Chambers CG, Zubair SM, Lienhard V JH. On the cost of electrodialysis for the desalination of high salinity feeds. Applied Energy. 2014;136:649-61.

[345] Baudler A, Schmidt I, Langner M, Greiner A, Schroder U. Does it have to be carbon? Metal anodes in microbial fuel cells and related bioelectrochemical systems. Energy & Environmental Science. 2015;8:2048-55.

[346] Chen S, Hou H, Harnisch F, Patil SA, Carmona-Martinez AA, Agarwal S, et al. Electrospun and solution blown three-dimensional carbon fiber nonwovens for application as electrodes in microbial fuel cells. Energy & Environmental Science. 2011;4:1417-21.

[347] Fricke K, Harnisch F, Schroder U. On the use of cyclic voltammetry for the study of anodic electron transfer in microbial fuel cells. Energy & Environmental Science. 2008;1:144-7.

[348] Garner LE, Thomas AW, Sumner JJ, Harvey SP, Bazan GC. Conjugated oligoelectrolytes increase current response and organic contaminant removal in wastewater microbial fuel cells. Energy & Environmental Science. 2012;5:9449-52.

[349] He Z, Mansfeld F. Exploring the use of electrochemical impedance spectroscopy (EIS) in microbial fuel cell studies. Energy & Environmental Science. 2009;2:215-9.

[350] Inglesby AE, Fisher AC. Enhanced methane yields from anaerobic digestion of Arthrospira maxima biomass in an advanced flow-through reactor with an integrated recirculation loop microbial fuel cell. Energy & Environmental Science. 2012;5:7996-8006.

[351] Li W-W, Yu H-Q, He Z. Towards sustainable wastewater treatment by using microbial fuel cells-centered technologies. Energy & Environmental Science. 2014;7:911-24.

[352] Malvankar NS, Tuominen MT, Lovley DR. Biofilm conductivity is a decisive variable for high-current-density Geobacter sulfurreducens microbial fuel cells. Energy & Environmental Science. 2012;5:5790-7.

[353] Qiao Y, Bao S-J, Li CM. Electrocatalysis in microbial fuel cells-from electrode material to direct electrochemistry. Energy & Environmental Science. 2010;3:544-53.

[354] Rinaldi A, Mecheri B, Garavaglia V, Licoccia S, Di Nardo P, Traversa E. Engineering materials and biology to boost performance of microbial fuel cells: a critical review. Energy & Environmental Science. 2008;1:417-29.

[355] Zhang F, Jacobson KS, Torres P, He Z. Effects of anolyte recirculation rates and catholytes on electricity generation in a litre-scale upflow microbial fuel cell. Energy & Environmental Science. 2010;3:1347-52.

[356] Cheng S, Logan BE. Ammonia treatment of carbon cloth anodes to enhance power generation of microbial fuel cells. Electrochemistry Communications. 2007;9:492-6.

[357] Oh SE, Logan BE. Voltage reversal during microbial fuel cell stack operation. Journal of Power Sources. 2007;167:11-7.

[358] Nam J-Y, Cusick RD, Kim Y, Logan BE. Hydrogen generation in microbial reverse-electrodialysis electrolysis cells using a heat-regenerated salt solution. Environmental science & technology. 2012;46:5240-6.

[359] Logan BE, Call D, Cheng S, Hamelers HV, Sleutels TH, Jeremiasse AW, et al. Microbial electrolysis cells for high yield hydrogen gas production from organic matter. Environmental Science & Technology. 2008;42:8630-40.

[360] Luo X, Nam J-Y, Zhang F, Zhang X, Liang P, Huang X, et al. Optimization of membrane stack configuration for efficient hydrogen production in microbial reverse-electrodialysis electrolysis cells coupled with thermolytic solutions. Bioresource technology. 2013;140:399-405.

[361] Hidayat S, Song YH, Park JY. A comparison of mono- and multi-valent ions as stack feed solutions in microbial reverse-electrodialysis electrolysis cells and their effects on hydrogen generation. International Biodeterioration and Biodegradation. 2016;113:28-33.

[362] Luo X, Nam JY, Zhang F, Zhang X, Liang P, Huang X, et al. Optimization of membrane stack configuration for efficient hydrogen production in microbial reverse-electrodialysis electrolysis cells coupled with thermolytic solutions. Bioresource Technology. 2013;140:399-405.

[363] Song YH, Hidayat S, Kim HK, Park JY. Hydrogen production in microbial reverse-electrodialysis electrolysis cells using a substrate without buffer solution. Bioresource Technology. 2016;210:56-60.

[364] Chisholm G, Kitson PJ, Kirkaldy ND, Bloor LG, Cronin L. 3D printed flow plates for the electrolysis of water: an economic and adaptable approach to device manufacture. Energy & Environmental Science. 2014;7:3026-32.

[365] Haber JA, Cai Y, Jung S, Xiang C, Mitrovic S, Jin J, et al. Discovering Ce-rich oxygen evolution catalysts, from high throughput screening to water electrolysis. Energy & Environmental Science. 2014;7:682-8.

[366] Spurgeon JM, Lewis NS. Proton exchange membrane electrolysis sustained by water vapor. Energy & Environmental Science. 2011;4:2993-8.

[367] Tran PD, Artero V, Fontecave M. Water electrolysis and photoelectrolysis on electrodes engineered using biological and bio-inspired molecular systems. Energy & Environmental Science. 2010;3:727-47.

[368] Pagliaro M, Konstandopoulos AG, Ciriminna R, Palmisano G. Solar hydrogen: fuel of the near future. Energy & Environmental Science. 2010;3:279-87.

[369] Shaner MR, Atwater HA, Lewis NS, McFarland EW. A comparative technoeconomic analysis of renewable hydrogen production using solar energy. Energy & Environmental Science. 2016;9:2354-71.

[370] Postnikov AV, Uvarov IV, Lokhanin MV, Svetovoy VB. Highly energetic phenomena in water electrolysis. Scientific Reports. 2016;6:39381.

[371] Walter MG, Warren EL, McKone JR, Boettcher SW, Mi Q, Santori EA, et al. Solar Water Splitting Cells. Chemical Reviews. 2010;110:6446-73.

[372] Kang D, Kim TW, Kubota SR, Cardiel AC, Cha HG, Choi KS. Electrochemical Synthesis of Photoelectrodes and Catalysts for Use in Solar Water Splitting. Chemical Reviews. 2015;115:12839-87.

[373] Fereidooni M, Mostafaeipour A, Kalantar V, Goudarzi H. A comprehensive evaluation of hydrogen production from photovoltaic power station. Renewable and Sustainable Energy Reviews. 2018;82:415-23.

[374] Low FW, Lai CW. Recent developments of graphene-TiO$_2$ composite nanomaterials as efficient photoelectrodes in dye-sensitized solar cells: A review. Renewable and Sustainable Energy Reviews. 2018;82:103-25.

[375] Ahmad H, Kamarudin SK, Minggu LJ, Kassim M. Hydrogen from photo-catalytic water splitting process: A review. Renewable and Sustainable Energy Reviews. 2015;43:599-610.

[376] Nikolaidis P, Poullikkas A. A comparative overview of hydrogen production processes. Renewable and Sustainable Energy Reviews. 2017;67:597-611.

[377] Yilmaz F, Balta MT, Selbaş R. A review of solar based hydrogen production methods. Renewable and Sustainable Energy Reviews. 2016;56:171-8.

[378] Dutton AG, Bleijs JAM, Dienhart H, Falchetta M, Hug W, Prischich D, et al. Experience in the design, sizing, economics, and implementation of autonomous wind-powered hydrogen production systems. International Journal of Hydrogen Energy. 2000;25:705-22.

[379] Tufa RA, Chanda D, Tundis L, Hnát J, Bouzek K, Veerman J, et al. Salinity gradient power driven water electrolysis for hydrogen production. Chemical Engineering Transactions. 2017;60:283-8.

[380] Chen X, Jiang C, Zhang Y, Wang Y, Xu T. Storable hydrogen production by Reverse Electro-Electrodialysis (REED). Journal of Membrane Science. 2017;544:397-405.

[381] Lee J, Yun J, Kwon SR, Chang WJ, Nam KT, Chung TD. Reverse Electrodialysis-Assisted Solar Water Splitting. Scientific Reports. 2017;7.

[382] Lattemann S, Höpner T. Environmental impact and impact assessment of seawater desalination. Desalination. 2008;220:1-15.

[383] Kingsbury RS, Coronell O. Osmotic Ballasts Enhance Faradaic Efficiency in Closed-Loop, Membrane-Based Energy Systems. Environmental Science & Technology. 2017;51:1910−7.

[384] van Egmond WJ, Starke UK, Saakes M, Buisman CJN, Hamelers HVM. Energy efficiency of a concentration gradient flow battery at elevated temperatures. Journal of Power Sources. 2017;340:71-9.

[385] Hwang J, Sekimoto T, Hsu W-L, Kataoka S, Endo A, Daiguji H. Thermal dependence of nanofluidic energy conversion by reverse electrodialysis. Nanoscale. 2017;9:12068-76.

[386] Cao L, Guo W, Ma W, Wang L, Xia F, Wang S, et al. Towards understanding the nanofluidic reverse electrodialysis system: well matched charge selectivity and ionic composition. Energy & Environmental Science. 2011;4:2259-66.

[387] Kim D-K, Duan C, Chen Y-F, Majumdar A. Power generation from concentration gradient by reverse electrodialysis in ion-selective nanochannels. Microfluid Nanofluid. 2010;9:1215-24.

[388] Kempener R, Neumann F. Salinity gradient energy technology brief, International Renewable Energy Agency. June 2014.

[389] Administration UEI. Levelized Cost and Levelized Avoided Cost of New Generation, Resources in the Annual Energy Outlook 2016. 2016.

[390] Andrjesdóttir Ó, Ong CL, Nabavi M, Paredes S, Khalil ASG, Michel B, et al. An experimentally optimized model for heat and mass transfer in direct contact membrane distillation. International Journal of Heat and Mass Transfer. 2013;66:855-67.

[391] Planungs-KG WWuIGC. Final Report Summary - REAPOWER (Reverse Electrodialysis Alternative Power Production). March 6th, 2015.

[392] Warsinger DM, Chakraborty S, Tow EW, Plumlee MH, Bellona C, Loutatidou S, et al. A review of polymeric membranes and processes for potable water reuse. Progress in Polymer Science. 2018.

[393] Paidar M, Fateev V, Bouzek K. Membrane electrolysis—History, current status and perspective. Electrochimica Acta. 2016;209:737-56.

[394] Pan Z, An L, Zhao T, Tang Z. Advances and challenges in alkaline anion exchange membrane fuel cells. Prog Energ Combust. 2018;66:141-75.

[395] Merle G, Wessling M, Nijmeijer K. Anion exchange membranes for alkaline fuel cells: A review. Journal of Membrane Science. 2011;377:1-35.

[396] Li X, Zhang H, Mai Z, Zhang H, Vankelecom I. Ion exchange membranes for vanadium redox flow battery (VRB) applications. Energy & Environmental Science. 2011;4:1147-60.

[397] Criscuoli A, Drioli E. Energetic and exergetic analysis of an integrated membrane desalination system. Desalination. 1999;124:243-9.

[398] André S, Janne G. Environmental impacts by running an osmotic power plant. In: Research NIfW, editor.: Norwegian Institute for Water Research, Norway, 2012.

[399] Miller S, Shemer H, Semiat R. Energy and environmental issues in desalination. Desalination. 2015;366:2-8.

[400] D'Angelo A, Tedesco M, Cipollina A, Galia A, Micale G, Scialdone O. Reverse electrodialysis performed at pilot plant scale: Evaluation of redox processes and simultaneous generation of electric energy and treatment of wastewater. Water Research. 2017;125:123-31.